

# Isotope Geochemical and Geochronologic Studies of Basement Units in the Central Western Carpathians (Slovakia)

Dissertation

Andreas S. Gaab  
2005

# Isotope Geochemical and Geochronologic Studies of Basement Units in the Central Western Carpathians (Slovakia)

Dissertation  
zur Erlangung des Grades  
Doktor der Naturwissenschaften  
am Fachbereich Geowissenschaften  
der Johannes Gutenberg-Universität Mainz

Andreas Simon Gaab  
geboren am 02.04.1976  
in Gräfelting

Mainz, 29. März 2005

Tag der mündlichen Prüfung

10. Mai 2005

# Contents

<b>1</b>	<b>Introduction</b>	<b>1</b>
<b>2</b>	<b>Alpine reworking of Ordovician protoliths in the Western Carpathians: Geochronological and geochemical data on the Muráň Gneiss Complex, Slovakia</b>	<b>4</b>
1	Introduction . . . . .	6
2	Geological Setting . . . . .	8
3	Sample Description . . . . .	10
4	Analytical Methods . . . . .	11
5	Geochemistry . . . . .	13
6	U-Pb dating . . . . .	15
7	Isotope Geochemistry . . . . .	16
8	Discussion and Conclusions . . . . .	21
	Acknowledgements . . . . .	23

<b>3</b>	<b>Zircon U-Pb geochronology and Isotopic Characterization for the pre-Mesozoic basement of the Northern Veporic Unit (Central Western Carpathians, Slovakia)</b>	<b>28</b>
1	Introduction . . . . .	30
2	Geological Setting . . . . .	31
3	Analytical Techniques . . . . .	32
4	Sample Description . . . . .	33
4.1	Kralova Hola . . . . .	33
4.2	Koleso valley . . . . .	34
4.3	Uplaz and Drotacka . . . . .	34
4.4	Mihalikovo quarry . . . . .	36
4.5	Hoškova valley . . . . .	36
5	U-Pb zircon dating . . . . .	37
5.1	SHRIMP dating . . . . .	37
5.2	Conventional dating . . . . .	37
5.3	Discussion of the U-Pb data . . . . .	42
6	Geochemistry (Koleso Valley) . . . . .	44
6.1	Main and Trace Elements . . . . .	44
6.2	WR-Pb-Pb . . . . .	44
6.3	Sr and Nd Isotopes . . . . .	49
7	Conclusion . . . . .	53
	Acknowledgements . . . . .	54
<b>4</b>	<b>Redistribution of REE and of U, Th, Pb, Sr, and Rb during intrusion and auto-metasomatism of the Dlhá Dolina granite (Gemeric Unit, Eastern Slovakia)</b>	<b>58</b>
1	Introduction . . . . .	60
2	Geological Setting . . . . .	60
3	Sample Description . . . . .	62

3.1	Petrographical Description . . . . .	63
4	Geochemistry . . . . .	64
4.1	Main and trace elements . . . . .	64
4.2	REE and Tetrad effect . . . . .	67
4.3	Lead Isotopes . . . . .	69
4.4	Sr isotopes . . . . .	71
5	Conclusions . . . . .	73
	Acknowledgements . . . . .	74
A	mineral abbreviations . . . . .	77
<b>5</b>	<b>CLEO: Common Lead Evaluation using Octave</b>	<b>78</b>
1	Introduction . . . . .	79
2	WR-Pb-Pb dating . . . . .	81
3	CLEO . . . . .	82
3.1	Capabilities . . . . .	83
3.2	Usage . . . . .	84
4	The Dlhá Dolina granite . . . . .	85
4.1	The WR-Pb-Pb data . . . . .	85
4.2	Discussion . . . . .	88
5	Summary . . . . .	89
	Acknowledgements . . . . .	89
A	Octave . . . . .	89
B	Analytical Technique . . . . .	90
<b>6</b>	<b>Analytical techniques</b>	<b>93</b>
1	Microwave assisted digestion of granitoid material . . . . .	94
2	Column chemistry for Sr and Nd separation and loading for TIMS measurements . . . . .	97
3	Relative-Sensitivity-Factor quantification for ICPMS analysis .	98

TABLE OF CONTENTS

---

3.1	Results on IRM . . . . .	103
	<b>Danksagung</b>	<b>106</b>
	<b>Complete Reference List</b>	<b>107</b>
	<b>Curriculum Vitae</b>	<b>121</b>

# List of Tables

<b>1</b>	<b>Introduction</b>	
<b>2</b>	<b>Alpine reworking of Ordovician protoliths in the Western Carpathians: Geochronological and geochemical data on the Muráň Gneiss Complex, Slovakia</b>	
1	Whole rock geochemical data. Samples sorted by $SiO_2$ content. Major (given in $wt\%$ as oxides) and trace elements (given in $ppm$ ) measured with XRF. REE, Rb and Sr measured with ICPMS. <i>nd</i> for not determined . . . . .	12
2	Vapor digestion single zircon U-Pb data for the felsic gneiss, sample UP1115. . . . .	13
3	Pb-Pb-WR data for samples of the Muráň area. Reproducibility is generally better than 500 ppm. . . . .	18
4	$^{87}Sr/^{86}Sr$ - and $^{143}Nd/^{144}Nd$ -whole rock isotopic compositions. Isotopic compositions are also recalculated to the Alpine overprint. For Nd values are reported as $\epsilon Nd$ and the $T_{DM}^{Nd}$ are given. . . . .	19



---

<b>3</b>	<b>Zircon U-Pb geochronology and Isotopic Characterization for the pre-Mesozoic basement of the Northern Veporic Unit (Central Western Carpathians, Slovakia)</b>	
1	Data for the SHRIMP analyses of the Kralova Hola. Concordia diagram shown in Fig. 5 . . . . .	38
2	Data for the conventional U-Pb single grain zircon analyses shown in Fig. 5. MG - multi grain; SG - single grain; CLC - single grain with CL control. . . . .	39
	(continued) Data for the conventional U-Pb single grain zircon analyses shown in Fig. 5. MG - multi grain; SG - single grain; CLC - single grain with CL control. . . . .	40
3	Details on multi grain analyses of sample 03GA50. <i>Pb*</i> and results given in table 2. . . . .	41
4	Compilation of the intercept ages shown in Fig. 5. Reinterpreted data from Putiš et al. (2001) and the data from Gaab et al. (in press) are included. . . . .	42
5	Geochemistry for the samples from the Koleso valley. Main elements are given in wt%, trace element in ppm. 'bd' for below detection limit. . . . .	45
6	WR-Pb-Pb data for samples from the Koleso valley and from Kralova Hola. Multiple splits were measured for each samples to observe the whole range of Pb isotopic composition. . . . .	46
7	Sr and Nd isotopic data for the Koleso area and two Kralova Hola samples. Initial values calculated for 460 Ma. . . . .	50

---

<b>4</b>	<b>Redistribution of REE and of U, Th, Pb, Sr, and Rb during intrusion and auto-metasomatism of the Dlhá Dolina granite (Gemic Unit, Eastern Slovakia)</b>	
1	Short description of the samples used for this study, more detailed description in Dianiška et al. (2002). Numbers refer to location in cross section (Fig. 1). Mineral abbreviations are given on page 77. . . . .	63
2	Geochemical data for the Dlhá Dolina complex. Main and trace elements analysed with XRF, REE analysed with ICPMS. <i>NA</i> for not available, <i>BD</i> for below detection. 0.006 ppm Eu assumed for samples with Eu below detection limit. Tetrad effect ( $TE_{1,3}$ ) calculated according Irber (1999). $Eu/Eu^* = \frac{Eu_N}{\sqrt{Gd_N * Sm_N}}$ . . . . .	65
3	Sr isotopic composition of the Dlhá Dolina drill core samples. Isotopic analyses are reproduced twice. . . . .	71
<b>5</b>	<b>CLEO: Common Lead Evaluation using Octave</b>	
1	Main and sub menu of <i>CLEO</i> . . . . .	82
2	$^{206}Pb/^{204}Pb$ , $^{207}Pb/^{204}Pb$ , $^{208}Pb/^{204}Pb$ , $^{207}Pb/^{206}Pb$ ratios for the samples of the Dlhá Dolina drill core. Measurements are corrected for fractionation. Errors are absolute. R gives the correlation of the error on the $^{206}Pb/^{204}Pb$ , $^{207}Pb/^{204}Pb$ and $^{207}Pb/^{206}Pb$ measurements. . . . .	84

**6 Analytical techniques**

1	Details for the method used for measurements on <i>Element2</i> . . . . .	99
2	Analyses of IRM GSP-2 of two independent microwave dissolution procedures and two independent analysis sequences. GSP-2b and GSP-2eI used as standard. Reference value after Raczek et al. (2001). . . . .	102
3	Analyses of IRM JG-1 of two independent microwave dissolution procedures and two independent analysis sequences. GSP-2b and GSP-2eI used as standard. Reference value after Dulski (2001). For JG-1a and JG-1b too low concentrations were measured and these analyses are classified as outliers. . . . .	103
4	Analyses of IRM JG-2 of two independent microwave dissolution procedures and two independent analysis sequences. GSP-2b and GSP-2eI used as standard. Reference value after Dulski (2001). . . . .	104

# List of Figures

## 1 Introduction

## 2 Alpine reworking of Ordovician protoliths in the Western Carpathians: Geochronological and geochemical data on the Muráň Gneiss Complex, Slovakia

1	Geologic Map of Slovakia modified after Plašienka (1997). Location of Fig. 2 indicated. Inlay depicts political boundaries of Slovakia with major rivers for overview. . . . .	7
2	Geologic Map of the Muráň area after Janák et al. (2001b). Study area is indicated by the rectangle. Note the location of the Muráň Gneiss Complex directly at the contact to the Gemic unit in the East. . . . .	8
3	Chondrite normalized REE-pattern (CI chondrite after Taylor and McLennan (1985)). . . . .	14
4	Concordia diagram for single zircon vapor digestion analyses of the felsic gneiss UP1115. . . . .	15
5	Representative cathodoluminescence images for zircons of sample UP1115 in a polished mount. Inherited cores and magmatic zoning present in some zircons. Most zircons experienced metamictisation and show nebulous CL. . . . .	16

6	$^{207}\text{Pb}/^{204}\text{Pb}$ vs. $^{206}\text{Pb}/^{204}\text{Pb}$ and $^{208}\text{Pb}/^{204}\text{Pb}$ vs. $^{206}\text{Pb}/^{204}\text{Pb}$ - diagram. Felsic gneiss and amphibolite samples form a linear array in both diagrams. Mica schists plot distinct in a small array. Stacey and Kramers (1975, lower line, (S&K)) and Upper Crustal (after Zartman and Haines, 1988, upper line, (Z&H)) evolution line drawn with labels in Ma. . . . .	17
7	Sr-Nd isotopic compositions recalculated to 88 Ma. Solid lines represent binary mixing (Langmuir et al., 1978) between end members similar to the most mafic and the most felsic sample (curvature = 0.012 and 0.024). Reservoirs plotted after Zindler and Hart (1986): BE - bulk earth; DM - depleted mantle; EM II - enriched mantle II; PREMA - prevalent mantle. . . . .	20
8	$\epsilon\text{Nd}$ isotopic evolution with time. Depleted mantle model and two-step calculations after Liew and Hofmann (1988). . . . .	21

**3 Zircon U-Pb geochronology and Isotopic Characterization  
 for the pre-Mesozoic basement of the Northern Veporic Unit  
 (Central Western Carpathians, Slovakia)**

1	Geological map of the Veporic Unit. Sample locations are indicated and location name used in this paper given. Outline of Slovakia with major rivers given in the inlay. Bratislava (BR) and Kosice (KO) indicated. . . . .	31
2	Zircon CL images for the Kralova Hola samples 02GA14 and 02GA17. Scale bar indicates 50 $\mu\text{m}$ . . . . .	34
3	Zircon CL images for samples from the Northern Veporic Unit. Localities shown in Fig. 1. Scale bar indicates 50 $\mu\text{m}$ . . . . .	35
4	Zircon CL images for samples from the Northern Veporic Unit. Locality shown in Fig. 1, Sample Mihalikovo (03GA50). Scale bar indicates 50 $\mu\text{m}$ . . . . .	36

---

5	Compilation of the U-Pb zircon data to identify the two main magmatic/metamorphic events recorded in the Veporic basement. Intercept ages and error bars are indicated by the arrows. Please note that the x- and y- axis are shifted for each sample. Data from Gaab et al. (in press) and from Putiš et al. (2001) given for comparison. Please note that the discordia lines for the latter dataset differ from the originally published ones. Detailed argumentation on page 43. The Kralova Hola data are measured on SHRIMP (Table 1), all other data are TIMS measurements (Table 2). Lower intercept ages are recent except for the Muran sample (see Tab. 4). . . . .	43
6	$^{206}\text{Pb}/^{204}\text{Pb}$ vs. $^{207}\text{Pb}/^{204}\text{Pb}$ and $^{206}\text{Pb}/^{204}\text{Pb}$ vs. $^{208}\text{Pb}/^{204}\text{Pb}$ diagrams for the samples presented in table 6. Evolution lines in the upper diagram drawn for the reservoirs after Zindler and Hart (1986) and the model after Stacey and Kramers (S&K; 1975). . . . .	47
7	Principal component analyses of the common lead data presented in this study (table 6) together with the common lead data published in Gaab et al. (in press). . . . .	48
8	$\epsilon\text{Nd}$ vs. $^{87}\text{Sr}/^{86}\text{Sr}$ diagram. Isotopic compositions are calculated back to initial values. Data for the High Tatra (HT), Western Tatra (WT), Low Tatra (LT) (Poller et al., 2001a, in press) and the Kralova Hola samples are calculated to 330 Ma, data from the Koleso valley and the Muráň area (Gaab et al., in press) are calculated to 460 Ma. . . . .	51

---

<b>4</b>	<b>Redistribution of REE and of U, Th, Pb, Sr, and Rb during intrusion and auto-metasomatism of the Dlhá Dolina granite (Gemic Unit, Eastern Slovakia)</b>	
1	Simplified geological map of the Gemic Unit modified after Broska et al. (2002) and cross section through the Dlhá Dolina subsurface granite modified after Dianiška et al. (2002). Vertical position of the samples indicated by numbers (compare with table 1). . . . .	61
2	Harker diagrams for the granites occurring in the Gemic Unit. Data for the Dlhá Dolina (black rimmed symbols) given in table 2. Reference data (grey circles) for the Gemic Granites from (Broska and Uher, 2001). . . . .	66
3	REE diagram normalized to chondrite (Taylor and McLennan, 1985). A: The drill core samples. Data given in table 2. B: Modelling of crystal fractionation for this dataset. Sample DD-908 and DD-783 shown in solid used as initial composition, sample GA-577 shown as reference. Grey lines represent 10, 30, 50, 70, and 90 % of fractionation. Detailed discussion in the text. . . . .	67
4	Comparison of the Tetrad effect observed in the Dlhá Dolina samples with the data from Irber (1999). Data given in table 2.	69
5	$^{207}\text{Pb}/^{204}\text{Pb}$ vs. $^{206}\text{Pb}/^{204}\text{Pb}$ diagram and $^{208}\text{Pb}/^{204}\text{Pb}$ vs. $^{206}\text{Pb}/^{204}\text{Pb}$ for the samples of the Dlhá Dolina subsurface granite. $\kappa_{today}$ calculated for reference lines and the age of 241 Ma. Data published by Gaab et al. (submitted). . . . .	70

6	$^{87}\text{Rb}/^{86}\text{Sr}$ vs. $^{87}\text{Sr}/^{86}\text{Sr}$ diagram for Gemeric Granites. Black symbols are the data presented in this study (table 3). WR data compiled by Cambel et al. (1990) shown in grey, localities given in the key. Reference line corresponding to 241 Ma shown (black line). Fields of the WR “isochrons” (dark grey field) and the WR-Biotite “isochrons” (light grey field) of the Cambel et al. (1990) dataset indicated. Biotite data points are not shown due to their high $^{87}\text{Rb}/^{86}\text{Sr}$ . . . . .	72
<b>5 CLEO: Common Lead Evaluation using Octave</b>		
1	$^{207}\text{Pb}/^{204}\text{Pb}$ vs. $^{206}\text{Pb}/^{204}\text{Pb}$ diagram and $^{208}\text{Pb}/^{204}\text{Pb}$ vs. $^{206}\text{Pb}/^{204}\text{Pb}$ for the samples of the Dlhá Dolina subsurface granite. Note the good linear correlation in the $^{207}\text{Pb}/^{204}\text{Pb}$ vs. $^{206}\text{Pb}/^{204}\text{Pb}$ diagram, which corresponds to an $^{207}\text{Pb}/^{206}\text{Pb}$ age of $241\pm 0.5$ Ma. Same symbols for samples used in all diagrams. $\kappa_{today}$ calculated for reference lines and the age of 241 Ma. . . . .	86
2	Detail from the $^{207}\text{Pb}/^{204}\text{Pb}$ vs. $^{206}\text{Pb}/^{204}\text{Pb}$ diagram with lead evolution curves drawn for the reservoirs after Zartman and Haines (1988). Ticks on the evolution curves for 0 (right), 500, 1000, 1500 and 2000 Ma (left). . . . .	87
3	Two dimensional diagram for the two principal components with the largest variance. . . . .	88



**6 Analytical techniques**

- 1 Detail for the assembly of the vessels for the microwave assisted digestion. PTFE beakers containing the sample and acid are introduced to the pressure safe microwave vessel. *HCl* is added outside the beaker to the vessel to ensure pressure equilibrium. . . . . 94
- 2 P-T diagram for the three digestion steps used for microwave assisted digestion. Acids used for the first and second step are *HF - HNO<sub>3</sub>*, for the last step *HCl*. Temperature limits shown in the diagram, energy of the microwave oven indicated at the top of each diagram. . . . . 95

# 1 Zusammenfassung für Fachfremde

Ziel dieser Arbeit ist es mithilfe von geochemischen und isotopengeochemischen Daten Aussagen über das Alter und den Ursprung von Grundgebirgseinheiten in den Zentralen Westlichen Karpathen zu treffen.

Grundlage zur Bestimmung des Alters dieser Gesteine bildet die Einzelzirkon U-Pb Methode, wofür Uran und die Bleiisotopie von Zirkonen massenspektrometrisch bestimmt wird. Für die geochemische Klassifizierung der Einheiten wurden hauptsächlich die Seltenen Erd Elemente (SEE) und die radioaktiven Uran-Blei, Rubidium-Strontium und die Samarium-Neodym Zerfallssysteme benutzt.

Die Karpathen bilden die östliche Fortsetzung der Alpen. Sie wurden wie diese während der Alpenen Gebirgsbildung (Orogenese) aufgefaltet. Der alpine Gebirgsgürtel entstand in geologisch relativ junger Zeit zwischen 120 und 60 Millionen Jahren vor heute durch die Kollision der Afrikanischen Platte im Süden mit der Eurasischen Platte im Norden. Während dieser Gebirgsbildung wurden durch die Intrusion von Graniten neue Gesteine gebildet (z.B. Poller et al., 2001b) und bereits vorhandene Gesteine durch Deformation und Metamorphose im Aussehen und Zusammensetzung verändert (z.B. Janák et al., 2001b). Der Grossteil der Gesteine der Zentralen Westlichen Karpathen sind jedoch erheblich älter.

Die Zentralen Westlichen Karpathen können in drei unterschiedliche Grundgebirgseinheiten eingeteilt werden, von denen zwei im Rahmen dieser Arbeit bearbeitet wurden:

Im Nordwesten, zwischen der Hohen Tatra und den Kleinen Karpathen aufgeschlossen, finden sich magmatische Gesteine, die grösstenteils als Granite klassifiziert werden. Diese Gesteine gehören zu der Tatriscen Einheit und wurden, wie z.B. in Poller and Todt (2000) gezeigt wird, während der Variskischen Gebirgsbildung zwischen 400 Ma und 310 Ma vor heute gebildet.

Nach Süden anschliessend finden sich zum einem leicht deformierte Granite, zum anderen stark deformierte und überprägte Gneisse und Amphibolite, welche zu der Veporischen Einheit gezählt werden. Die Granite können grösstenteils ebenso der Variskischen Gebirgsbildung zugeordnet werden, jedoch sind Teile dieser Einheit erheblich älter als die Gesteine der Tatriscen Einheit. Geochronologische Daten zu diesen Gesteinen existieren kaum. Der erste Teil der Arbeit beschäftigt sich daher mit der Entwicklung und dem Alter der Veporischen Grundgebirgseinheiten und mit den geochemischen Veränderungen, den die Alpine und die Variskische Gebirgsbildung in diesen Gesteinen verursacht haben (Kapitel 2 und 3).

Als südlichste Grundgebirgseinheit schliesst die Gernerische Einheit an. Sie besteht hauptsächlich aus Sedimenten, welche aus vulkanischem Material entstanden sind. Das Alter der Sedimente kann anhand von Mikrofossilien als Früh-Palaeozoisch, also zwischen 500 und 400 Ma vor heute, bestimmt werden (z.B. Vozárová et al., 1998). Die sedimentären Gesteine, die leicht metamorph überprägt sind, werden von einigen Graniten durchschlagen. Sie haben jedoch einen anderen Charakter als die Granite, die in der Tatriscen und der Veporischen Einheit vorkommen. Sie weisen einen hohen Anteil an Turmalin auf und zeichnen sich durch hohe Gehalte von seltenen Metallen wie Niob, Tantal und Zinn aus. Das Alter der Granite, wie in Kapitel 4 gezeigt wird, ist vergleichsweise jung und liegt bei 250 Ma vor heute. Somit sind diese Granite während dem Perm entstanden.

Am Ende dieser Arbeit werden Details zur Analytik und Auswertung von Bleiisotopendaten gegeben (Kapitel 5). Die kombinierte Methodik zur Bestimmung der Strontium und Neodym Isotopie und der Seltenerdelementkonzentrationen, wie sie während dieser Arbeit verwendet wurde, wird in Kapitel 6 beschrieben.

## 2 Zusammenfassung

In dieser Arbeit werden geochronologische und isotopengeochemische Daten zur Entwicklung der Zentralen Westlichen Karpathen präsentiert. Die Karpathen bilden die östliche Fortsetzung der Alpen und können in drei Alpine Grundgebirgsdecken unterteilt werden, von denen zwei, die Veporische und die Gemerische, bearbeitet wurden. In der Veporischen Einheit wurden polymetamorphe Grundgebirgseinheiten untersucht, um deren genaue Altersstellung zu definieren und sie isotopengeochemisch zu klassifizieren. Dagegen wurde in der Gemerischen Einheit, welche die Veporische Einheit überlagert, ein spezialisierter S-Typ Granit im Detail untersucht, um die petrogenetischen Prozesse, die zur magmatischen Entwicklung dieses Granits geführt haben, zu identifizieren.

U-Pb Datierungen an Zirkonen der Veporischen Grundgebirgseinheiten zeigen für die gesamte Veporische Einheit ordovizische Entstehungsalter an (440-470 Ma). Diese Datierungen revidieren publizierte kambrische Entstehungsalter dieses Grundgebirges. Die Isotopensignatur ( $\epsilon Nd$  und  $^{87}Sr/^{86}Sr$ ) der ordovizischen Grundgebirgseinheiten, bestehend aus stark überprägten Amphiboliten und Gneissen, ist von der Signatur der sich im Norden anschließenden Tatriscen Einheit gut unterscheidbar. Die Blei-isotopenzusammensetzung dieser Gesteine ist stark krustal geprägt und überschneidet sich mit der der Tatriscen Einheit. Zusammen mit den  $T_{DM}^{Nd}$  Altern sind diese Einheiten vergleichbar mit prävariskischen Einheiten der Alpen. Somit kann das ordovizische Grundgebirge zu den peri-Gondwana Terranen gezählt werden, die an einem aktiven Kontinentalrand im Norden von Gondwana gebildet wurden.

In den Gesteinen der Veporischen Einheit wurde im Weiteren eine starke metamorphe Überprägung und intensiver felsischer Magmatismus karbonis-

chen Alters erkannt (320-350 Ma). Dieses Ereignis ist zeitgleich mit dem Magmatismus, welcher hauptsächlich in der sich im Norden anschließenden Tatrischen Einheit beobachtet wird. Dieser gehört der variskischen Orogenese an.

Intensive alpine Deformation und Metamorphose konnte in der südlichen Veporischen Einheit anhand der Einzelzircondatierungen und der Isotopendaten der ordovizischen Einheiten nachgewiesen werden.

Am Dlhá Dolina Granit in der Gemerischen Einheit können starke Fraktionierungs- und Auto-Metasomatose-Effekte beobachtet werden. Durch die magmatische Fraktionierung wird eine Anreicherung der SEE erzeugt, wogegen die Metasomatose die SEE stark verarmt. Es kommt sogar zur Ausbildung eines Tetraden Effektes im SEE Muster, welche den starken Einfluss von Fluiden während der spät-magmatischen Phase belegt. Gesamtgesteins Pb-Pb Daten beschränken das minimale Intrusionsalter dieses Granites auf 240 Ma. Dieses Alter ist in guter Übereinstimmung mit den Sr-Isotopendaten der magmatisch dominierten Gesteine, wohingegen die stark metasomatisch geprägten Gesteine ein zu radiogenes  $^{87}\text{Sr}/^{86}\text{Sr}_{ini}$  aufweisen.

Während dieser Arbeit wurde intensiv mit der Blei-Isotopenzusammensetzung von Gesamtgesteinsproben gearbeitet. Um die Auswertung dieser Daten optimieren zu können wurde ein Computerscript für das GPL Programm *Octave* erstellt. Die Hauptaufgabe dieses Scripts besteht darin, Regressionen für geochronologische Anwendungen gemäß York (1969) zu berechnen. Ausserdem können  $\mu$  und  $\kappa$ -Werte für diese Regressionen berechnet und eine Hauptkomponentenanalyse, welche hilfreich für den Vergleich von zwei Datensätzen ist, durchgeführt werden.

Am Ende der vorliegenden Arbeit wird die analytische Methode für einen Mikrowellen beschleunigten Säureaufschluss von granitoidem Material zur Bestimmung der Sr- und Nd-Isotopenzusammensetzung und der Element-

konzentrationen vorgestellt. Diese kombinierte Methode nutzt ein TIMS für die Sr und Nd Isotopenmessungen und eine Einzelkollektor-ICPMS zur Bestimmung der SEE, Rb und Sr Konzentrationen, welche mithilfe von relativen Sensitivitätsfaktoren gegenüber einem internen Standard quantifiziert werden. Diese Methode wird durch Messungen von internationalen Referenzmaterialien bewertet. Die Ergebnisse zeigen eine Reproduzierbarkeit von  $<10\%$  für die Elementkonzentrationen und von  $<5\%$  für Elementverhältnisse.

### 3 Abstract

This study presents geochronological and geochemical data for the evolution of the Central Western Carpathians. The basement units of the Veporic unit, one of three Alpine basement nappes, are mainly studied during the course of this work. In this unit the poly-metamorphic basement was studied to clarify its age and to classify it isotope geochemically. Additional to the Veporic basement units, a specialized S-type granite from in the Gemic unit, overlying the Veporic unit, is studied in detail to identify petrogenetic processes responsible for the magmatic evolution of this granite.

The zircon U-Pb dating for basement units in the Veporic Unit reveal Ordovician precursor age for the whole unit (440-470 Ma). These ages revise published Cambrian precursor ages. The isotopic signature, i.e.  $\epsilon Nd$  and  $^{87}Sr/^{86}Sr$ , for these Ordovician basement units is distinct from the signatures observed for magmatic rocks in the Tatric unit to the North. The WR-PbPb isotopic composition of these basement rocks reveals a strong crustal influence and overlap with the the WR-PbPb isotopic composition of the Tatric unit. Together with the  $T_{DM}^{Nd}$  ages, these are well comparable with pre-Variscan units described in the Alps. Thus belong the Ordovician basement units to the peri-Gondwana terranes, which were formed at the northern active continental margin of Gondwana.

Carboniferous metamorphism and felsic magmatism is also recognized in the Veporic unit (320-350 Ma). This event is contemporaneous with the magmatism observed mainly in the Tatric Unit to the North and belongs to the Variscan orogeny.

Intensive Alpine deformation and metamorphism can be observed in the single zircon U-Pb data and in the isotopic data for the Southern Veporic Unit.

The Dlhá Dolina granite in the Gemic unit shows effects of extensive fractionation and auto-metasomatism. Magmatic fractionation creates an

increase in the REE concentration in these rocks, whereas the metasomatic processes result in a depletion and in the generation of a Tetrad effect in the REE pattern, which shows the strong influence of fluids during the late magmatic phase. WR-Pb-Pb data constrain a minimum intrusion age of 240 Ma for the Dlhá Dolina pluton, which is in agreement with Sr isotopic data observed for the magmatic dominated samples, whereas the samples with a strong metasomatic influence have too radiogenic  $^{87}\text{Sr}/^{86}\text{Sr}_{ini}$ .

The Pb isotopic composition of whole rock (WR) samples was used extensively during this study. Therefore a script for the GPL software *Octave* was written to evaluate these datasets. The main purpose of this script is the calculation of York (1969) regression lines for geochronological applications. Additional  $\mu$  and  $\kappa$ -values can be calculated for regression lines and, useful for comparison of different datasets, principal component analyses can be calculated.

At the end of this work, the analytical technique for microwave-assisted acid digestion of granitoid material for isotopic and elemental analyses will be presented. This technique uses a TIMS for Sr and Nd isotopic measurements and a single collector ICPMS for determination of the REE, Rb and Sr concentrations quantified by relative sensitivity factors (RSF) relative to an internal standard. This method will be evaluated by measurements of international reference materials. These results in a precision of <10% for the elemental concentrations and of <5% for elemental ratios.



# Chapter 1

## Introduction

This work presents the results obtained during the course of the PhD study on “Isotope Geochemical and Geochronologic Studies of Basement Units in the Central Western Carpathians (Slovakia)” and consists of three main parts:

- Geochronological and isotopic studies of the pre-Variscan basement in the Veporic Unit (Chapter 2 and Chapter 3)
- Geochemical and isotopic constraints on the evolution and timing of a specialized S-type granitoid intrusion in the Gemeric Unit (Chapter 4)
- Presentation of a computer script for the evaluation of isotopic Pb data using the GPL program *Octave* (Chapter 5) and details on analytical techniques used for this work (Chapter 6)

These parts are presented as manuscripts ready for publication. Chapter 2 will be printed in a special issue for *Lithos* edited by BB. Chapter 5 is submitted to *Computers & Geosciences*. Chapter 3 and 4 are planned for submission to *Swiss Bulletin of Mineralogy and Petrology* and to *Geologica Carpathica*, respectively.

The first part is split in two chapters:

Chapter 2 presents the first single zircon U-Pb ages for the pre-Variscan basement in the Southern Veporic Unit. It results in an Ordovician precursor age for the felsic Muráň gneiss. This leads to a dichotomy with published Cambrian multi grain U-Pb ages from the Northern Veporic Unit (Putiš et al., 2001). In order to resolve this apparent age progression of basement units from North to South, single and multi grain zircon U-Pb ages are presented in Chapter 3 for the Northern Veporic Unit. These data fortify the Ordovician precursor ages presented in Chapter 2. Thus a re-interpretation of the data published by Putiš et al. (2001) is proposed. This results in a common Pre-Variscan evolution of the basement units from the Veporic Unit, no progression of the formation age can be observed.

Geochemical and Pb, Sr, and Nd isotopic data are presented in both Chapters to characterize the samples and to compare the Veporic Unit to other units of the Central Western Carpathians.

The second part (Chapter 4) concerns about the evolution of a granitoid plutonic complex sampled by drill cores in the Gemeric Unit (Dlhá Dolina valley). Geochemical, Pb and Sr isotopic data are presented to resolve the effects produced by magmatic fractionation and by metasomatic overprint. The isotopic data for this intrusion constrains a minimum intrusion age of 240 Ma, which is in good agreement with published data on similar intrusions in the Gemeric Unit.

Chapter 5 presents a new computer script for *Octave* to evaluate Pb isotopic data. This script was used for evaluation of all Pb isotopic datasets presented in this work. To show the capabilities of this script the Pb dataset of the Dlhá Dolina intrusion is presented and discussed in this Chapter in detail.

In Chapter 6 details about the analytical techniques used for this work are presented. This includes the microwave assisted digestion of granitoid samples for determination of REE, Rb and Sr concentrations using Relative Sensitivity Factors (RSF) and details on the column chemistry for the isotopic measurements.

# Chapter 2

The study presented in this chapter uses single zircon U-Pb geochronological data to identify the protolith age of the Muráñ Gneiss Complex and Pb, Sr, and Nd isotopic data to constrain the geodynamic context of this unit. The isotopic systematics of this complex are partially reset by intense Alpine deformation, nevertheless some conclusions on the sources can be drawn, as will be shown in the following.

A.S. Gaab performed all analyses presented in this chapter and prepared the manuscript. UP provided an additional sample used for U-Pb single zircon dating and introduced the author to the methods used for this work. MJ introduced to the regional geology and supported the author during field work. WT admitted the entry to the clean lab and to the mass spectrometer.

The manuscript presented in this chapter will be published in a special issue of *Lithos* edited by BB. Positive reviews by KS, GO, MK and BB were applied to the manuscript. Parts of this study were also presented by Gaab et al. (2003b) and Gaab et al. (2003c) on international meetings.

# Alpine reworking of Ordovician protoliths in the Western Carpathians: Geochronological and geochemical data on the Muráň Gneiss Complex, Slovakia

A.S., Gaab<sup>a,\*</sup> MJ<sup>b</sup> UP<sup>a</sup> WT<sup>a</sup>

<sup>a</sup>*Max-Planck-Institut für Chemie, Abt. Geochemie, P.O. Box 3060, 55020 Mainz, Germany*

<sup>b</sup>*Geological Institute; Slovak Academy of Sciences; P.O. Box 106; 84005 Bratislava 45; Slovak Republic*

---

## Abstract

Magmatic protoliths of Ordovician age have been identified in the metamorphic rocks of the Muráň Gneiss Complex, Veporic Unit (Central Western Carpathians). Vapor digestion single zircon U-Pb dating yields an intrusion age of  $464 \pm 35$  Ma (upper intercept) for the granite protolith. A lower intercept age of  $88 \pm 40$  Ma records amphibolite facies metamorphic overprint in the Cretaceous, during the Alpine orogeny. Geochemical and isotopic data suggest crustal origin of the orthogneiss.  $\epsilon Nd_{ini}$  are between -2.5 and -5 and corresponding  $T_{DM}^{Nd}$  range between 1.3-1.5 Ga (two-step approach).  $^{87}Sr/^{86}Sr_{ini}$  ratios vary between 0.7247 and 0.7120, and a steep REE pattern further constrains the crustal affinity of these rocks. Associated amphibolite bodies have  $\epsilon Nd_{ini}$  values of 6.5,  $^{87}Sr/^{86}Sr_{ini}$  ratio of 0.7017, and a flat REE pattern. They are interpreted as MORB derived metabasites. Pb, Sr and Nd isotopic variations observed for the Muráň Gneiss Complex can be explained by an intense Alpine metamorphism.

These basement rocks of the Central Western Carpathians are interpreted as Ordovician magmatic rocks intruded at an active Gondwana margin. They represent the eastern prolongation of Cambro-Ordovician units, which were part of the peri-Gondwana superterrane and accreted to Laurussia during Variscan orogeny. Alpine metamorphic overprint is the most dominant feature and no Variscan metamorphic overprint is recorded by the isotopic data of this unit.

*Key words:* Western Carpathians, Gondwana, Ordovician, basement, Alpine orogeny

---

\* Andreas S. Gaab

*Email address:* gaab@mpch-mainz.mpg.de (A.S., Gaab).

## 1 Introduction

Ordovician magmatic complexes are recognized in many areas of the Central European Variscides, like in the Bohemian Massif (e.g. Hegner and Kröner, 2000; Kröner et al., 2000), in SW Poland (Oliver et al., 1993) or in the Black Forest (Chen et al., 2000). Metabasic rocks and orthogneisses with Ordovician protolith ages occur also in the basement of the Alps, e.g. in the Austroalpine units (Miller and Thöni, 1995; Poller et al., 1997; Schaltegger et al., 1997). These magmatic rocks are interpreted as fragments of an active continental margin of Gondwana, and are grouped together under the name “Hun Superterrane” (Stampfli and Borel, 2002; von Raumer et al., 2002). Ordovician granitoids are considered to be the products of this active margin magmatism forming a longitudinal zone (von Raumer et al., 2002). Terranes were detached from Gondwana due to opening of back-arc oceans following the subduction of the mid-ocean ridge of a former peri-Gondwana ocean, the Proto-Tethys (Stampfli and Borel, 2002). These terranes collided with Laurussia during the Variscan orogeny.

The Central Western Carpathians represent a tectonic system that extends eastward from the Alps and its pre-Tertiary complexes comprise six principal Slovakocarpethian (analogous to the Austroalpine in the Alps), north-verging superunits (Fig. 1): the Tatric, Veporic and Gemeric thick-skinned basement/cover sheets, and the Fatric, Hronic and Silicic detachment cover-nappe systems (e.g. Plašienka et al., 1997). The Central Western Carpathians developed during several orogenic cycles.

During Mesozoic-Cenozoic times the Western Carpathians evolved as a complex subduction-collisional orogenic belt. They resulted from collision of European and Apulian continental domains located between two oceanic sutures - Meliatic in the south and Penninic in the north (e.g. Plašienka et al., 1997; Plašienka, 1997). High-pressure, blueschist facies metamorphism was related to subduction of Meliatic ocean in Jurassic time (Faryad, 1995). Subsequent continental collision during Cretaceous caused regional metamorphism. The most intense metamorphism affected the Veporic unit, especially its south-eastern parts at the contact to the Gemeric unit (Plašienka et al., 1999; Janák et al., 2001b).

Pre-Alpine tectonometamorphic evolution was generally related to the subduction-collisional processes during Variscan orogeny, resulting from convergence, accretion and amalgamation of crustal blocks derived from Gondwana with Laurussia (e.g. von Raumer and Neubauer, 1993; Plašienka et al., 1997). Variscan metamorphism and magmatism is well documented in all crystalline complexes of the Central Western Carpathians, especially in the Tatric unit with only weak Alpine recrystallization (e.g. Janák et al., 1996; Poller and Todt, 2000).

Pre-Variscan history of the Central Western Carpathians is not very well

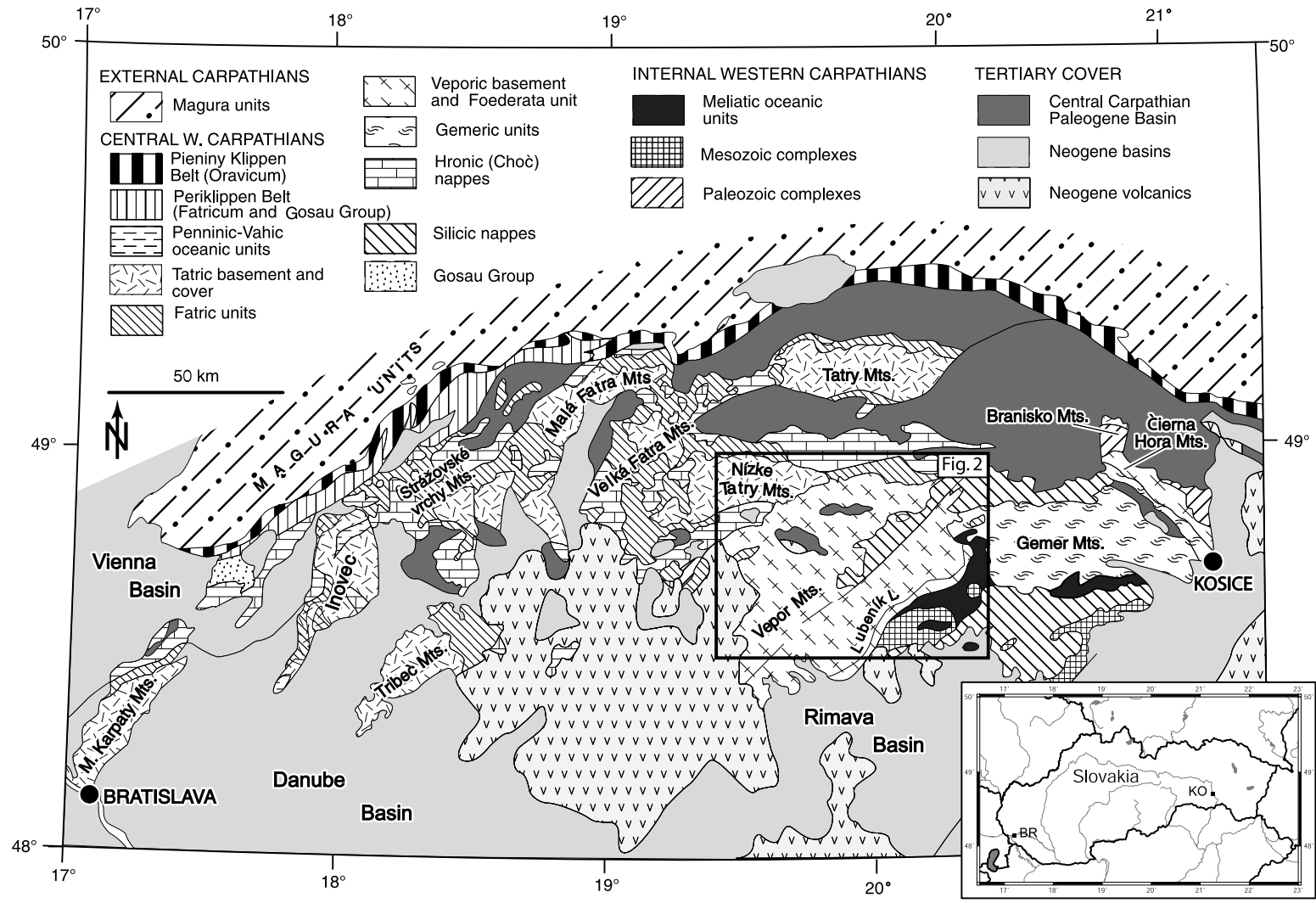


Fig. 1. Geologic Map of Slovakia modified after Plasienka (1997). Location of Fig. 2 indicated. Inlay depicts political boundaries of Slovakia with major rivers for overview.

known. Volcanic activity and sedimentation in the Early Paleozoic time occurred in the adjacent Gemic unit (e.g. Grecula, 1982) where both Variscan and Alpine metamorphic overprint reached mostly greenschist facies (e.g. Faryad, 1997), except minor Variscan amphibolite facies rocks (Bajaník and Hovorka, 1981).

Metagranitoids of Late Cambrian and Ordovician protolith age have been identified only recently in the polymetamorphosed complexes of the Veporic unit (Putiš et al., 2001; Janák et al., 2002; Gaab et al., 2003b). This study presents new geochemical and geochronological data on the protolith and the timing of metamorphic recrystallization of the Muráň Gneiss Complex in the Veporic Unit. It demonstrates the response of Ordovician magmatic rocks and their isotopic system to Alpine deformation and metamorphism under amphibolite facies conditions (ca. 600° C; 10kbar, Janák et al., 2001b). The aim of this study is to recognize the Pre-Variscan elements in the Central Western Carpathians, arguing that they possibly belonged to the former peri-Gondwana superterrane in the Early Palaeozoic time and to constrain the timing of metamorphism.

## 2 Geological Setting

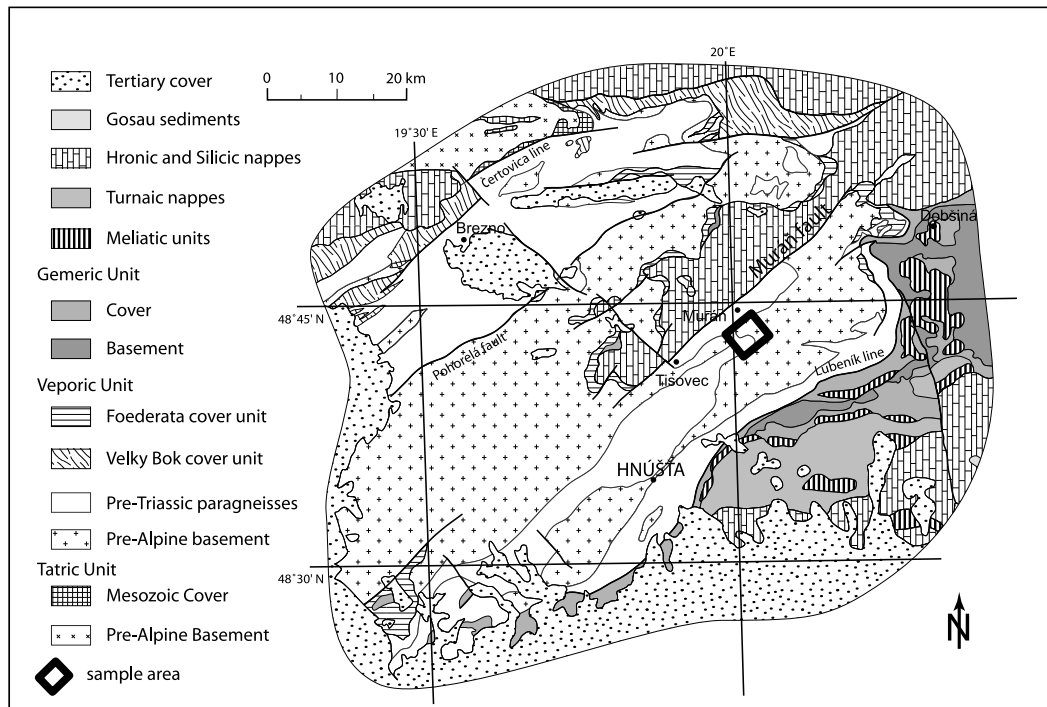


Fig. 2. Geologic Map of the Muráň area after Janák et al. (2001b). Study area is indicated by the rectangle. Note the location of the Muráň Gneiss Complex directly at the contact to the Gemic unit in the East.



The Muráň Gneiss Complex is part of the Veporic Unit. It is exposed east of the Muráň tectonic line and west of the Lubeník tectonic line, the transition from the Veporic Unit to the Gemeric Unit (Fig. 2).

The Veporic Unit consists of pre-Alpine basement complexes assembled during the Variscan orogeny (Bezák, 1991, and references therein) that are overlain by the Upper Palaeozoic-Triassic sedimentary cover (Fig. 2). Polymetamorphic pre-Alpine basement comprises granitoids, migmatites, gneisses and amphibolites, mostly mylonitized due to the Alpine overprint. Mica schists, phyllites and fine-grained gneisses of metavolcanosedimentary protolith are of uncertain age (Early to Late Palaeozoic). The tectonometamorphic history of this basement was interpreted as pre-Alpine with only greenschist facies Alpine overprint (Korikovský et al., 1989; Bezák, 1991; Kováčik et al., 1996). In contrast, Méres and Hovorka (1991) and more recently Plašienka et al. (1999), Lupták et al. (2000) and Janák et al. (2001b) emphasized that Alpine overprint reached amphibolite facies conditions.

In the central and north-eastern part of the Veporic Unit locally preserved para-autochthonous cover include Upper Permian sandstones and conglomerates, Scythian quartzites and slates, and Middle-Upper Triassic carbonates and shales (Foederata unit). The south-eastern rim of the Veporic Unit is composed of Carboniferous, Permian and Scythian clastic sequences partly forming an allochthonous unit overlying the Foederata cover unit to the north-west. All these Veporic cover units were affected by Alpine metamorphism of low to medium grade (Lupták et al., 2003, and references therein). Its metamorphic grade increases from anchi- and epizone (350-400° C; 4-5 kbar) in the Mesozoic cover (Lupták et al., 2003) to amphibolite facies (500-620° C; 7-10 kbar) in the basement (Janák et al., 2001b). This regional metamorphism with a geothermal gradient of ca. 15° C/km corresponds to a medium to high-pressure type. This was generated by crustal thickening due to an overburden formed by the Gemeric basement sheet and the Meliatic accretionary complex during the Cretaceous continental collision.

Lithology and metamorphism of Muráň Gneiss Complex were investigated by several authors. Felsic gneisses, designated as "granite-gneiss" or "orthogneiss", were attributed to either granitoid (Klinec, 1976) or rhyolitic protolith (Hovorka et al., 1987), or both (Kováčik et al., 2001). Amphibolite layers were interpreted as product of basaltic, concomitant volcanism (Hovorka et al., 1987). Based on whole-rock Sr isotopic studies, Kováčik et al. (2001) proposed that the protolith of "orthogneisses" was crustal, about 420 Ma old. Metamorphism of the Muráň Gneiss Complex rocks was attributed largely to Variscan orogeny. According to Hovorka et al. (1987), metamorphic conditions reached only greenschist to lower amphibolite facies, whereas Kováčik et al. (2001) estimated partial melting conditions for orthogneisses during the Variscan orogeny. Janák et al. (2001b) calculated metamorphic conditions of 620° C and 9-10 kbar for overlying meta-sedimentary mica schists and sug-

gested this metamorphism as Alpine, reaching the highest metamorphic grade (staurolite + biotite + kyanite) within the Veporic unit. Published geochronological data for these micaschists provide Cretaceous metamorphic ages. The data include in-situ  $^{40}\text{Ar} - ^{39}\text{Ar}$  UV laser dating of white mica (72 - 77 Ma, Janák et al., 2001b), electron microprobe dating of metamorphic monazite ( $92 \pm 16$  Ma, Janák et al., 2001a) and Sm-Nd dating of garnet ( $109 \pm 6$  Ma, Lupták et al., 2004).

The deformational structures in the area are dominated by a flat or moderately NE-dipping metamorphic/mylonitic foliation ( $S_1$ ). The foliation planes bear a distinct stretching lineation ( $L_1$ ) plunging generally to the east. These structures were formed during the first Alpine deformation ( $AD_1$ ) stage within a large-scale sub-horizontal ductile shear zone. This shear zone is interpreted as a low-angle detachment fault zone that parallels the basement/cover interface and lithological boundaries within the Veporic cover, as well as the original Veporic/Gemic overthrust contact (Janák et al., 2001b, and references therein).

### 3 Sample Description

Three major rock types occur in the Muráň Gneiss Complex: felsic gneiss, amphibolite (both generalized as pre-Alpine basement in Fig. 2) and mica schist (generalized as pre-Triassic paragneiss in Fig. 2).

The most prominent lithology is a coarse grained felsic gneiss with K-feldspar, albite, quartz, biotite, phengitic white mica and minor garnet. This gneiss is intercalated with amphibolite bodies, several tens of meters in thickness. Amphibolite is fine- to medium-grained with tschermakitic hornblende, epidote, garnet, plagioclase and quartz as major minerals. At the contact between the felsic gneiss and the amphibolite, a strongly deformed, banded gneiss with variable amount of mafic and felsic components is formed. Some centimeter thick layers of amphibolite are locally preserved in this banded gneiss. This gneiss complex is overlain by a medium grained kyanite- and staurolite-bearing mica schist (for detailed description of this unit see Kováčik et al., 1996; Janák et al., 2001b).

Several samples were collected in the area between Muráň and Tisovec (Fig. 2) to cover the whole compositional range of the gneisses. The sampled area is approximately 25 km<sup>2</sup> and is situated around the coordinate point WGS-84 48°42' N; 20°01' E. For U-Pb zircon dating, sample UP1115 was collected from a homogeneous felsic outcrop. For geochemistry, samples were taken from the amphibolite (02GA21), the felsic gneiss (02GA19, 03GA06, and 03GA11) and the banded gneiss (03GA07 to 03GA10, 02GA18 sampled at Muránska Lehota: 48°43'46" N; 20°02'45" E). Sample 03GA08 is a 10cm wide amphibolite layer

in the banded gneiss.

For Pb-Pb whole rock analyses, additional samples of the banded gneiss (UP1112; UP1115; UP1125; 02GA20), together with samples of the overlying mica schists (UP1111; UP1113; 02GA22), were analyzed in order to characterize the whole range of Pb isotopic compositions.

#### 4 Analytical Methods

Major and trace element analyses were measured by XRF at the University Mainz using powder and glass tablets. For determination of REE, the samples were dissolved using a three step microwave assisted  $HF - HNO_3$ -digestion (Totland et al., 1995) of approx. 100mg powdered sample (CEM MARS5, XP-1500, temperature controlled; step one:  $HF - HNO_3$ , 40min, max.  $200^\circ C$ ; step two:  $HF - HNO_3$ , 25min, max.  $220^\circ C$ ; step three:  $HCl - HNO_3$ , 30min, max.  $120^\circ C$ ).

REE, Rb, Sr and Pb concentrations were analyzed on a Finnigan Element2 single collector ICP-MS at the Max-Planck-Institut für Chemie, Mainz. Quantification was achieved by external calibration with  $In$  as internal standard. Machine drift was corrected using  $^{115}In - ^{187}Re$  (Cheatham et al., 1993). Accuracy for elemental concentrations is better than 15%. For elemental ratios the accuracy is better than 5%, because these are less sensitive to drift and matrix effects.

For Sr and Nd isotopic analyses, the samples were dissolved using microwave-assisted digestion of 50-150 mg whole-rock powder (as previously described). After dissolution, column chemistry in a clean lab was applied following the method of White and Patchett (1984). Isotopic ratios were measured on a multi-collector TIMS (Finnigan MAT 261) in static mode.

Pb isotopes were measured on  $HF - HNO_3$ ,  $HBr$  leachates of fresh rock splits. After extraction in 0.5 mol  $HBr$  and resin column chemistry, common Pb was measured using static multi-collection on a MAT 261 TIMS (Arndt and Todt, 1994).

Single zircon vapor digestion analyses were performed on  $HF - HNO_3$  and  $HCl$  dissolved single zircons without column chemistry. A  $^{205}Pb$  and  $^{233}U$  mixed spike was added prior to dissolution (Wendt and Todt, 1991; Poller et al., 2000). After correction for fractionation, the blank, common lead, and spike contribution were subtracted. The ISOPLOT macro was used to evaluate the U-Pb zircon data (Ludwig, 2001). In addition to the dated ones, zircons from the same sample were imaged with an cathodo-luminescence detector (CL) on a Hitachi 5450 at the MPI Mainz from polished zircon mounts.

CHAPTER 2: ALPINE REWORKING OF THE ORDOVICIAN MURÁŇ GNEISS

	03GA06 felsic	03GA11 felsic	02GA19 felsic	02GA18 banded	03GA10 banded	03GA09 banded	03GA07 banded	03GA08 mafic	02GA21 amph
<i>SiO<sub>2</sub></i>	76.9	76.0	75.9	72.8	71.0	68.6	67.6	56.0	47.0
<i>TiO<sub>2</sub></i>	0.05	0.04	0.03	0.18	0.35	0.24	0.25	1.72	1.87
<i>Al<sub>2</sub>O<sub>3</sub></i>	12.81	13.6	12.47	13.73	14.72	14.34	14.5	15.16	14.07
<i>Fe<sub>2</sub>O<sub>3</sub></i>	0.83	0.86	1.00	2.91	2.49	4.81	4.98	9.8	13.11
<i>MnO</i>	0.01	0.02	0.02	0.05	0.03	0.07	0.07	0.17	0.2
<i>MgO</i>	0.08	0.05	0.03	0.66	1.01	2.19	2.35	4.81	6.38
<i>CaO</i>	0.24	0.67	0.54	2.72	2.29	4.47	4.47	7.59	11.34
<i>Na<sub>2</sub>O</i>	4.16	5.61	3.78	3.73	4.12	4.03	4.06	3.42	3.46
<i>K<sub>2</sub>O</i>	3.94	2.39	4.4	2.16	1.66	0.54	0.68	0.32	0.44
<i>P<sub>2</sub>O<sub>5</sub></i>	0.01	0.01	0.01	0.03	0.05	0.04	0.04	0.2	0.15
<i>Sum</i>	99.5	99.6	98.2	99.0	99.2	100.0	99.8	99.9	99.4
<i>Sc</i>	2	1	3	9	7	19	21	30	48
<i>V</i>	3	4	4	38	44	97	108	238	337
<i>Cr</i>	2	3	8	13	18	48	50	112	136
<i>Co</i>	64	73	86	59	74	60	63	52	58
<i>Ni</i>	<i>nd</i>	2	4	3	8	8	9	37	67
<i>Cu</i>	7	3	3	4	2	5	4	36	24
<i>Zn</i>	2	1	3	27	31	26	31	86	100
<i>Ga</i>	15	16	17	17	17	15	15	20	21
<i>Y</i>	23	53	47	17	17	13	14	53	35
<i>Zr</i>	79	83	111	92	165	86	83	238	119
<i>Nb</i>	9	8	8	7	8	5	4	6	7
<i>Ba</i>	605	183	291	538	463	167	208	18	<i>nd</i>
<i>Pb</i>	19	15	14	11	16	4	7	7	6
<i>Th</i>	13.4	17.5	15.8	6.4	31	5.6	5.1	4.4	<i>n-d</i>
<i>U</i>	3.7	6.7	5.4	3	4.1	2.2	0.4	1.4	0.3
<i>Rb</i>	59	39	93	74	33	7	10	2	36
<i>Sr</i>	40	49	22	131	262	190	227	127	262

	03GA06	03GA11	02GA19	02GA18	03GA10	03GA09	03GA07	03GA08	02GA21
<i>La</i>	4.5	6	9.9	15	35	10	9.8	12	4.9
<i>Ce</i>	<i>nd</i>	<i>nd</i>	28	31	71	19	18	29	14
<i>Pr</i>	1.2	1.8	2.9	3.2	7.9	1.9	1.9	3.8	2.1
<i>Nd</i>	4.4	6.7	11	11	29	6	6.5	16	11
<i>Sm</i>	1.1	2	3	2.1	5.3	1.2	1.3	4.2	3.4
<i>Eu</i>	0.04	0.069	0.1	0.4	0.92	0.29	0.3	1.1	1.5
<i>Gd</i>	1.1	2.3	3	1.9	4.1	1.2	1.2	5	4.5
<i>Tb</i>	0.23	0.48	0.5	0.3	0.42	0.16	0.18	0.81	0.7
<i>Dy</i>	1.7	3.9	4.2	1.9	2.1	1.1	1.2	5.2	4.9
<i>Ho</i>	0.42	0.96	1	0.4	0.31	0.24	0.26	1.1	1
<i>Er</i>	1.6	3.5	3.3	1.2	0.67	0.77	0.8	3.3	2.9
<i>Tm</i>	0.3	0.66	0.5	0.2	0.076	0.12	0.13	0.5	0.5
<i>Yb</i>	2	4.5	4.5	1.5	0.43	0.79	0.9	3	3.2
<i>Lu</i>	0.33	0.67	0.6	0.2	0.069	0.13	0.14	0.45	0.4
<i>Eu*<sup>a</sup></i>	0.11	0.097	0.10	0.61	0.6	0.75	0.74	0.74	1.20
<i>Sm/Nd</i>	0.25	0.31	0.27	0.19	0.18	0.20	0.20	0.26	0.31

$$^a Eu^* = Eu_N / \sqrt{Sm_N * Gd_N}$$

Table 1. Whole rock geochemical data. Samples sorted by *SiO<sub>2</sub>* content. Major (given in *wt%* as oxides) and trace elements (given in *ppm*) measured with XRF. REE, Rb and Sr measured with ICPMS. *nd* for not determined

grain no.	Measured atomic ratios <sup>a</sup>						Corrected ages (Ma) <sup>b</sup>						
	$\frac{U_{tot}}{Pb_{rad}}$	$\frac{^{206}Pb}{^{204}Pb}$	$2\sigma_m^c$	$\frac{^{207}Pb}{^{206}Pb}$	$2\sigma_m^c$	$\frac{^{208}Pb}{^{206}Pb}$	$2\sigma_m^c$	$\frac{^{206}Pb}{^{238}U}$	$2\sigma_m$	$\frac{^{207}Pb}{^{235}U}$	$2\sigma_m$	$\frac{^{207}Pb}{^{206}Pb}$	$2\sigma_m$
I	12.44	985	59	0.07003	26	0.11562	54	444	5	442	12	430	60
E	13.09	267	6	0.11029	33	0.19314	59	431	4	434	14	453	84
B	14.72	751	11	0.07535	20	0.10348	62	385	2	396	5	456	25
H	16.20	2961	149	0.05930	8	0.59314	12	240	1	254	2	388	15
A	17.12	548	15	0.08223	21	0.12246	40	332	3	347	7	443	47
D	17.17	359	3	0.09567	30	0.15241	65	332	2	344	6	421	42

<sup>a</sup> corrected for fractionation

<sup>b</sup> corrected for blank, spike and common lead

<sup>c</sup>  $2\sigma_m$  refer to the  $2\sigma$  deviation of the weighted mean of 2-6 blocks (20-60 ratios). Last significant digits given.

Table 2. Vapor digestion single zircon U-Pb data for the felsic gneiss, sample UP1115.

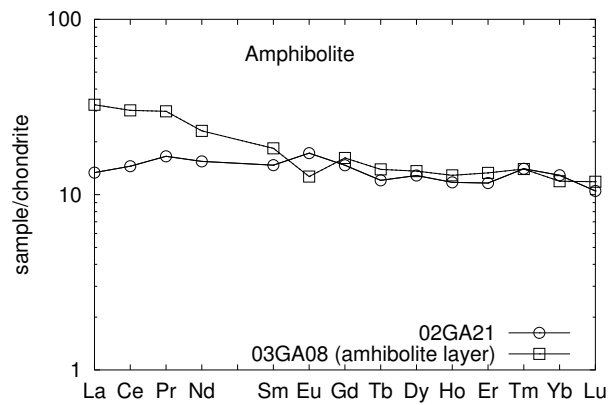
## 5 Geochemistry

According to major element classification, amphibolites resemble a typical basaltic composition (total alkali content: 3.9 wt%,  $SiO_2$ : 46.99 wt%, Table 1) and according to the AFM-classification have a tholeiitic character. The amphibolite has a Zr/Y ratio of 3.4 and a Zr content of 119 ppm, which is characteristic for MORB (Pearce and Norry, 1979).

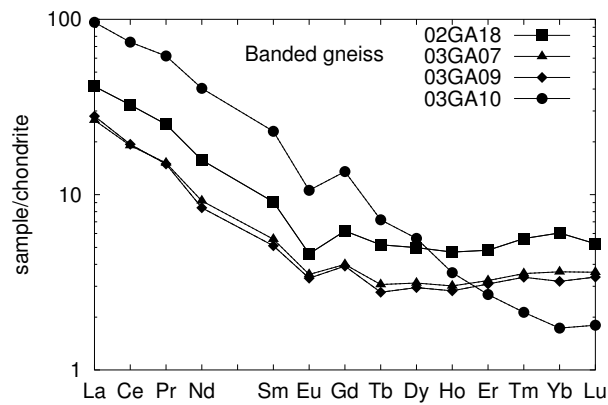
Banded as well as felsic gneiss with a  $SiO_2$  content of 67.6 to 75.9 wt% and a total alkali content of 4.8 to 8.2 wt% are sub-alkaline granitoid rocks (McDonalds, 1986). The felsic gneiss has very low Ca, Mg and Fe concentrations. These concentrations increase for the banded gneiss with decreasing  $SiO_2$  drastically towards the contents measured in the amphibolite. Such a linear correlation with  $SiO_2$  can be observed for all samples and most elements (Table 1). This indicates that banded gneisses are binary mixing products of the felsic gneiss and the amphibolite.

The REE diagrams display three different pattern. The amphibolite depicts a flat REE pattern at ten times chondritic values (Fig. 3(a)). In contrast, the most felsic samples (Fig. 3(c)) have slightly U-shaped pattern with a pronounced negative Eu-anomaly ( $Eu^* \approx 0.1$ ), whereas the banded gneiss shows steeper pattern with small negative Eu-anomalies ( $Eu^*$ : 0.60 to 0.75, Table 1, Fig. 3(b)).

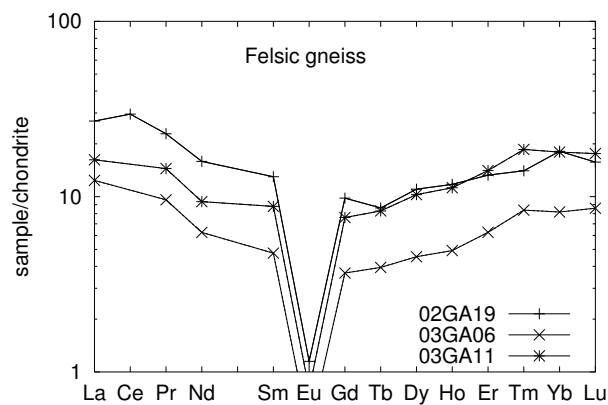
Sample 03GA08, a 10cm wide amphibolite layer surrounded by more felsic banded gneiss, has similar HREE concentrations as the amphibolite (02GA21), but displays a small negative Eu-anomaly and a slightly enriched pattern for LREE (Fig. 3(a)). This indicates, that small bodies of amphibolite are influenced by the felsic members.



(a)



(b)



(c)

Fig. 3. Chondrite normalized REE-pattern (CI chondrite after Taylor and McLennan (1985)).

## 6 U-Pb dating

Single zircon U-Pb vapor digestion analyses were performed on zircons from the felsic gneiss UP1115. Measured  $^{206}\text{Pb}/^{204}\text{Pb}$  ratios range between 250 and 3000 (Table 2). Common lead correction was applied with an isotopic composition in agreement with the WR-Pb-Pb data ( $^{206}\text{Pb}/^{204}\text{Pb}$ : 18.413;  $^{207}\text{Pb}/^{204}\text{Pb}$ : 15.699;  $^{208}\text{Pb}/^{204}\text{Pb}$ : 38.502; Fig. 6(a)). Six data points define a discordia line with an upper intercept of  $464\pm 35$  Ma and a lower intercept of  $88\pm 40$  Ma (MSWD: 0.36). Two of these points are nearly concordant with  $^{206}\text{Pb}/^{238}\text{U}$  ages of  $444\pm 5$  Ma and  $431\pm 4$  Ma. Four zircons are clearly discordant with  $^{206}\text{Pb}/^{238}\text{U}$  ages younger than 385 Ma (Fig. 4).

Many zircons from the sample UP1115 have prismatic habit and show oscillatory zoning in CL-imaging (upper two zircons in Fig. 5). They have clearly a magmatic origin, indicating that the upper intercept age of  $464\pm 35$  Ma reflects the intrusion age of the granite protolith of the gneiss. Some zircon grains (e.g. upper and middle left zircon in Fig. 5) show a possible inherited core on CL-images. Such cores were not present in the crystals analyzed for U-Pb as no pre-Ordovician  $^{207}\text{Pb}/^{206}\text{Pb}$  ages were obtained. Most zircons of sample UP1115 (e.g. two lowermost grains in Fig. 5) show a nebulous pattern in their CL-image and the magmatic zoning is overprinted. This suggest lead loss as mechanism, which produced the discordancy during Alpine metamorphism. The  $U_{\text{tot}}/Pb_{\text{rad}}$  ratio in the zircons increases from the concordant zircons (12.44 and 13.09) to higher values for the more discordant ones (14.72

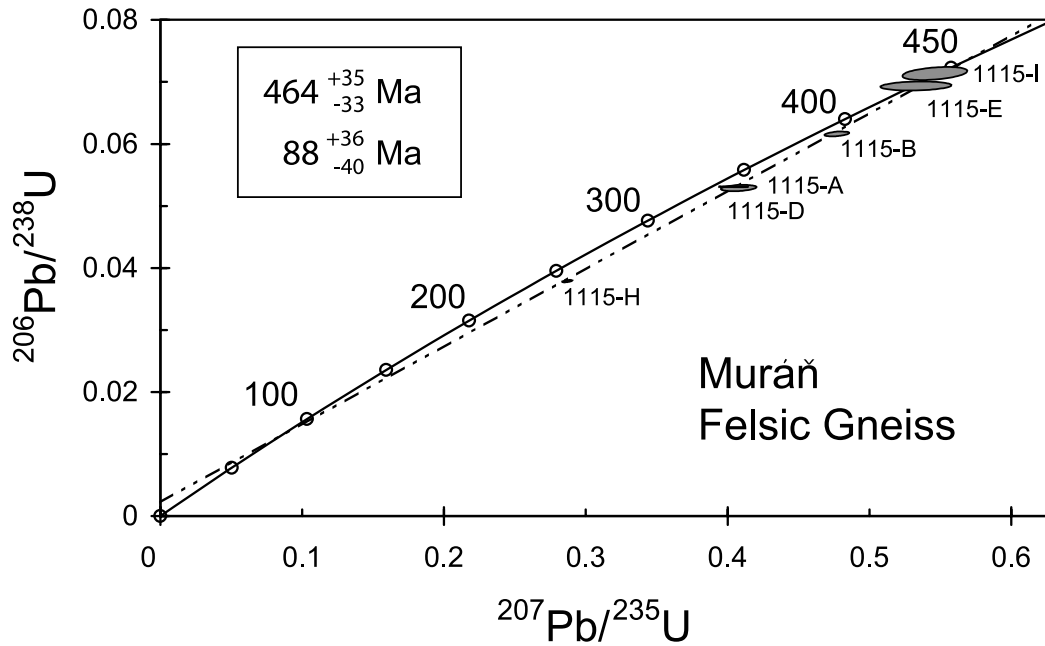


Fig. 4. Concordia diagram for single zircon vapor digestion analyses of the felsic gneiss UP1115.

to 17.17, Table 2), which is coherent with this interpretation.

## 7 Isotope Geochemistry

Mica schists form a narrow array in the  $^{206}\text{Pb}/^{204}\text{Pb}$  vs.  $^{207}\text{Pb}/^{204}\text{Pb}$  diagram (18.4-18.6 and 15.6-15.7, respectively). The  $^{208}\text{Pb}/^{204}\text{Pb}$  ratios are between 39.0 and 39.2. This coincides well with the evolution of upper crustal lead according to Zartman and Haines (1988) and resembles an isotopic composition, which evolved till 400 to 500 Ma in a crustal environment (Fig. 6).

$^{206}\text{Pb}/^{204}\text{Pb}$  and  $^{207}\text{Pb}/^{204}\text{Pb}$  ratios for amphibolites are between 18.3-18.4 and 15.6-15.7, respectively. These ratios are distinct from those reported for typical MORB (17.7-18.7 and 15.43-15.53, respectively, Sun, 1980). The evolution line for the upper mantle plots at less radiogenic ratios out of the range of Fig. 6 (18.2-18.3 and 15.46-15.47 for lead evolved till 100 to 200 Ma, Zartman and Haines, 1988). Also the  $^{208}\text{Pb}/^{204}\text{Pb}$  ratios are slightly higher than the reported values for MORB (38.3-38.6 vs. 37.6-38.2, Sun, 1980). The lead isotopic composition coincides well with the Stacey and Kramers (1975) model composition at 100 to 200 Ma. This can also be interpreted as a mixture of

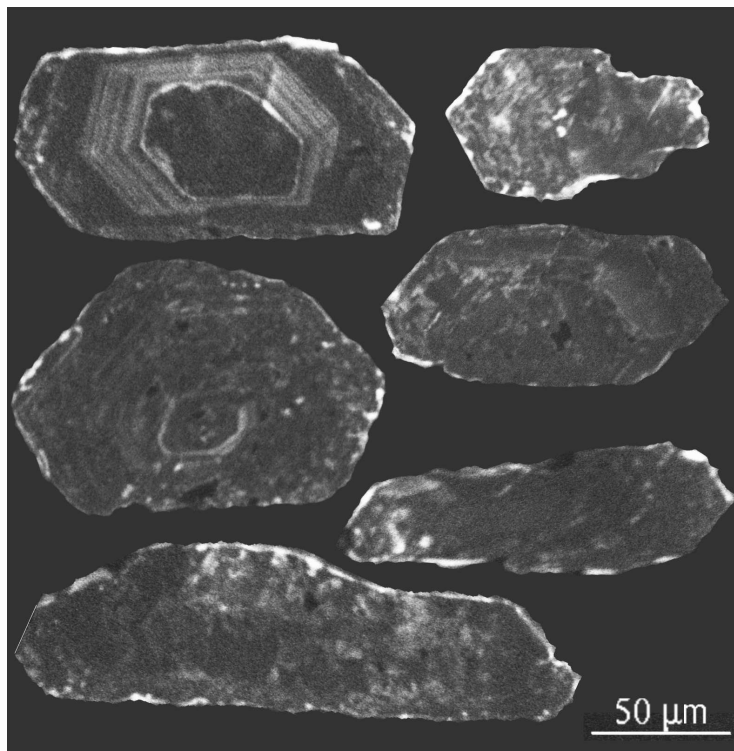


Fig. 5. Representative cathodoluminescence images for zircons of sample UP1115 in a polished mount. Inherited cores and magmatic zoning present in some zircons. Most zircons experienced metamictisation and show nebulous CL.



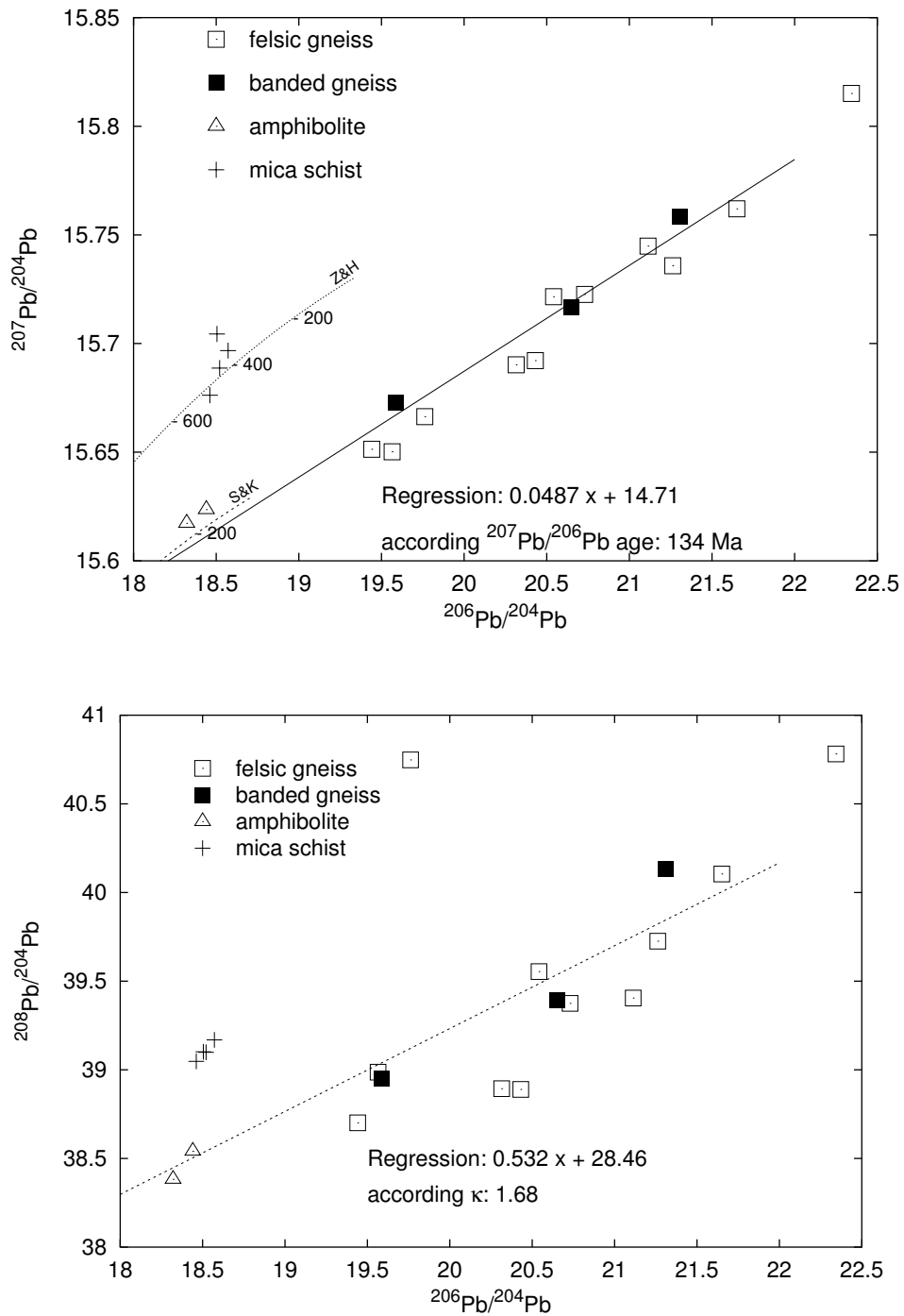


Fig. 6.  $^{207}\text{Pb}/^{204}\text{Pb}$  vs.  $^{206}\text{Pb}/^{204}\text{Pb}$  and  $^{208}\text{Pb}/^{204}\text{Pb}$  vs.  $^{206}\text{Pb}/^{204}\text{Pb}$ -diagram. Felsic gneiss and amphibolite samples form a linear array in both diagrams. Mica schists plot distinct in a small array. Stacey and Kramers (1975, lower line, (S&K)) and Upper Crustal (after Zartman and Haines, 1988, upper line, (Z&H)) evolution line drawn with labels in Ma.

	$\frac{^{206}\text{Pb}}{^{204}\text{Pb}}$	$\frac{^{207}\text{Pb}}{^{204}\text{Pb}}$	$\frac{^{208}\text{Pb}}{^{204}\text{Pb}}$
Felsic and banded gneiss			
UP1112-1	20·315	15·690	38·894
UP1112-2	20·431	15·692	38·889
UP1115-1	21·308	15·758	40·132
UP1115-2	20·651	15·717	39·391
UP1124-1	22·343	15·815	40·782
UP1124-2	21·651	15·762	40·104
UP1125-1	21·262	15·736	39·725
UP1125-2	20·729	15·723	39·375
02GA18A	19·565	15·650	38·987
02GA18B	19·762	15·666	40·748
02GA18D	19·441	15·651	38·701
02GA19A	19·585	15·673	38·950
02GA20A	21·113	15·745	39·405
02GA20B	20·542	15·722	39·554
Amphibolite			
02GA21A	18·321	15·617	38·383
02GA21B	18·440	15·624	38·540
Mica schist			
UP1111	18·521	15·689	39·099
UP1113-1	18·462	15·676	39·048
UP1113-2	18·505	15·704	39·102
02GA22	18·572	15·697	39·169

Table 3. Pb-Pb-WR data for samples of the Muráň area. Reproducibility is generally better than 500 ppm.

upper crustal lead with a more primitive lead sampled from the upper mantle (Fig. 6).

Gneisses with high felsic component display a large range of lead isotopic compositions, but align in a linear array converging at lower ratios with array of the amphibolites (Table 3, Fig. 6). All gneisses together depict a good linear correlation with a correlation coefficient of  $r=0.981$ . The mafic samples plot at lower ratios, whereas the more felsic samples (according to their higher U content, Table 1) at more radiogenic  $^{206}\text{Pb}/^{204}\text{Pb}$  and  $^{207}\text{Pb}/^{204}\text{Pb}$  ratios. The slope of this reference line corresponds to an  $^{207}\text{Pb}/^{206}\text{Pb}$  age of 134 Ma. The regression line is calculated according to York (1969).

A similar good linear correlation ( $r=0.905$ , one outlier) is present on the  $^{206}\text{Pb}/^{204}\text{Pb}$  vs.  $^{208}\text{Pb}/^{204}\text{Pb}$  diagram (Fig. 6); the slope of the regression corresponds to a  $\kappa_{(today)}$ -ratio of 1.48 (calculated for 134 Ma).

$^{87}\text{Sr}/^{86}\text{Sr}$  and  $^{143}\text{Nd}/^{144}\text{Nd}$  ratios show a large range for the investigated sam-

sample	$\frac{^{87}Sr}{^{86}Sr}{}^a$	$2\sigma$	$\frac{^{87}Rb}{^{86}Sr}{}^b$	$\frac{^{87}Sr}{^{86}Sr}{}^{464} Ma$	$\frac{^{143}Nd}{^{144}Nd}{}^a$	$2\sigma$	$\frac{^{147}Sm}{^{144}Nd}{}^b$	$\epsilon Nd_0 Ma$	$\epsilon Nd_{464} Ma$	$T_{DM}^{Nd} [Ga]^c$
03GA06	0.739353	8	4.13	0.712038	0.512170	13	0.16	-9.1	-5.0 <sup>d</sup>	1.4 <sup>d</sup>
03GA11	0.735952	8	2.25	0.721048	0.512249	11	0.19	-7.6	-3.9 <sup>d</sup>	1.5 <sup>d</sup>
02GA19	0.802601	10	11.78	0.724741	0.512301	6	0.17	-6.6	-2.6 <sup>d</sup>	1.3 <sup>d</sup>
02GA18	0.715566	11	1.60	0.704998	0.512329	5	0.12	-6.0	-1.5	1.3
03GA10	0.710557	6	0.36	0.708150	0.512312	7	0.12	-6.4	-1.6	1.2
03GA09	0.707833	8	0.11	0.707077	0.512266	9	0.12	-7.3	-3.0	1.4
03GA07	0.707990	8	0.13	0.707126	0.512263	18	0.12	-7.3	-3.0	1.4
03GA08	0.706629	6	0.04	0.706366	0.512733	6	0.16	1.9	3.9	1.1
02GA21	0.705956	53	0.65	0.701662	0.512971	10	0.20	6.5	6.5	1.2

<sup>a</sup> measured on TIMS *MAT261* multicollection. Errors on the last digits are given as  $2\sigma$  deviation of the weighted mean (6-25 blocks)

<sup>b</sup> measured on single collector ICP-MS *Element2* (Table 1)

<sup>c</sup> calculated using the depleted mantle model after Liew and Hofmann (1988)

<sup>d</sup> two step model at 88 Ma ( $^{147}Sm/^{144}Nd = 0.12$ ) according Liew and Hofmann (1988)

Table 4.  $^{87}Sr/^{86}Sr$ - and  $^{143}Nd/^{144}Nd$ -whole rock isotopic compositions. Isotopic compositions are also recalculated to the Alpine overprint. For Nd values are reported as  $\epsilon Nd$  and the  $T_{DM}^{Nd}$  are given.

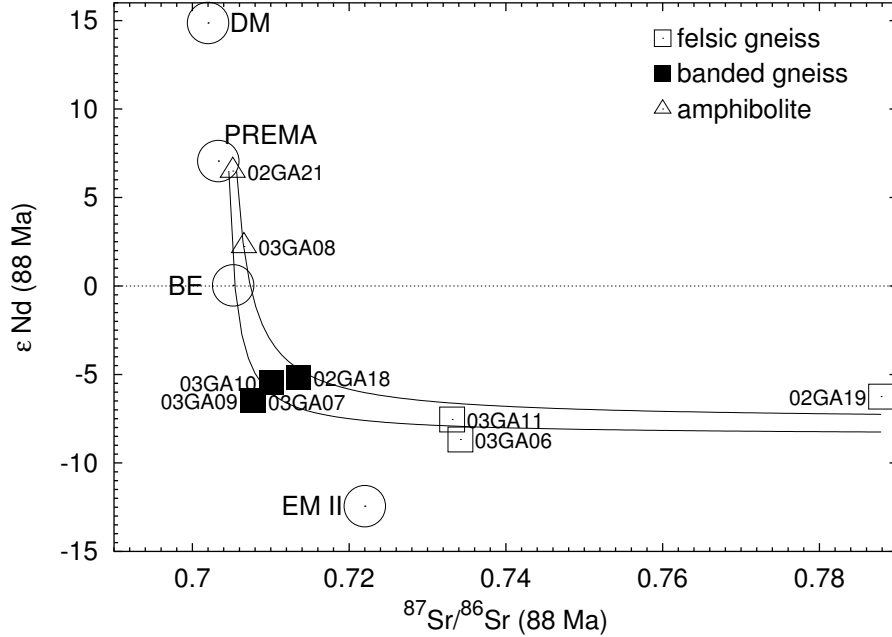


Fig. 7. Sr-Nd isotopic compositions recalculated to 88 Ma. Solid lines represent binary mixing (Langmuir et al., 1978) between end members similar to the most mafic and the most felsic sample (curvature = 0.012 and 0.024). Reservoirs plotted after Zindler and Hart (1986): BE - bulk earth; DM - depleted mantle; EM II - enriched mantle II; PREMA - prevalent mantle.

ples, which correlates with the geochemistry of the gneiss suite. The most radiogenic felsic gneisses has  $^{87}\text{Sr}/^{86}\text{Sr}_{meas}$  values of  $0.802601 \pm 10$ . The  $\epsilon Nd_{meas}$  values of -6.6 are low (Table 4).  $^{87}\text{Sr}/^{86}\text{Sr}_{ini}$  values for all felsic gneisses range between 0.725 and 0.712 and  $\epsilon Nd_{ini}$  between -5.0 and -2.6, which is typical for crustal dominated rocks. The banded gneisses have lower  $^{87}\text{Sr}/^{86}\text{Sr}_{ini}$  values at 0.704-0.708 and  $\epsilon Nd_{ini}$  values of -3 to 1.5. Finally, amphibolites have unradiogenic ratios for  $^{87}\text{Sr}/^{86}\text{Sr}_{ini}$  of 0.702 and for  $\epsilon Nd_{ini}$  of 6.5. This is similar to the prevalent MORB composition (Zindler and Hart (1986), Fig. 7).

Banded gneisses have  $^{87}\text{Sr}/^{86}\text{Sr}$  ratios close to amphibolite and  $^{143}\text{Nd}/^{144}\text{Nd}$  ratios close to felsic gneiss. When recalculating the isotopic composition to the Alpine metamorphic event at 88 Ma, using the Rb/Sr and Sm/Nd ratios measured with ICP-MS, the mixing correlation between the three units can be approved. In Fig. 7 mixing hyperbola (after Langmuir et al., 1978) are displayed using a felsic and a mafic end-member with elemental concentrations and isotopic compositions comparable to those observed for the samples. This mixing array models the isotopic range observed for the banded gneisses well. If the isotopic composition is recalculated to initial values or to a Variscan event around 320 Ma the mixing array does not model the isotopic range as good.

$T_{DM}^{Nd}$  model ages are slightly younger for amphibolites than for felsic gneisses.

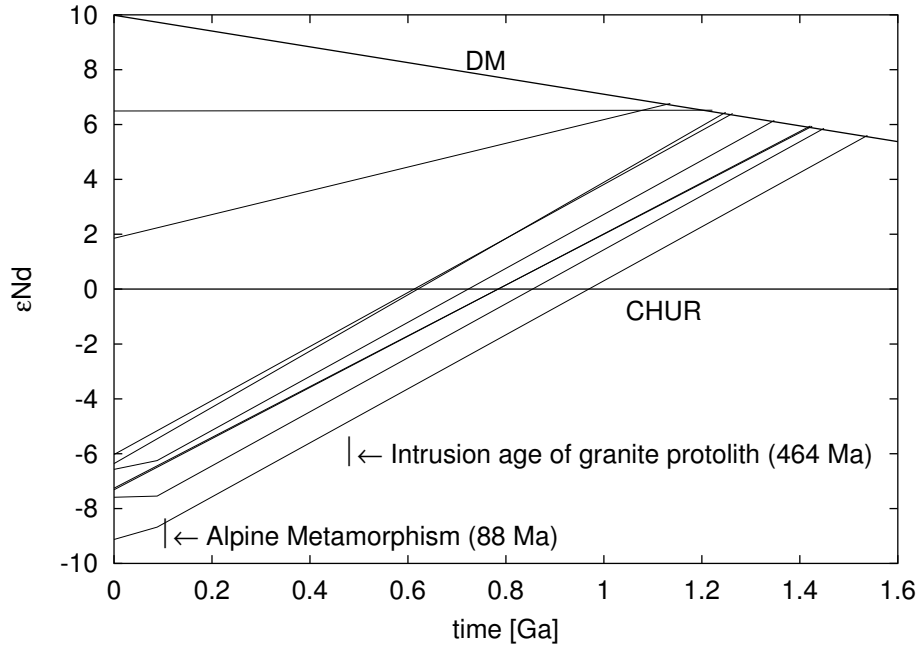


Fig. 8.  $\epsilon Nd$  isotopic evolution with time. Depleted mantle model and two-step calculations after Liew and Hofmann (1988).

They increase from 1.1 Ga for the mafic samples to 1.5 Ga for the felsic samples with a two step approach applied for the most evolved samples (see Table 4, Fig. 8). The two-step evolution is calculated using the Alpine overprint at 88 Ma recorded by the U-Pb zircon discordia according to the approach by Liew and Hofmann (1988). The  $T_{DM}^{Nd}$  of the banded gneisses are probably disturbed by the deformation in Alpine time, which results in too young  $T_{DM}^{Nd}$  model ages. Thus reasonable model ages for the initial granitoid range between 1.3 and 1.5 Ga. These  $T_{DM}^{Nd}$  are in good agreement with values observed for other peri-Gondwanan terranes (Murphy and Nance, 2002).

## 8 Discussion and Conclusions

Several important consequences arise from our geochronological, geochemical and isotopic data obtained for the Muráň Gneiss Complex in the Veporic unit. Felsic gneisses record an Ordovician magmatic intrusion age of  $464 \pm 35$  Ma. These rocks were deformed and metamorphosed under amphibolite facies conditions during the Alpine orogeny, in the Cretaceous ( $88 \pm 40$  Ma). No evidence for Variscan metamorphism was found from the U-Pb single zircon dating. All measured zircons plot on a discordia line inconsistent with a metamorphic or magmatic event during Variscan time (Fig. 4). This is in contrast to previous studies on the Muráň Gneiss Complex, which interpret deformation and metamorphism as Variscan (Kováčik et al., 2001).

The whole rock isotopic data presented in this paper is consistent with the evolution recorded by zircons:

The WR-Pb-Pb data reveals an Cretaceous age of homogenization (Fig. 6), which is too old compared to the lower discordia intercept, but is well comparable with published data on metamorphism (Janák et al., 2001b,a; Lupták et al., 2004) and fits within the limits of the WR-Pb-Pb method. The Nd isotopic evolution yields reasonable  $T_{DM}^{Nd}$  ages when a two-step modeling with an Alpine event is employed (Fig. 8). The Sr and Nd isotopic variations can be interpreted as binary mixing during Alpine metamorphism (Fig. 7).

Felsic gneisses have geochemical features of crustal dominated granitoids. Their Nd and Sr isotopic compositions are typical for evolved crustal rocks together with the enriched REE pattern and pronounced Eu-Anomaly. The  $T_{DM}^{Nd}$  model ages range between 1.3 and 1.5 Ga and thus are significantly older than the intrusion ages. This suggests that most material was reworked older crustal material, which is a typical feature for the peri-Gondwanan terranes (Liew and Hofmann, 1988; von Raumer et al., 2003; Kröner et al., 2000; von Raumer et al., 2003).

The geochemistry of amphibolites resembles typical MORB affinity. This is supported by a flat REE pattern, the Zr/Y ratio as well as the Nd and Sr isotopic compositions, which are similar to the prevalent MORB composition (Zindler and Hart (1986), Fig. 7). With  $\epsilon Nd_{ini}$  values of 6.5 and  $T_{DM}^{Nd}$  of 1.2 Ga they are well comparable e.g. with gabbros and quartz-eclogites from the Ötztal basement in the Austroalpine units of the Eastern Alps (Miller and Thöni, 1995). The Pb-Pb-WR data do not support the MORB character of the protolith of the Muráň Gneiss Complex amphibolites, because they do not follow the evolution line of upper mantle, thus showing a contamination with lead (Fig. 6), which is quite probable due to their low Pb concentration.

The banded gneiss is interpreted to have been formed during Alpine deformation and metamorphism as a mixture of amphibolite and felsic gneiss. This is already indicated by the common deformational structures and the linear correlation of the major and trace elements (Table 1). Furthermore, in the  $^{87}Sr/^{86}Sr$  vs.  $\epsilon Nd$  diagram a mixing hyperbola can be fitted to the data when the isotopic compositions are recalculated to an Alpine overprint (88 Ma; Fig. 7).

Considering the paleotectonic correlations during the Early Palaeozoic time, the Central Western Carpathians possibly belonged to the assembly of microplates and crustal blocks derived from the northern margin of Gondwana (“Hun superterrane”, Stampfli, 1996; Stampfli and Borel, 2002; von Raumer et al., 2002, 2003)). According to such scenario, the Central Western Carpathians were most probably a lateral prolongation of this superterrane, further east of the Bohemian Massif and the Alps. Ordovician rocks in the Central Western

Carpathians resulted from magmatism at an active Gondwana margin, tracing a continuation of considerably large orogenic belt obscured in the pre-Alpine basement.

Amphibolite facies overprint is also observed in gneisses of Cambro-Ordovician protolith in the northern parts of the Veporic Unit (e.g. Putiš et al., 1997). Locally eclogite facies metamorphism of metabasites from this area has been reported (Janák et al., 2003). Published geochronological data (multigrain zircon U-Pb dating (Putiš et al., 2001) and electron microprobe dating of monazite (Janák et al., 2002)) suggest Variscan age of the high-grade metamorphism in the Northern Veporic Unit. However, single zircon U-Pb data on gneisses from this Unit does not give evidence for Variscan metamorphism (Gaab, unpublished data). Similar to the zircon data presented in this study, only Ordovician magmatic and Alpine metamorphic events can be identified. Thus further research should be addressed to the importance of Alpine metamorphism versus Variscan metamorphism for the evolution of the whole Veporic Unit.

### Acknowledgements

We would like to thank MK, IB, IP and DP for their help during field work and for fruitful discussions. For constructive and thorough reviews by KS, GO and MK and especially BB are acknowledged. AH is gratefully acknowledged for providing the opportunity to perform this study at MPI, Mainz. Field work was partially supported by grants VEGA 3167 and APVT-20-020002 (to MJ) from the Slovak grant agencies. TR and SG are thanked for useful discussions during this study.

### References

- Arndt, N., Todt, W., 1994. Formation of 1.9 Ga Old Trans-Hudson Continental Crust: Pb Isotopic Data. *Chemical Geology* 118, 9–26.
- Bajaník, Š., Hovorka, D., 1981. The amphibolite facies metabasites of the Rakovec Group of Gemericum (the Western Carpathians). *Geologický Zborník - Geologica Carpathica* 32, 679–705.
- Bezák, V., 1991. Metamorphic conditions of the Veporic unit in the Western Carpathians. *Geologický Zborník - Geologica Carpathica* 42, 219–222.
- Cheatham, M., Sangrey, W., White, W., 1993. Sources of error in external calibration ICP-MS analysis of geological samples and an improved non-linear drift correction procedure. *Spectrochimica Acta Part B* 48B, E487–E506.

- Chen, F., Hegner, E., Todt, W., 2000. Zircon ages and Nd isotopic and chemical compositions of orthogneisses from the Black Forest, Germany: evidence for a Cambrian magmatic arc. *International Journal of Earth Science* 88, 791–802.
- Faryad, S. W., 1995. Phase petrology and P-T conditions of mafic blueschists from the Meliata unit, West Carpathians, Slovakia. *Journal of Metamorphic Geology* 13, 701–714.
- Faryad, S. W., 1997. Metamorphic petrology of the Early Paleozoic low-grade rocks in the Gemericum. In: Grecula, P., Hovorka, D., Putiš, M. (Eds.), *Geological Evolution of the Western Carpathians*. Mineralia Slovaca - Monograph, Geocomplex, 309–314.
- Gaab, A., Poller, U., Todt, W., Janák, M., 2003b. Geochemical and Isotopic Characteristics of the Muráň Gneiss Complex, Veporic Unit (Slovakia). *Journal of the Czech Geological Society* 48, 52.
- Grecula, P., 1982. Gemericum: segment of the Paleotethyan riftogene basin within Alpine Variscides. *Mineralia Slovaca - Monograph* 2, 108pp.
- Hegner, E., Kröner, A., 2000. Review of Nd isotopic data and xenocrystic and detrital zircon ages from the pre-Variscan basement in the eastern Bohemian Massif: speculations on palinspastic reconstructions. In: Franke, W., Haak, V., Onken, O., Tanner, D. (Eds.), *Orogenic Processes: Quantification and Modelling in the Variscan Belt*, vol. 179. Geological Society, London, 113–129.
- Hovorka, D., Dávidová, M.-Ľ., Fejdi, P., Gregorová, Z., Határ, J., Kátlovský, V., Pramuka, S., Spišiak, J., 1987. The Muráň gneisses of the Kohút Crystalline Complex. *Acta Geologica et Geographica Universitatis Comenianae* 42, 5–101.
- Janák, M., Cosca, M., Finger, F., Plašienka, D., Koroknai, B., Lupták, B., Horváth, P., 2001a. Alpine (Cretaceous) metamorphism in the Western Carpathians: P-T-t paths and exhumation of the Veporic core complex. *Geologisch-Paläontologische Mitteilungen Innsbruck* 25, 115–118.
- Janák, M., Finger, F., Plašienka, D., Petřík, I., Humer, B., Méres, Š., Lupták, B., 2002. Variscan high P-T recrystallization of Ordovician granitoids in the Veporic unit (Nízke Tatry Mountains, Western Carpathians): new petrological and geochronological data. *Geolines* 14, 38–39.
- Janák, M., Méres, Š., Ivan, P., 2003. First evidence for omphacite and eclogite facies metamorphism in the veporic unit of the Western Carpathians. *Journal of the Czech Geological Society* 48, 69.
- Janák, M., O'Brien, P. J., Hurai, V., Reutel, C., 1996. Metamorphic evolution and fluid composition of garnet-clinopyroxene amphibolites from the Tatra Mountains, Western Carpathians. *Lithos* 39, 57–59.
- Janák, M., Plašienka, D., Frey, M., Cosca, M., Schmidt, S., Lupták, B., Méres, Š., 2001b. Cretaceous evolution of a metamorphic core complex, the Veporic unit, Western Carpathians (Slovakia): P-T conditions and *in situ*  $^{40}\text{Ar}/^{39}\text{Ar}$  UV laser probe dating of metapelites. *Journal of Metamorphic Geology* 19, 197–216.



- Klinec, A., 1976. Geologická mapa Slovenského Rudohoria a Nízkych Tatier. Geologický Ústav Dionýza Štura, Bratislava.
- Korikovsky, S. P., Krist, E., Boronikhin, V. A., 1989. Staurolite-chloritoid schists from the Klenovec region: prograde metamorphism of high alumina rocks of the Kohút zone-Veporides. *Geologický Zborník - Geologica Carpathica* 39, 187–200.
- Kováčik, M., Král', J., Bachlinski, R., 2001. The "Muráň" orthogneisses: contribution to tectonics, origin, metamorphism and Sr-isotopes constraint (Southern Veporicum, Western Carpathians). *Slovak Geological Magazine* 7, 202–211.
- Kováčik, M., Král', J., Maluski, H., 1996. Metamorphic rocks in the Southern Veporicum basement: their Alpine metamorphism and thermochronologic evolution. *Mineralia Slovaca* 28, 185–202.
- Kröner, A., Štípská, P., Schlumann, K., Jaekel, P., 2000. Chronological constraints on the pre-Variscan evolution of the Bohemian Massif, Czech Republic. In: Franke, W., Haak, V., Onken, O., Tanner, D. (Eds.), *Orogenic Processes: Quantification and Modelling in the Variscan Belt*, vol. 179. Geological Society, London, 175–197.
- Langmuir, C. H., Vocke, R. D., Hanson, G. N., 1978. A general mixing equation with applications to Icelandic basalts. *Earth Planetary Science Letters* 37, 380–392.
- Liew, T., Hofmann, A., 1988. Precambrian crustal components, plutonic associations, plate environment of Hercynian Fold Belt of central Europe: Indications from a Nd and Sr isotopic study. *Contributions to Mineralogy and Petrology* 98, 129–138.
- Ludwig, K. R., 2001. Isoplot/ex rev. 3.49 A geochronological Toolkit for Microsoft Excel. Berkeley Geochronological Center; Special Publications No. 1a .
- Lupták, B., Janák, M., Plašienka, D., Schmidt, S. T., Frey, M., 2000. Chloritoid-kyanite schists from the Veporic unit, Western Carpathians, Slovakia: implications for Alpine (Cretaceous) metamorphism. *Swiss Bulletin of Mineralogy and Petrology* 80, 211–222.
- Lupták, B., Janák, M., Plašienka, D., Schmidt, S. T., 2003. Alpine low-grade metamorphism of the Permian-Triassic sedimentary rocks from the Veporic Superunit, Western Carpathians: Phyllosilicate composition and "crystallinity" data. *Geologický Zborník - Geologica Carpathica* 54, 367–375.
- Lupták, B., Thöni, M., Janák, M., Petrík, I., 2004. Sm-Nd isotopic chronometry of garnets from the veporic unit, Western Carpathians: some preliminary age results and P-T constraints. *Geolines* 17.
- McDonalds, G. A., 1986. Chemical composition of Hawaiian lavas. In: Coats, R. R., Hay, R. L., Anderson, C. A. (Eds.), *Studies in vulcanology: a memoir in honor of Howel Williams*, 116. Geological Society of America, 477–522.
- Méres, Š., Hovorka, D., 1991. Geochemistry and metamorphic evolution of the Kohút crystalline complex mica schists (Western Carpathians). *Acta*

- Geologica et Geographica Universitatis Comenianae 47, 15–66.
- Miller, C., Thöni, M., 1995. Origin of eclogites from the Austroalpine Ötztal basement (Tirol, Austria) - Geochemistry and Sm-Nd vs. Rb-Sr isotope systematics. *Chem. Geol.* 122, 199–225.
- Murphy, J. B., Nance, R. D., 2002. Sm-Nd isotopic systematics as tectonic tracers: an example from West Avalonia in the Canadian Appalachians. *Earth-Science Reviews* 59, 77–100.
- Oliver, G., Corfu, F., Krogh, T., 1993. U-Pb ages from SW Poland: evidence for a Caledonian suture zone between Baltica and Gondwana. *Journal of the Geological Society, London* 150, 355–369.
- Pearce, J., Norry, M., 1979. Petrogenetic implications of Ti, Zr, Y and Nb variations in volcanic rocks. *Contrib. Mineral. Petrol.* 69, 33–47.
- Plašienka, D., 1997. Cretaceous tectonochronology of the Central Western Carpathians, Slovakia. *Geologický Zborník - Geologica Carpathica* 48, 99–111.
- Plašienka, D., Grecula, P., Putiš, M., Hovorka, D., Kováčik, M., 1997. Evolution and structure of the Western Carpathians: an overview. In: Grecula, P., Hovorka, D., Putiš, M. (Eds.), *Geological Evolution of the Western Carpathians. Mineralia Slovaca - Monograph*, 1–24.
- Plašienka, D., Janák, M., Lupták, B., Milovský, R., Frey, M., 1999. Kinematics and metamorphism of a Cretaceous core complex: the Veporic unit of the Western Carpathians. *Physics and Chemistry of the Earth (A)* 24, 651–658.
- Poller, U., Janák, M., Kohút, M., Todt, W., 2000. Early Variscan Magmatism in the Western Carpathians: U-Pb zircon data from granitoids and orthogneisses of the Tatra Mts (Slovakia). *International Journal of Earth Science* 89, 336–349.
- Poller, U., Nægler, T., Liebetrau, V., Galetti, G., 1997. The Mönchalpgneiss - Geochemical characteristics and Sm-Nd data of a polymetamorphic S-type granitoid (Silvretta nappe / Switzerland). *European Journal of Mineralogy* 9, 411–422.
- Poller, U., Todt, W., 2000. U-Pb single zircon data of granites from the High Tatra Mountains (Slovakia): implications for the geodynamic evolution. *Transactions of the Royal Society* 91, 235–243.
- Putiš, M., Filová, I., Korikovskiy, S. P., Kotov, A. B., Madarás, J., 1997. Layered metaigneous complex of the veporic basement with features of the Variscan and Alpine thrust tectonics (Western Carpathians). In: Grecula, P., Hovorka, D., Putiš, M. (Eds.), *Geological Evolution of the Western Carpathians. Mineralia Slovaca - Monograph, Geocomplex*, 175–196.
- Putiš, M., Kotov, A., Korikovskiy, S., Salnikova, E., Yakoleva, S., Berezhnaya, N., Kovach, V., Plotkina, J., 2001. U-Pb zircon ages of dioritic and trondhjemitic rocks from a layered amphibolitic complex crosscut by granite vein (Veporic basement, Western Carpathians). *Geologický Zborník - Geologica Carpathica* 52, 49–60.
- Schaltegger, U., Nægler, T., Corfu, E., Maggetti, M., Galetti, M. G., Stosch, H., 1997. A Cambrian island arc in the Silvretta nappe, a comparison. *Swiss*

- Bulletin of Mineralogy and Petrology 77, 337–350.
- Stacey, J. S., Kramers, J. D., 1975. Approximation of terrestrial lead isotope evolution by a two-stage model. *Earth Planetary Science Letters* 26, 207–221.
- Stampfli, G., 1996. The intra-Alpine terrain: a palaeotethyan remnant in the Alpine Variscides. *Eclogae Helvetiae* 89, 12–42.
- Stampfli, G. M., Borel, G. D., 2002. A plate tectonic model for the Paleozoic and Mesozoic constrained by dynamic plate boundaries and restored synthetic oceanic isochrons. *Earth Planetary Science Letters* 196, 17–33.
- Sun, S.-S., 1980. Lead isotopic study of young volcanic rocks from mid-ocean ridges, ocean islands and island arcs. *Philosophical Transactions of The Royal Society* 297, 409–445.
- Taylor, S., McLennan, S., 1985. *The continental crust: its composition and evolution*. Blackwell, Oxford.
- Totland, M., Jarvis, I., Jarvis, K., 1995. Microwave digestion and alkali fusion procedures for the determination of platinum-group elements and gold in geological materials by ICP-MS. *Chemical Geology* 124, 21–36.
- von Raumer, J., Neubauer, F., 1993. Late Precambrian and Palaeozoic evolution of the Alpine basement - an overview. In: von Raumer, J., Neubauer, F. (Eds.), *Pre-Mesozoic geology in the Alps*. Springer-Verlag, Berlin, 625–639.
- von Raumer, J., Stampfli, G., Borel, G., Bussy, F., 2002. Organization of pre-Variscan basement areas at the north-Gondwanan margin. *International Journal of Earth Science* 91, 35–52.
- von Raumer, J. F., Stampfli, G. M., Bussy, F., 2003. Gondwana-derived microcontinents – the constituents of the Variscan and Alpine collisional orogens. *Tectonophysics* 365, 7–22.
- Wendt, J., Todt, W., 1991. A vapor digestion method for dating single zircons by direct measurement of U and Pb without chemical separation. *Terra Abstracts* 3, 507–508.
- White, W., Patchett, J., 1984. Hf-Nd-Sr isotopic and incompatible element abundances in island arcs: implications for magma origins and crust-mantle evolution. *Earth Planetary Science Letters* 67, 167–185.
- York, D., 1969. Least squares fitting of a straight line with correlated errors. *Earth Planetary Science Letters* 5, 320–324.
- Zartman, R., Haines, S., 1988. The plumbotectonic model for Pb isotopic systematics among major terrestrial reservoirs - A case for bi-directional transport. *Geochimica et Cosmochimica Acta* 52, 1327–1339.
- Zindler, A., Hart, S., 1986. Chemical Geodynamics. *Annual Review of Earth and Planetary Sciences* 14, 493.

# Chapter 3

The purpose of the study presented in this chapter is to clarify the apparent dichotomy, which arises from the U-Pb zircon age obtained for the Muráň Gneiss presented in Chapter 2 and published multi-grain U-Pb zircon data (Putiš et al., 2001). Therefore detailed sampling for U-Pb geochronology was performed in the Northern Veporic Unit in 2004 and combined with isotopic data for samples from the Koleso valley sampled in 2002.

The manuscript and all analyses presented in this chapter were prepared by A.S. Gaab. UP introduced the author to analytical methods used for this manuscript. MJ made this work possible by introducing to the regional geology and supporting the author during field work. WT admitted the entry to the clean lab and to the mass spectrometer.

This manuscript will be submitted to the Swiss Bulletin of Mineralogy and Petrology.

# Zircon U-Pb geochronology and Isotopic Characterization for the pre-Mesozoic basement of the Northern Veporic Unit (Central Western Carpathians, Slovakia)

A.S. Gaab<sup>a,\*</sup> UP<sup>a</sup> MJ<sup>b</sup> WT<sup>a</sup>

<sup>a</sup> *Max-Planck-Institut für Chemie; Abt. Geochemie; P.O. Box 3060; 55020 Mainz; Germany*

<sup>b</sup> *Slovak Academy of Sciences; Geological Institute; P.O. Box 106; 84005 Bratislava 45; Slovak Republic*

---

## Abstract

Ordovician magmatism is observed in the whole Veporic unit. New single and multi grain zircon U-Pb dating reveal an intensive magmatic activity between 460-470 Ma and a minor magmatic phase around 440 Ma in the Northern Veporic Unit. Carboniferous ages of SHRIMP and single grain TIMS U-Pb dating in this unit document intense metamorphism and magmatism during Variscan orogeny (330-350 Ma).

Previously published multi grain U-Pb data in the same area have been interpreted to show Cambrian precursor ages. A new interpretation of this multi grain data is suggested, revealing an Ordovician ( $464 \pm 23$ ) precursor age and a Carboniferous metamorphic overprint. With this new interpretation and published data on the Southern Veporic Unit a common Ordovician precursor age for the whole Veporic unit is documented.

The isotopic signature for the Pre-Variscan basement in the Veporic unit is distinct from the Tatric unit, only the metasedimentary Lower Unit in the Western Tatra reveals comparable  $^{87}\text{Sr}/^{86}\text{Sr}_{ini}$  and  $\epsilon Nd_{ini}$  as the felsic gneisses in the Veporic basement. These gneisses are characterized by  $^{87}\text{Sr}/^{86}\text{Sr}_{ini,460}$  between .712 and .715 and by  $\epsilon Nd_{meas,460}$  between -8 and -11. The amphibolites of the Veporic basement are characterized by high  $^{87}\text{Sr}/^{86}\text{Sr}_{ini,460}$  of 0.708-0.710 and  $\epsilon Nd_{ini,460}$  of 4.5-5.6. A primitive gabbro with  $\epsilon Nd_{ini,460}$  of 5.9 and  $^{87}\text{Sr}/^{86}\text{Sr}_{ini}$  of .7028 occurs in the Northern Veporic basement. This signature is similar to a mafic component observed in the Southern Veporic Unit.

The Variscan Kralova Hola granites show complete distinct signatures as the gneisses and amphibolites, but reveal a marked similarity with diorites and granites from the High Tatra Mountains with  $^{87}\text{Sr}/^{86}\text{Sr}_{ini,330}$  of .7013-0.7016 and  $\epsilon Nd_{ini,330}$  of -0.5-1.2.

*Key words:* Ordovician, zircon, geochronology, isotope geochemistry

---

## 1 Introduction

The pre-Variscan history of the Central Western Carpathians is not very well known. Late Cambrian to Ordovician protolith ages for meta-granitoids have been identified only recently in the polymetamorphosed complexes of Veporic Unit (Putiš et al., 2001; Janák et al., 2002; Gaab et al., in press). The Veporic Unit is one of three thick skinned north-verging Slovakocarpathian superunits (e.g. Plašienka et al., 1997). Its tectonic position is between the Tatric Unit in the North, which is dominated by Variscan magmatism (e.g. Poller and Todt, 2000), and the Gemeric Unit in the South, which is dominated by Palaeozoic sediments intruded by Permian granites (e.g. Vozárová et al., 1998; Poller et al., 2002).

Reliable radiometric ages on the Veporic Unit, especially U-Pb zircon ages for the pre-Variscan history, i.e. older than 360 Ma, are only sparsely available. U-Pb multi grain dating by Putiš et al. (2001) reveals Cambrian protolith ages ( $514\pm 24$  Ma) and Carboniferous ages ( $348\pm 31$  Ma) in the polymetamorphosed complexes of the northern region.  $^{40}\text{Ar} - ^{39}\text{Ar}$  step heating dating of an amphibolite revealed a staircase pattern with old apparent ages of up to 440 Ma indicating old grains which were partially reset by metamorphism (Maluski et al., 1993). Janák et al. (2002) presents chemical Th-U-Pb monazite dating with Ordovician (450-490 Ma) and Carboniferous ages ( $342\pm 27$ ). Janák et al. (2002) interpreted this as a record of pre-Variscan granitoid magmatism and Variscan metamorphic overprint. Gaab et al. (in press), based on single zircon U-Pb dating, constrained an Ordovician age for the protolith ( $464\pm 40$  Ma) and a Cretaceous age ( $82\pm 40$ ) for the metamorphic overprint of the so called “Muráň Orthogneiss” in the southern part of the Veporic unit.

The U-Pb geochronological data imply significant differences in timing of pre-Variscan granitoid magmatism in the Veporic Unit. The purpose of this study is to resolve this age progression in detail by presenting single zircon U-Pb data from the basement rocks of the Northern Veporic Unit. The results together with a re-interpretation of the multi-grain data published by Putiš et al. (2001) argue against this dichotomy and a coeval evolution of the whole Veporic unit during Palaeozoic times is suggested by this study.

---

\* Andreas S. Gaab

*Email address:* gaab at mpch-mainz.mpg.de (A.S. Gaab).

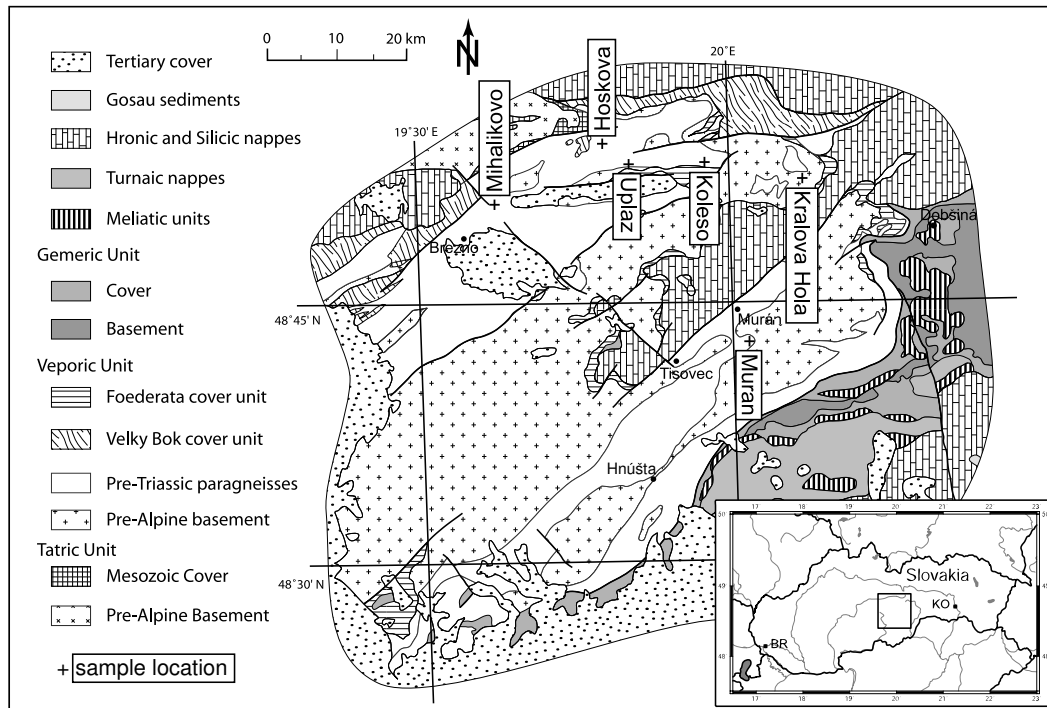


Fig. 1. Geological map of the Veporic Unit. Sample locations are indicated and location name used in this paper given. Outline of Slovakia with major rivers given in the inlay. Bratislava (BR) and Kosice (KO) indicated.

In order to characterize the Northern Veporic Unit additional to the U-Pb zircon data this study presents isotopic data for gneisses from the Koleso valley. This data are compared to the Tatric unit and to the southern part of the Veporic unit to resolve similarities and different source contributions.

## 2 Geological Setting

The Veporic Unit consist of pre-Alpine basement complexes assembled during the Variscan orogeny (Bezák, 1991, and references therein) that are overlain by Upper Palaeozoic to Triassic sedimentary cover sequences (Fig. 1). The poly-metamorphic basement comprises granitoids, migmatites, gneisses and amphibolites, mostly mylonitized during Alpine overprint. In the Central and North-Eastern part of the Veporic unit locally preserved para-autochthonous cover include Upper Permian sandstones and conglomerates, Scythian quartzites and slates, and Middle to Upper Triassic carbonates and shales (Foederata unit). The South-Eastern rim of the Veporic unit is composed of Carboniferous, Permian and Scythian clastic sequences partly forming an allochthonous unit overlying the Foederata cover unit to the North-West.

Variscan magmatic and metamorphic events in the Veporic basement have

been determined by U-Pb dating of zircons in the granitoids, migmatites and orthogneisses (Cambel et al., 1990; Putiš et al., 2001). The Variscan age (330-370 Ma) of some Veporic granitoids has been documented also by chemical Th-U-Pb electron microprobe dating of monazite (Finger et al., 2003; Thöni et al., 2003). Some hornblende from basement amphibolites preserved pre-Alpine ages (346-377 Ma; Dallmeyer et al., 1996; Král' et al., 1996), however the  $^{40}\text{Ar} - ^{39}\text{Ar}$  do not show well plateau ages, suggesting metamorphic overprint. In the northern parts of the Veporic unit, in the Koleso valley, garnet-bearing metabasites bear evidence of eclogite facies metamorphism of unknown age (Janák et al., 2003). The host rocks of these eclogites show Variscan age of metamorphic recrystallization, based on Th-U-Pb chemical microprobe dating of monazite (Janák et al., 2002).

The grade of Alpine metamorphic overprint in the Northern Veporic unit is not very well constrained, although at least greenschist to lower amphibolite facies conditions have been suggested for the basement (Putiš et al., 1997). Janák et al. (2001b) documented that Alpine overprint in the southeastern parts of the Veporic basement reached middle amphibolite facies conditions (up to 620°C and 10 kbar). All the Veporic cover units were affected by Alpine metamorphism of low to medium grade (Lupták et al., 2000, 2003). Published geochronological data provide Cretaceous metamorphic ages. The data include  $^{40}\text{Ar} - ^{39}\text{Ar}$  dating of micas and amphibole (Maluski et al., 1993; Dallmeyer et al., 1996; Kováčik et al., 1996; Král' et al., 1996; Koroknai et al., 2001; Janák et al., 2001a) electron microprobe dating of metamorphic monazite (Janák et al., 2001b) and Sm-Nd dating of garnet (Lupták et al., 2004).

### 3 Analytical Techniques

The SHRIMP (Sensitive High Resolution Ion Microprobe) analyses were performed at the ANU in Canberra. The standards used were SL13 and FC-1 and measured for reference after 3 spot analyses. Operating procedures for U, Th, and Pb isotopic measurements followed those described by Compston et al. (1984) and Williams (1998). For ratio calculation the SQUID program, version 1.02, was used (Ludwig, 2001b).

Isotope dilution U-Pb zircon analyses were performed at the MPI for Chemistry in Mainz. Digestion of the single zircon grains was performed in teflon bombs according to Wendt and Todt (1991) at 200°C with  $\text{HF} - \text{HNO}_3$  after addition of  $^{205}\text{Pb} - ^{233}\text{U}$  mixed spike. The multi grain fractions were weighted and, after addition of  $^{205}\text{Pb} - ^{233}\text{U}$  mixed spike, digested with  $\text{HF} - \text{HNO}_3$  in teflon bombs. Pb and U were separated using resin column chemistry after complete dissolution for the single as well as for the multi-grain analyses. The isotopic composition was measured on a Finnigan MAT 261 in dynamic mode



equipped with an SEM. Common lead correction was applied using the Stacey and Kramers (1975) model composition at 460 Ma.

Main and trace elements were analyzed on powder and melt tables by RFA at the University of Mainz. For Sr and Nd isotopic analyses the powdered whole rock samples were dissolved using a microwave assisted acid digestion as described in Gaab et al. (in press) and were separated using column chemistry according to White and Patchett (1984). For WR-Pb-Pb analyses rock splits were leached in  $HF - HNO_3$  and Pb was separated using resin column chemistry as described in Gaab et al. (submitted). The isotopic data for Pb, Sr and Nd was measured at the MPI for Chemistry in Mainz using a Finnigan MAT261 in static mode.

## 4 Sample Description

Samples for single and multi grain U-Pb zircon studies were taken on the southern slope of the mountain ridge “Kráľ’ovohol’ske Tatry” north of the village Helpa in Central Slovakia. Additionally the Hoškova sample was taken along the northern slope of this mountain ridge according to the outcrop described in Putiš et al. (2001). Samples for the geochemical studies were sampled in the Koleso valley north-east from Helpa and on top of Kralova Hola (Fig. 1).

The location names were assigned according to the topographic map “Turistická mapa 1:50 000 ‘Nízke Tatry Kráľ’ova Hol’a’ no.123, 3.vydanie”.

### 4.1 Kralova Hola

Kralova Hola is the easternmost peak along the Kráľ’ovohol’ske Tatry mountain ridge. Sample 02GA14 was taken near the top at  $48^\circ 52' 20''N$ ;  $20^\circ 09' 20''E$ . It is a strongly mylonitized granite with feldspar-augen. Additionally the only weakly deformed sample 02GA17 was sampled at  $48^\circ 50' 40''N$ ;  $20^\circ 07' 52''E$ . Petrographically and geochemically these two samples are very similar, only the grade of tectonic deformation is different. These samples were used for geochemical and for isotopic analyses.

Zircon CL images for both samples are shown in Fig. 2. In general, the zircons are simple euhedral magmatic zircons with magmatic zoning as seen by oscillatory magmatic growth in Fig. 2. No metamorphic rim can be observed. Only a minor part of the zircons exhibit small remnants of cores. The zircons of these samples were analyzed by SHRIMP (table 1).

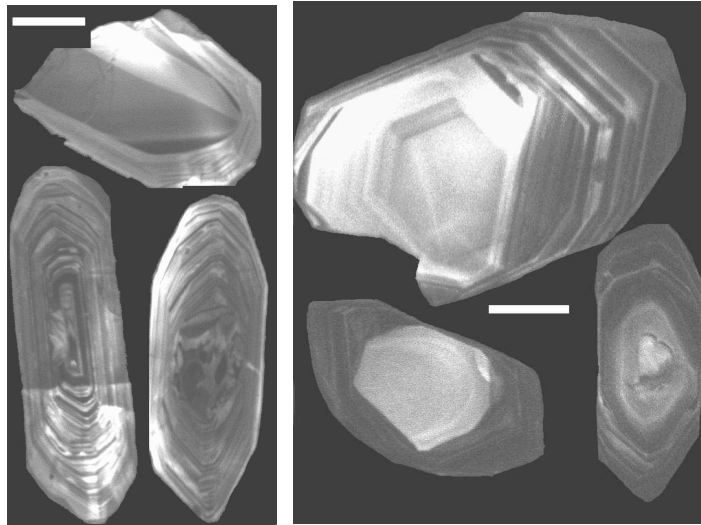


Fig. 2. Zircon CL images for the Kralova Hola samples 02GA14 and 02GA17. Scale bar indicates 50 $\mu$ m.

#### 4.2 *Koleso valley*

In the Koleso valley a large variety of basement rocks occur. Most prominent are felsic gneisses with variable amount of quartz present (table 5). Intercalated with these felsic gneisses are garnet-bearing amphibolites. All samples show intense deformation and exhibit lineations.

For the U-Pb zircon dating sample 03GA18, a granitoid boudin in strongly deformed felsic gneisses was sampled at 48° 53' 55" N; 19° 59' 15" E. The zircons of this sample (Fig. 3(a)) show magmatic zoning and also resorption rims with metamorphic overgrowth.

For geochemical analyses samples for the felsic gneisses (02GA01, 02GA06 and 02GA10) and for the amphibolites (02GA04, 02GA11 and 02GA12) were collected in this valley. In addition, a gabbro with magmatic features, sample 02GA08, was sampled for comparison with the amphibolites. To record the Pb isotopic variation of these rocks, samples 02GA01-02GA12 and samples 03GA25-03GA32, taken from the same outcrop as sample 03GA18, were used for WR-Pb-Pb analyses.

#### 4.3 *Uplaz and Drotacka*

Samples for U-Pb single zircon analyses were taken at 48° 52' 50" N; 19° 54' 50" E on the southern slope of the Král'ovohol'ske mountain ridge 3.5 km north of Závadka nad Hronom.

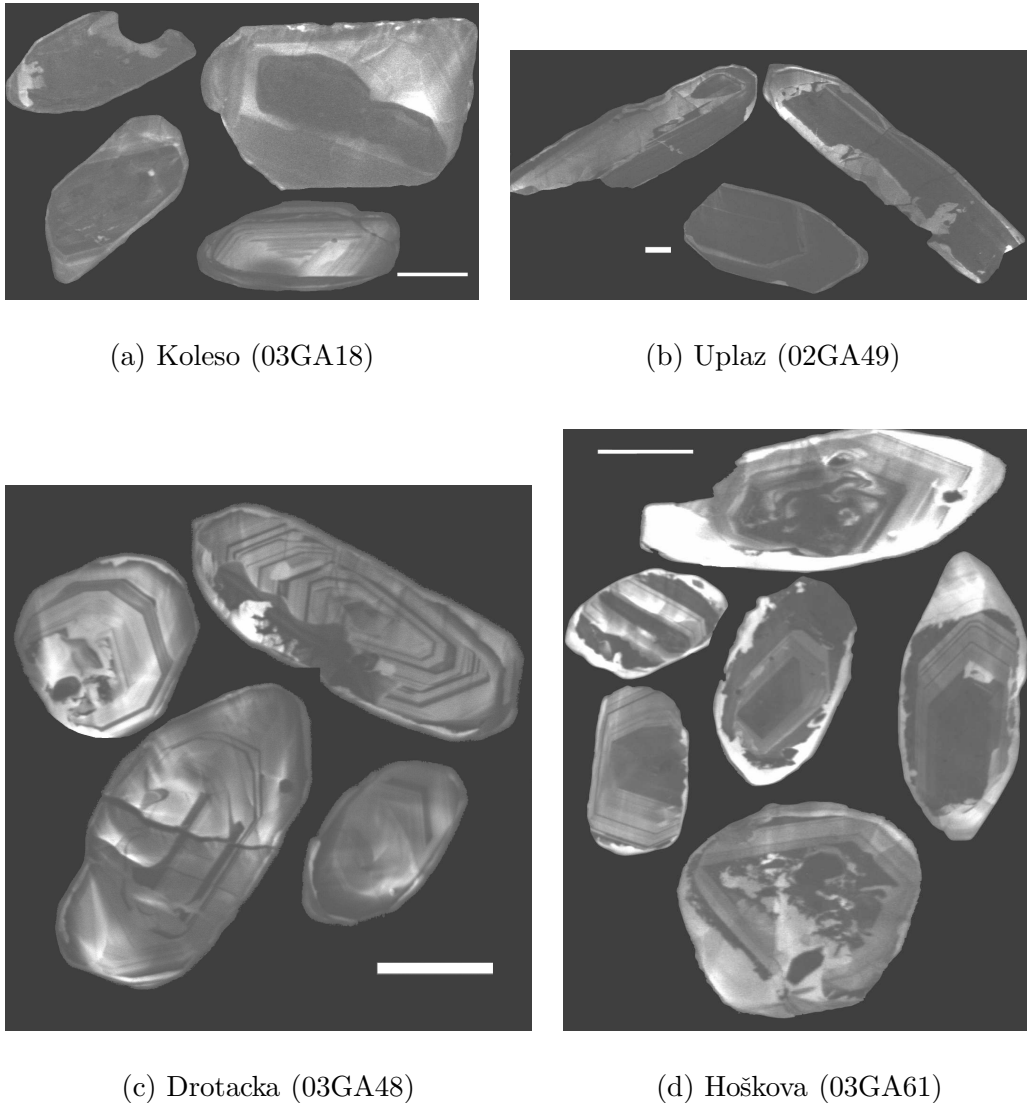


Fig. 3. Zircon CL images for samples from the Northern Veporic Unit. Localities shown in Fig. 1. Scale bar indicates 50 $\mu$ m.

Sample 03GA48 resembles a fine-grained metagranite, very untypical for the basement in this area. It was sampled on the Drotacka ridge. CL zircon images are shown in Fig. 3(c). The zircons show intensive magmatic zoning. Nevertheless, resorption structures can be observed in most grains.

In the Uplaz valley sample 03GA49 was taken along a roadside cliff. This sample resembles an intermediate to felsic gneiss, strongly deformed and quite similar to the felsic gneisses in the Koleso valley. CL zircon images are shown in Fig. 3(b) and reflect intense resorption features with magmatic zoning present in the inner parts of the zircons.

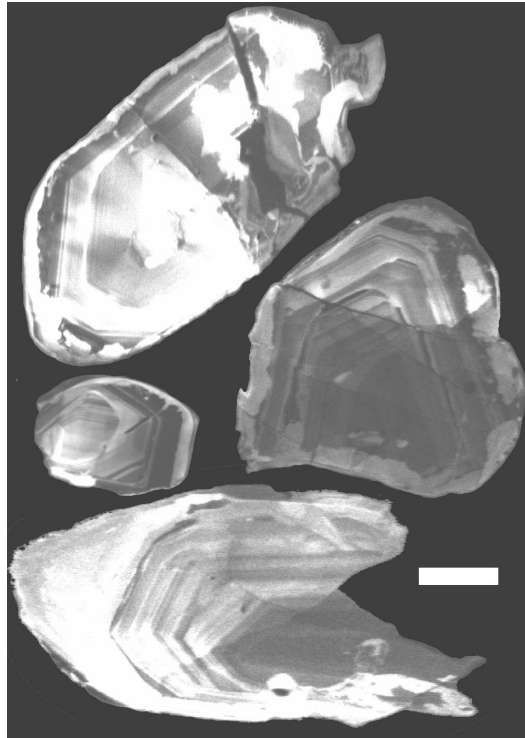


Fig. 4. Zircon CL images for samples from the Northern Veporic Unit. Locality shown in Fig. 1, Sample Mihalikovo (03GA50). Scale bar indicates 50 $\mu$ m.

#### 4.4 *Mihalikovo quarry*

Directly above the abandoned quarry near the Mihalikovo valley at 48° 50' 05" N; 19° 39' 35" E sample 03GA50 was taken at a small cliff consisting of strongly layered and deformed intermediate gneisses. The CL images of the zircons from this sample are shown in Fig. 4. The inner parts of these zircons show magmatic zoning, but the zircons also exhibit intensive resorption and metamorphic rims.

#### 4.5 *Hoškova valley*

The sample 03GA61 is taken near to the outcrop described for the sample VBNT-76L in Putiš et al. (2001) at 48° 55' 22" N; 19° 53' 55" E. The sampled cliff is 50 m above the road opposite to the small creek on the southern slope of the ridge. The cliff consists of strongly banded amphibolites interlayered with Pl-Qtz rich felsic gneisses.

Zircons for this felsic gneiss are presented in Fig. 3(d) on the left side. They show magmatic zoning in the inner parts but also strong resorption structures and rims with a bright CL intensity most probable linked to a metamorphic overprint.

## 5 U-Pb zircon dating

U-Pb zircon dating presented in this study was performed on 7 samples from the Northern Veporic Unit. Locations of these samples are indicated in Fig. 1 and zircon CL images of each sample are shown in Fig. 2 to Fig. 4. The data for the individual grains are given in table 1 for the SHRIMP analyses and in table 2 for the conventional analyses. The concordia diagrams are presented in Fig. 5 as a compilation of all samples to pronounce similarities and differences observed for the samples. The table 4 presents the exact upper and lower intercept ages for all samples investigated in this study. Discordia ages and diagrams were generated using ISOPLOT (Ludwig, 2001a).

### 5.1 SHRIMP dating

The samples from Kralova Hola (02GA14 and 03GA17) were dated by SHRIMP. Both samples belong to the same lithological unit, which is demonstrated by similar geochemical and isotopic composition of these samples (table 5). Also the zircon populations of both samples are very similar (Fig. 2).

The individual measurements for each sample do not result in a concordant age (table 1). The small discordancy of the zircons is probably produced by the tectonic and metamorphic overprint. Both samples, the strongly deformed as well as the undeformed, result in the same age. A good overlap of both samples can be observed in the concordia diagram (Fig. 5) and ages of  $345\pm 11$  and  $349\pm 26$  are obtained calculating with a discordia with recent lead loss (table 4). This age of  $\approx 350$  Ma is, in accordance with the CL images (Fig. 2), interpreted as intrusion age.

Cores are present to a minor extent in zircons of both samples and reveal  $^{207}\text{Pb}/^{206}\text{Pb}$  ages between 1500 and 1700 Ma.

### 5.2 Conventional dating

The *Koleso* and the *Uplaz* samples reveal similar upper intercept ages of  $462\pm 10$  and  $467\pm 8$  Ma, respectively (table 4). Individual grains are discordant and a discordia line with a lower intercept at recent times can be inferred (Fig. 5).  $^{206}\text{Pb}/^{204}\text{Pb}$  ratios are between 80 and 900 for the *Koleso* sample and between 65 and 2650 for the *Uplaz* sample (table 2). One zircon of the *Koleso* sample reveals an old  $^{207}\text{Pb}/^{206}\text{Pb}$  age of 1500 Ma. Two grains of this sample reveal slightly older ages as the upper intercept age of the discordia (table 2)

zircon grain no.	location name	$^{204}\text{Pb}/^{206}\text{Pb}$	measured ratios $^{207}\text{Pb}/^{206}\text{Pb}$	$^{208}\text{Pb}/^{206}\text{Pb}$	$^{206}\text{Pb}/^{238}\text{U}$	$^{207}\text{Pb}/^{235}\text{U}$	$^{206}\text{Pb}/^{238}\text{U}$	$^{207}\text{Pb}/^{235}\text{U}$	1 $\sigma$	cor.	$^{206}\text{Pb}/^{238}\text{U}$	1 $\sigma$	calculated ages $^{207}\text{Pb}/^{235}\text{Pb}$	1 $\sigma$
		err	% err	err										
2.1	Kralova Hola	9.7E-5	.0544	0.8	.220	0.9	0.0580	0.0003	0.427	0.006	0.68	356.9	3.8	399
2.2	02GA14	2.5E-4	.0559	0.8	.197	1.0	0.0555	0.0002	0.405	0.007	0.50	362.2	3.8	349
3.1	--	1.6E-4	.0546	1.0	.167	1.4	0.0554	0.0004	0.400	0.008	0.47	353.8	3.7	386
9.1	--	8.9E-5	.0546	0.9	.212	1.1	0.0563	0.0003	0.417	0.007	0.62	361.4	3.9	328
9.2	--	6.1E-5	.0539	0.7	.185	0.9	0.0569	0.0003	0.418	0.005	0.76	348.9	3.6	299
11.1	--	1.5E-4	.0569	1.1	.164	1.5	0.0572	0.0003	0.428	0.010	0.49	348.9	3.7	298
17.1	--	7.1E-5	.0545	0.8	.173	1.0	0.0572	0.0003	0.421	0.006	0.68	350.9	3.6	341
18.1	--	1.9E-5	.0546	0.9	.212	1.1	0.0559	0.0003	0.420	0.006	0.73	355.8	3.6	328
23.1	--	5.0E-4	.0612	0.7	.205	1.0	0.0569	0.0003	0.422	0.009	0.37	354.0	3.7	368
24.1	--	8.4E-5	.0547	1.2	.136	1.7	0.0587	0.0004	0.433	0.009	0.57	367.4	4.0	348
32.1	--	7.5E-5	.0555	0.9	.186	1.3	0.0577	0.0004	0.431	0.007	0.66	362.4	3.8	389
41.1	--	1.5E-4	.0542	0.8	.136	1.2	0.0570	0.0004	0.409	0.007	0.55	358.8	3.7	284
45.1	--	6.0E-5	.0533	1.0	.212	1.0	0.0569	0.0003	0.413	0.006	0.62	354.9	3.7	304
48.1	--	5.3E-5	.0543	0.9	.238	1.1	0.0582	0.0003	0.429	0.008	0.67	367.7	3.8	349
50.1	--	2.3E-5	.0533	0.6	.010	3.0	0.0585	0.0003	0.428	0.004	0.86	362.5	3.7	325
50.2	--	2.5E-5	.0533	0.6	.199	0.9	0.0563	0.0003	0.410	0.005	0.81	354.2	3.6	326
52.1	--	--	.0542	0.7	.162	1.1	0.0580	0.0003	0.432	0.004	0.85	364.1	3.7	379
53.1	--	2.0E-4	.0554	1.1	.206	1.3	0.0571	0.0003	0.410	0.012	0.38	360.3	3.9	306
60.1	--	1.6E-5	.0537	0.9	.218	1.1	0.0583	0.0004	0.427	0.006	0.66	366.4	3.8	348
68.2	--	4.9E-5	.0543	0.7	.138	1.1	0.0583	0.0002	0.431	0.004	0.76	365.8	3.7	352
68.1	--	3.7E-5	.1037	0.5	.184	0.8	0.2546	0.0019	3.634	0.039	0.88	1436.6	13.8	1682
17.1	Kralova Hola	1.5E-4	.0540	1.1	.046	2.9	0.0581	0.0006	0.416	0.009	0.80	362.0	4.8	279
22.1	02GA17	1.4E-4	.0564	1.7	.177	2.3	0.0555	0.0005	0.422	0.015	0.80	350.5	4.1	387
22.2	--	3.8E-5	.0541	0.5	.030	1.6	0.0573	0.0003	0.424	0.003	0.80	366.8	3.7	353
27.1	--	7.4E-5	.0549	1.1	.106	1.7	0.0573	0.0004	0.428	0.008	0.80	359.7	4.0	363
29.1	--	4.7E-4	.0571	2.3	.145	3.4	0.0571	0.0008	0.409	0.029	0.26	359.2	5.6	206
29.2	--	2.1E-4	.0571	0.5	.029	1.8	0.0563	0.0007	0.400	0.008	0.80	338.3	3.4	371
41.1	--	6.1E-5	.0547	1.1	.041	2.8	0.0573	0.0004	0.420	0.009	0.58	360.6	3.8	361
41.2	--	8.2E-5	.0539	1.0	.038	2.9	0.0575	0.0003	0.429	0.005	0.81	341.2	3.6	314
44.1	--	1.6E-5	.0544	0.7	.229	1.3	0.1281	0.0010	1.667	0.020	0.90	359.7	4.0	377
47.1	--	2.6E-4	.0587	1.8	.228	2.2	0.0569	0.0005	0.431	0.020	0.32	358.2	4.4	410
44.2	--	6.7E-5	.0946	0.6	.100	1.4	0.0546	0.0003	0.398	0.007	0.52	783.1	10.3	1501

Table 1. Data for the SHRIMP analyses of the Kralova Hola. Concordia diagram shown in Fig. 5

sample name	location name	type	Pb* (ng)	Pb <sub>comm</sub> (ng)	U <sub>tot</sub> /Pb <sub>lead</sub>	<sup>206</sup> Pb/ <sup>207</sup> Pb	2σ	corrected ratios		calculated ages		used for discordia						
								<sup>207</sup> Pb/ <sup>206</sup> Pb	2σ	<sup>206</sup> Pb/ <sup>238</sup> U	2σ		<sup>207</sup> Pb/ <sup>235</sup> U	2σ				
K62	Protacka	CLC	0.013	0.013	11.2	71	1.6	0.2476	0.0063	0.5436	0.0166	-	-	-	+			
K30	---	CLC	0.025	0.022	13.1	85	1.2	0.2169	0.0013	0.4699	0.0020	443	6	368	40	-	+	
K66	---	CLC	0.054	0.010	16.1	281	14.1	0.1024	0.0004	0.1907	0.0014	353	3	340	22	249	162	+
K18	Hoskova	CLC	0.004	0.007	17.5	45	0.6	0.3521	0.0015	0.8113	0.0052	360	11	149	92	-	-	-
L107	---	CLC	0.039	0.078	18.8	48	0.6	0.3520	0.0014	0.8431	0.0027	294	15	274	69	-	-	-
L151	---	CLC	0.004	0.002	15.6	62	1.4	0.2586	0.0009	0.5794	0.0051	395	8	208	90	-	-	-
L17	---	CLC	0.007	0.004	12.2	82	0.7	0.2066	0.0012	0.4564	0.0029	492	8	279	40	-	-	-
L125	---	CLC	0.021	0.003	13.2	217	2.4	0.1138	0.0006	0.2324	0.0015	425	3	382	13	128	77	-
K89	---	CLC	0.034	0.016	13.9	129	1.1	0.1645	0.0003	0.3668	0.0010	398	3	382	13	285	82	*
K29	---	CLC	0.045	0.008	14.7	275	12.2	0.1037	0.0010	0.1845	0.0017	387	4	371	27	272	193	*
L28	---	CLC	0.103	0.009	16.2	542	7.6	0.0802	0.0002	0.1364	0.0011	346	2	348	6	363	34	*
K43	---	CLC	0.344	0.018	20.3	1082	3.0	0.0666	0.0003	0.0987	0.0008	280	2	286	3	329	17	*
L17	Mihalikovo	MG	121.160	2.702	15.9	2864	8.7	0.0607	0.0001	0.0945	0.0002	349	8	361	8	437	12	+
M1	---	MG	280.442	5.719	14.8	3166	6.8	0.0607	0.0001	0.0815	0.0002	378	23	389	21	457	24	+
L39	---	MG	156.576	3.125	16.2	3197	9.4	0.0603	0.0001	0.0939	0.0002	343	5	356	5	441	7	+
M3	---	MG	236.672	4.414	15.4	3222	6.7	0.0607	0.0001	0.0822	0.0002	364	16	377	15	458	19	+
M2	---	MG	324.799	6.397	16.3	3250	6.7	0.0607	0.0001	0.0905	0.0002	343	11	358	11	469	14	+
L2	---	MG	129.719	2.504	15.9	3299	9.6	0.0601	0.0001	0.0945	0.0002	349	13	362	12	440	15	+
L42	---	MG	90.165	1.290	16.4	4445	10.8	0.0590	0.0001	0.0897	0.0002	340	6	353	6	439	6	+
L50	---	CLC	0.290	0.407	15.6	62	0.2	0.2882	0.0005	0.6696	0.0018	354	4	352	13	341	216	+
L76	---	CLC	0.050	0.020	14.0	155	11.1	0.1472	0.0005	0.2318	0.0033	392	6	389	57	374	374	+
K61	---	CLC	0.055	0.016	14.9	195	17.0	0.1233	0.0003	0.2771	0.0010	369	5	340	51	142	344	+
K112	---	SG	0.186	0.042	12.5	277	4.5	0.1078	0.0006	0.2153	0.0022	440	3	439	13	430	79	*
K98	---	SG	0.156	0.026	11.8	349	4.4	0.0970	0.0002	0.1941	0.0006	462	9	457	13	434	41	*
L148	---	CLC	0.147	0.013	12.5	578	9.7	0.0801	0.0002	0.1623	0.0005	433	2	432	6	423	29	*
K101	---	CLC	0.121	0.009	12.8	621	8.4	0.0786	0.0001	0.1574	0.0008	426	2	428	5	437	22	*
L159	---	CLC	0.290	0.026	13.2	633	23.3	0.0780	0.0002	0.1490	0.0007	416	2	416	8	416	48	*
L8	---	SG	0.684	0.061	20.7	706	3.9	0.0742	0.0001	0.1152	0.0005	275	2	284	3	354	23	*
K45	---	SG	0.468	0.025	13.7	1005	6.2	0.0701	0.0001	0.1496	0.0002	392	1	399	2	441	8	*
K45	---	CLC	0.270	0.013	12.9	1099	92.1	0.0684	0.0002	0.1145	0.0010	427	3	427	11	424	57	*
K28	---	CLC	0.310	0.012	12.2	1321	31.2	0.0669	0.0001	0.1202	0.0005	449	2	450	5	456	17	*
K24	---	SG	1.408	0.045	16.0	1870	20.1	0.0634	0.0001	0.0932	0.0002	351	2	362	2	439	8	*

Table 2. Data for the conventional U-Pb single grain zircon analyses shown in Fig. 5. MG - multi grain; SG - single grain; CLC - single grain with CL control.

sample	location name	type	Pb* (ng)	Pb <sub>common</sub> (ng)	U <sub>det</sub> /Pb <sub>rad</sub>	<sup>206</sup> Pb/ <sup>204</sup> Pb	<sup>207</sup> Pb/ <sup>206</sup> Pb	corrected ratios	<sup>206</sup> Pb/ <sup>238</sup> U	<sup>207</sup> Pb/ <sup>235</sup> U	calculated ages	<sup>207</sup> Pb/ <sup>206</sup> Pb	2σ	used for discordance
A52-5	Koleso	SG	0.943	0.954	16.4	84	0.3	0.2292	0.0004	0.4605	0.0011	358	3	479
A25-2		SG	1.828	1.592	15.8	96	0.6	0.2081	0.0004	0.4048	0.0010	373	4	440
A55-4		SG	0.329	0.232	14.1	112	1.0	0.1859	0.0005	0.3453	0.0010	417	3	440
A55-1		SG	1.518	0.796	13.9	147	0.5	0.1566	0.0005	0.2647	0.0007	423	3	465
A25-5		SG	0.890	0.451	19.0	151	1.8	0.1538	0.0004	0.2593	0.0012	312	2	483
A52-7		SG	0.261	0.245	19.2	155	0.7	0.1502	0.0002	0.2509	0.0006	310	2	502
A52-1		SG	1.883	0.889	16.9	161	0.9	0.1447	0.0002	0.2419	0.0008	352	8	464
A52-2		SG	1.888	0.851	16.7	168	0.8	0.1426	0.0002	0.2412	0.0006	356	3	463
A55-2		SG	5.960	2.592	17.6	174	0.7	0.1502	0.0002	0.2236	0.0006	337	3	453
A25-3		SG	1.122	0.372	19.2	222	0.9	0.1222	0.0003	0.1748	0.0006	311	2	473
A25-1		SG	0.315	0.068	15.4	319	2.2	0.1016	0.0001	0.1239	0.0005	385	2	472
A52-3		SG	2.636	0.473	16.0	395	1.8	0.0931	0.0001	0.0989	0.0003	373	7	452
A52-6		SG	2.818	0.448	16.5	444	2.3	0.0888	0.0001	0.0883	0.0003	361	3	461
A25-4		SG	3.319	0.259	14.8	881	4.7	0.0728	0.0001	0.0455	0.0001	403	2	452
A55-5		SG	0.346	0.037	9.6	579	12.7	0.0621	0.0003	0.0982	0.0005	595	5	463
A55-3		SG	0.182	0.016	11.6	709	20.6	0.0777	0.0003	0.1059	0.0004	485	3	495
A52-4		SG	2.078	0.223	6.0	574	5.8	0.1185	0.0002	0.1622	0.0004	849	4	507
K30	Uplaz	CLC	0.290	0.381	12.9	67	0.2	0.2742	0.0006	0.6138	0.0019	432	3	1515
K64		CLC	0.710	0.293	12.7	170	1.2	0.1422	0.0002	0.2943	0.0007	433	2	459
K46		CLC	1.940	0.285	13.2	434	7.5	0.0895	0.0001	0.1954	0.0005	408	2	478
K60		CLC	4.360	0.332	13.1	825	3.4	0.0743	0.0001	0.1515	0.0004	413	3	55
L108		CLC	5.177	0.272	12.4	1072	19.5	0.0698	0.0002	0.1299	0.0005	498	2	448
K62		CLC	5.177	0.272	13.6	1202	18.4	0.0683	0.0001	0.1213	0.0003	404	8	465
L122		CLC	0.406	0.017	12.6	1229	27.8	0.0679	0.0002	0.1263	0.0003	432	2	442
L102		CLC	1.156	0.025	13.1	2617	21.0	0.0619	0.0001	0.0980	0.0003	421	2	461
														20
														7

Table 2 (continued). Data for the conventional U-Pb single grain zircon analyses shown in Fig. 5. MG - multi grain; SG - single grain; CLC - single grain with CL control.



analysis no.	sieve fraction [ $\mu\text{m}$ ]	weight of fraction [mg]	weight of spike [mg]	$HNO_3$ wash	$Pb^*$ / weight of fraction
M1	<74	8.778	.015	no	32
M2	<74	7.559	.015	no	43
M3	<74	6.029	.015	no	39
L39	<74	3.077	.019	yes	51
L2	<74	2.615	.019	yes	49
L17	<74	2.405	.016	yes	50
L42	<74	1.815	.012	yes	49

Table 3. Details on multi grain analyses of sample 03GA50.  $Pb^*$  and results given in table 2.

and they not used for regression (Fig. 5). Nevertheless plot these grains in agreement with the discordia line intersecting 462 Ma and recent times.

A slightly younger intrusion age of  $440 \pm 7$  is revealed by the single grain data of the *Mihalikovo* sample. This age is additionally constrained by multi grain data on the zircon sieve fraction  $<74 \mu\text{m}$ . The multi grain measurements, with  $^{206}\text{Pb}/^{204}\text{Pb}$  ratios between 2860 and 4450, result in an upper intercept age of  $443 \pm 6$  and recent lead loss (table 2 and 4). Details of the multi grain measurements are given in table 3. The ratio of the radiogenic lead ( $Pb^*$ ) and the weight of zircon fraction records the effect of the  $HNO_3$  wash step. Washed fractions have ratios of  $\approx 50$ , whereas the not washed fractions have lower ratios between 32 and 43 (Table 3). This suggest that during washing a large amount of less radiogenic minerals were dissolved resulting in an increase of the radiogenic lead measured. Nevertheless, this does not influence the results of the multi grain dating, because all fractions plot nicely on the one discordia line.

The single grain data of this sample plot closer to the concordia line than the multi grain data. The zircons used for single grain dating were mostly larger than  $100 \mu\text{m}$  (Fig. 4), whereas for the multi grain dating only zircons smaller than  $74 \mu\text{m}$  were used. Therefore a correlation between the discordancy and the grain size becomes apparent. Smaller zircons a larger discordancy (Fig. 5).

The youngest ages are revealed by the *Hoškova* and the *Drotacka* samples. The zircons plot reverse discordant and result in intercept ages of  $334 \pm 19$  and  $329 + 72 - 34$ , respectively (Fig. 5). As can be seen in table 2, the radiogenic lead concentrations and therefore the U concentrations in the zircons are very low. This results in a large common lead correction and most analyses could not be used for regression. The low  $^{206}\text{Pb}/^{204}\text{Pb}$  ratios were reproducible for separate dissolution steps for both samples, thus this is not due to contamination, but due to low U concentrations of the zircons.

Sample name	Location name	lower			upper			no. of points	MSWD	Probability of fit
		intercept	+2 $\sigma$	-2 $\sigma$	intercept	+2 $\sigma$	-2 $\sigma$			
03GA48	Drotacka	-	-	-	329	34	72	3	0	0.99
03GA61	Hoškova	0	0	0	334	19	19	4	1.2	0.31
03GA14	Kralova Hola	0	0	0	345	11	11	20	1.1	0.34
03GA17	Kralova Hola	0	0	0	349	26	26	11	2.3	0.02
VBNT-764a	Hoškova	464	8.3	23	1297	1100	790	2	0	1
VBNT-764b	Hoškova	333	120	110	489	77	50	2	0	1
03GA18	Kolesko	0	0	0	461.6	9.8	9.9	14	0.3	0.99
03GA49	Uplaz	0	0	0	468.6	7.8	7.9	8	0.76	0.62
UP1115	Muran	88	34	40	464	36	33	6	0.36	0.84
03GA50SG	Mihalikovo	0	0	0	439.8	6.6	6.6	9	0.47	0.88
03GA50MG	Mihalikovo	0	0	0	442.6	6.1	6.2	7	1.7	0.12

Table 4. Compilation of the intercept ages shown in Fig. 5. Reinterpreted data from Putiš et al. (2001) and the data from Gaab et al. (in press) are included.

### 5.3 Discussion of the U-Pb data

The compilation of all U-Pb zircon data is presented in Fig. 5 and in table 4. Additional to the samples presented in this study the single grain data presented in Gaab et al. (in press) and the multi grain data for the sample VBNT-76L published in Putiš et al. (2001) are included. Please note that the latter data are reinterpreted and the intercept ages do not correspond to the originally published. This will be discussed in more detail below.

A good accordance can be observed for Koleso (03GA18), Uplaz (03GA49) and Muráň sample (UP1115) (Gaab et al., in press). All these have an upper intercept age between 460 and 470 Ma. Most zircons of these samples are discordant. Only for sample UP1115 a Alpine lower intercept age of  $88 \pm 40$  Ma can be inferred (Gaab et al., in press). The other two samples show recent lead loss (see Table 2). This correspond with the increasing metamorphic grade of Alpine metamorphism in the Veporic unit from Northwest to the Southeast (Janák et al., 2001a).

The Mihalikovo sample (03GA50) yields a slightly younger upper intercept age of  $\approx 440$  Ma for both, the single grain analyses and the multi grain analyses. Two single zircons yield  $^{238}\text{U}/^{206}\text{Pb}$  ages older than 440 Ma ( $449 \pm 2$  Ma and  $462 \pm 9$  Ma) indicating slightly older components present in the zircons. Recent lead loss must be assumed for this sample.

A completely different age spectrum is given by the Drotacka (03GA48) and Hoškova sample (03GA61). Zircons of both samples have extremely low uranium and radiogenic lead contents. Nevertheless both samples yield discordia intercept ages between 320 and 360 Ma, wich is clearly distinct from the other samples. Similar Variscan ages can be also observed for the Kralova Hola samples (02GA14 and 02GA17). The ages between 340 and 350 Ma for these samples are comparable with intrusion ages of diorites and granites in the West Tatra mountains (Poller et al., 2000).

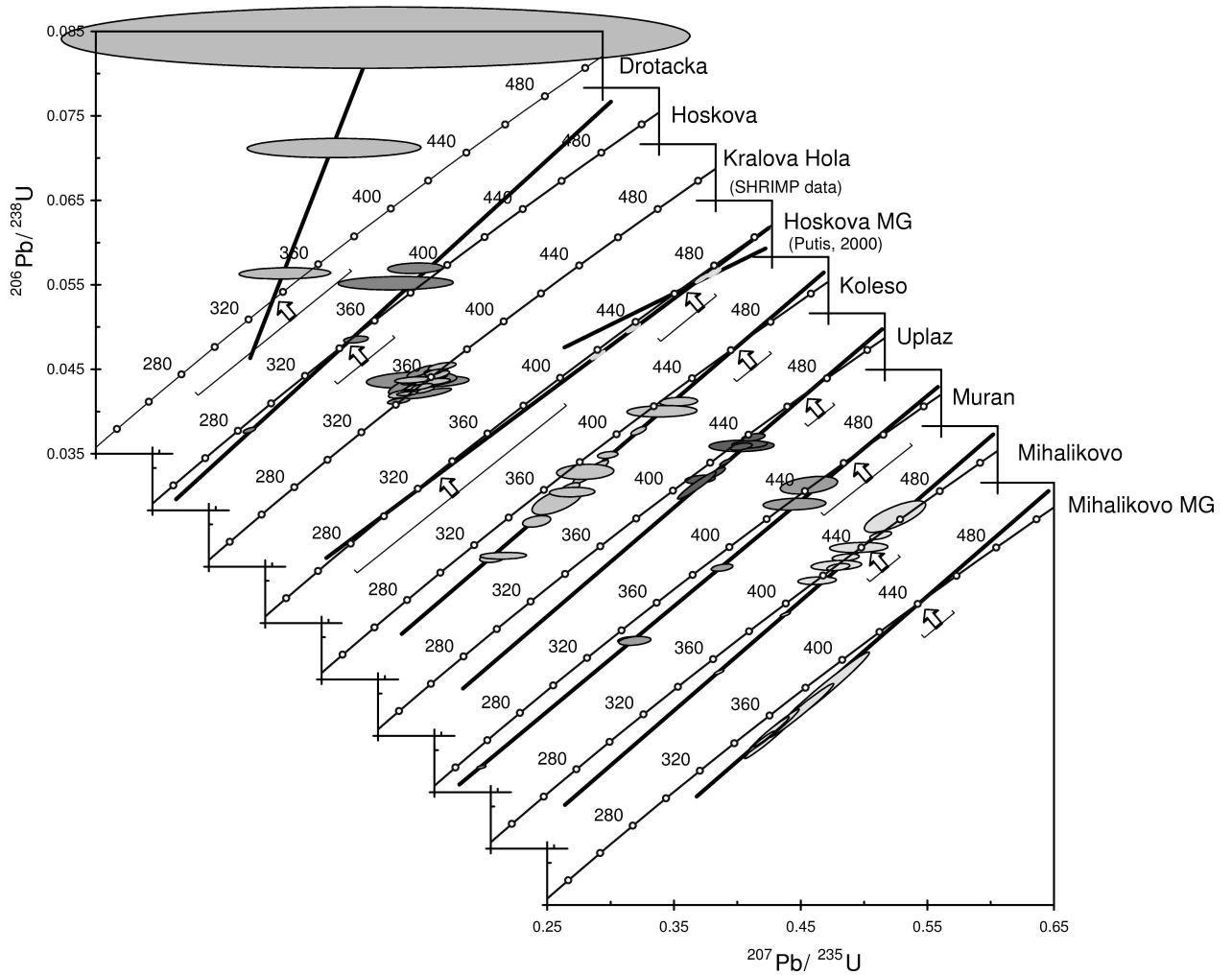


Fig. 5. Compilation of the U-Pb zircon data to identify the two main magmatic/metamorphic events recorded in the Veporic basement. Intercept ages and error bars are indicated by the arrows. Please note that the x- and y- axis are shifted for each sample. Data from Gaab et al. (in press) and from Putiš et al. (2001) given for comparison. Please note that the discordia lines for the latter dataset differ from the originally published ones. Detailed argumentation on page 43. The Kralova Hola data are measured on SHRIMP (Table 1), all other data are TIMS measurements (Table 2). Lower intercept ages are recent except for the Muran sample (see Tab. 4).

Previously published data by Putiš et al. (2001) is, as can be seen in Fig 5, in good accordance with the single and multi grain data of this study, if the data are reinterpreted. Putiš et al. (2001) calculated one discordia line from three of four multi grain data points and interpreted a Variscan metamorphic event at  $348 \pm 31$  Ma and a Cambrian magmatic event at  $514 \pm 24$  Ma. His complete dataset can also be interpreted using two distinct discordia lines and all measured data points. According to this interpretation, the discordia (for the abraded and the HF leached fraction) reveals Pre-Cambrian ages of 1300 Ma, similar to the few old grains observed by the single grain data presented in

this study, and a lower intercept at  $464 \pm 9 - 23$  Ma. The second discordia for the sieve fractions  $>80\mu\text{m}$  and  $>60\mu\text{m}$  reveals a similar upper intercept with a large error and a lower intercept at  $330 \pm 120$  Ma, which may corresponds to the Variscan magmatic event (see table 4).

With the new data presented in this study together with the re-interpretation of the data published by Putiš et al. (2001) a consistent history of the Northern Veporic Unit can be assumed.

## 6 Geochemistry (Koleso Valley)

Geochemical and isotope geochemical analyses were performed on samples from the Koleso Valley (Fig. 1). The results for the main and trace elements are given in table 5. The isotopic data is given in table 6 for the WR-Pb-Pb analyses and in table 7 for the Sr and Nd isotopic composition.

### 6.1 Main and Trace Elements

Samples are classified either as felsic gneisses or as amphibolites (see table 5). The  $\text{SiO}_2$  content of the samples from the Koleso valley vary from 74 to 46 wt%. The total alkali contents for the felsic gneisses are between 5 and 6 wt%, for the amphibolites between 1.4 and 3.2 wt%. No consistent predominance of  $\text{K}_2\text{O}$  vs.  $\text{Na}_2\text{O}$  can be observed for both lithologies. The felsic gneisses are enriched in  $\text{Pb}$ ,  $\text{U}$  and REE, which reflects a strong crustal affinity.

The gabbro shows a completely different geochemistry than the amphibolites. The gabbro has very high  $\text{MgO}$  concentrations of 22.5 wt% and relatively low  $\text{Fe}_2\text{O}_3$  concentrations of 9.75 wt%. Also  $\text{Cr}$  and  $\text{Ni}$  are quite enriched with 1212 and 354 ppm, respectively. In comparison to the amphibolites  $\text{P}_2\text{O}_5$  and the total alkali content is significantly lower. Therefore this gabbro reflects a complete different origin, being more primitive than the amphibolites.

### 6.2 WR-Pb-Pb

WR-Pb-Pb analyses were performed to gain information on possible sources and the evolution of this unit. This dataset will be compared to the WR-Pb-Pb dataset available for the Southern Veporic Unit (Gaab et al., in press). Additionally these datasets enable a comparison of the Veporic unit with data from the Tatric unit published by Poller et al. (2001). Samples for the gabbro from the Koleso and the granites from Kralova Hola were also included.

	Felsic Gneisses			Amphibolites			Gabbro
	02GA01	02GA06	02GA10	02GA04	02GA11	02GA12	02GA08
<i>SiO<sub>2</sub></i>	73.67	58.97	61.33	46.37	49.47	48.26	42.51
<i>Al<sub>2</sub>O<sub>3</sub></i>	11.9	21.9	19.73	13.4	18.43	16.64	9.75
<i>Fe<sub>2</sub>O<sub>3(t)</sub></i>	4.24	8.43	7.56	18.09	15.12	13.85	12.07
<i>MnO</i>	0.03	0.14	0.11	0.29	0.19	0.29	0.18
<i>MgO</i>	1.24	2.38	2.29	8.33	3.58	5.04	22.47
<i>CaO</i>	0.87	0.38	0.26	9.06	6.23	10.17	6.4
<i>Na<sub>2</sub>O</i>	2.32	1.34	0.84	1.51	1.28	0.75	0.76
<i>K<sub>2</sub>O</i>	2.96	3.72	4.98	0.13	1.93	0.77	0.15
<i>TiO<sub>2</sub></i>	0.77	0.96	1.03	3.68	1.75	1.52	0.6
<i>P<sub>2</sub>O<sub>5</sub></i>	0.07	0.08	0.06	0.38	0.31	0.33	0.04
<i>Sum</i>	98.89	99.69	99.41	101	98.96	99.23	99.79
<i>Sc</i>	13	13	14	42	39	42	27
<i>V</i>	76	113	104	512	165	285	144
<i>Cr</i>	57	95	84	22	798	884	1212
<i>Co</i>	63	44	37	98	93	98	88
<i>Ni</i>	29	46	45	37	206	326	354
<i>Cu</i>	3	20	10	37	40	29	36
<i>Zn</i>	63	147	129	146	92	128	78
<i>Ga</i>	17	31	30	28	23	21	11
<i>Rb</i>	101	69	206	3	74	24	8
<i>Sr</i>	224	161	156	387	202	377	67
<i>Y</i>	25	26	36	45	30	27	15
<i>Zr</i>	283	165	277	218	110	95	58
<i>Nb</i>	16	22	20	28	22	15	3
<i>Ba</i>	703	784	1281	bd	763	92	38
<i>Pb</i>	15	30	43	5	16	10	4
<i>Th</i>	14.9	16.1	19.4	bd	bd	bd	bd
<i>U</i>	2.6	4	2.3	bd	bd	0.9	bd
<i>La</i>	41	38	49	19	8	7	3
<i>Ce</i>	74	80	97	53	18	25	9
<i>Pr</i>	5	9	13	11	4	7	bd
<i>Nd</i>	28	34	42	30	10	7	3
<i>Sm</i>	4	7	9	8	1	6	2

Table 5. Geochemistry for the samples from the Koleso valley. Main elements are given in wt%, trace element in ppm. 'bd' for below detection limit.

The diagrams and the principal component analysis was performed using the computer script *CLEO* for *Octave* presented by Gaab et al. (submitted).

The Pb isotopic composition of the felsic gneisses in the Koleso valley are given in table 6. The  $^{206}\text{Pb}/^{204}\text{Pb}$  ratios range between 18.5 and 19.5, the  $^{207}\text{Pb}/^{204}\text{Pb}$  ratios between 15.64 and 15.77 (Fig. 6). The array of these samples plot nearly along the Upper Crustal evolution line (Zartman and Haines, 1988). No age information can be retrieved from the  $^{207}\text{Pb}/^{204}\text{Pb}$  vs.  $^{206}\text{Pb}/^{204}\text{Pb}$  diagram for these samples, because of the large scatter. This indicates that

	$\frac{^{206}\text{Pb}}{^{204}\text{Pb}}$	$\frac{2\sigma}{10^4}$	$\frac{^{207}\text{Pb}}{^{204}\text{Pb}}$	$\frac{2\sigma}{10^4}$	$\frac{^{208}\text{Pb}}{^{204}\text{Pb}}$	$\frac{2\sigma}{10^4}$	$\frac{^{207}\text{Pb}}{^{206}\text{Pb}}$	$\frac{2\sigma}{10^4}$
02GA01-1	18.6580	17	15.7051	16	39.2763	35	0.8417	0.03
02GA04-1	18.5152	56	15.6485	54	38.5485	118	0.8452	0.30
02GA06-1	18.3010	8	15.6706	6	38.5973	18	0.8563	0.01
02GA10-1	18.5306	13	15.7538	8	39.5476	28	0.8501	0.01
02GA10-2	18.9760	13	15.7262	9	40.5359	28	0.8287	0.01
03GA25-1	18.9812	14	15.7272	8	39.7666	31	0.8273	0.07
03GA25-2	18.8808	29	15.7148	14	39.6318	60	0.8311	0.12
03GA25-3	18.8026	8	15.6905	6	39.4111	16	0.8333	0.09
03GA25-4	18.9553	5	15.6961	17	39.2308	55	0.8269	0.14
03GA25-5	19.4093	12	15.7692	13	40.0601	26	0.8113	0.17
03GA25-6	18.9757	7	15.7263	7	39.6593	15	0.8276	0.06
03GA26-2	18.5400	8	15.6764	8	39.1016	17	0.8443	0.07
03GA31-1	18.8224	9	15.7175	8	39.2826	19	0.8338	0.07
03GA31-2	19.3528	6	15.7138	5	38.7783	12	0.8108	0.04
03GA32-1	18.9742	8	15.7155	7	39.5232	18	0.8271	0.06
03GA32-2	19.0425	17	15.7467	14	39.9142	36	0.8257	0.08
03GA32-3	18.8882	10	15.7200	9	39.5146	22	0.8311	0.07
03GA32-4	19.1397	55	15.7564	44	39.8874	114	0.8220	0.07
02GA11-1	18.7406	20	15.6828	14	38.6234	41	0.8368	0.03
02GA11-2	18.7852	5	15.6878	3	38.7153	13	0.8351	0.00
02GA11-3	18.7102	78	15.6813	57	38.7295	164	0.8381	0.45
02GA12-1	18.6988	14	15.6522	6	38.5560	29	0.8371	0.01
02GA12-2	18.7168	100	15.6769	67	38.6493	204	0.8376	0.68
02GA12-3	18.7326	70	15.7363	61	38.8699	146	0.8400	0.44
02GA08-1	18.9546	94	15.6327	67	38.3038	189	0.8247	0.64
02GA08-2	19.1008	59	15.6239	60	38.3501	119	0.8180	0.36
02GA14	19.2951	10	15.7054	9	38.7790	21	0.8140	0.01
02GA17	18.8792	10	15.7378	7	39.1364	21	0.8336	0.01

Table 6. WR-Pb-Pb data for samples from the Koleso valley and from Kralova Hola. Multiple splits were measured for each samples to observe the whole range of Pb isotopic composition.

multiple components were incorporated during formation of these gneisses. The  $^{208}\text{Pb}/^{204}\text{Pb}$  ratios vary between 38.5 and 40.7 for the Koleso gneisses.

The Kralova Hola samples plot within the range of the felsic gneisses at high  $^{207}\text{Pb}/^{204}\text{Pb}$  ratios between 15.62 and 15.64 and intermediate  $^{208}\text{Pb}/^{204}\text{Pb}$  ratios between 38.78 and 39.14 in Fig. 6. The gabbro plots distinct from the other samples at intermediate  $^{206}\text{Pb}/^{204}\text{Pb}$  and low  $^{207}\text{Pb}/^{204}\text{Pb}$  and low

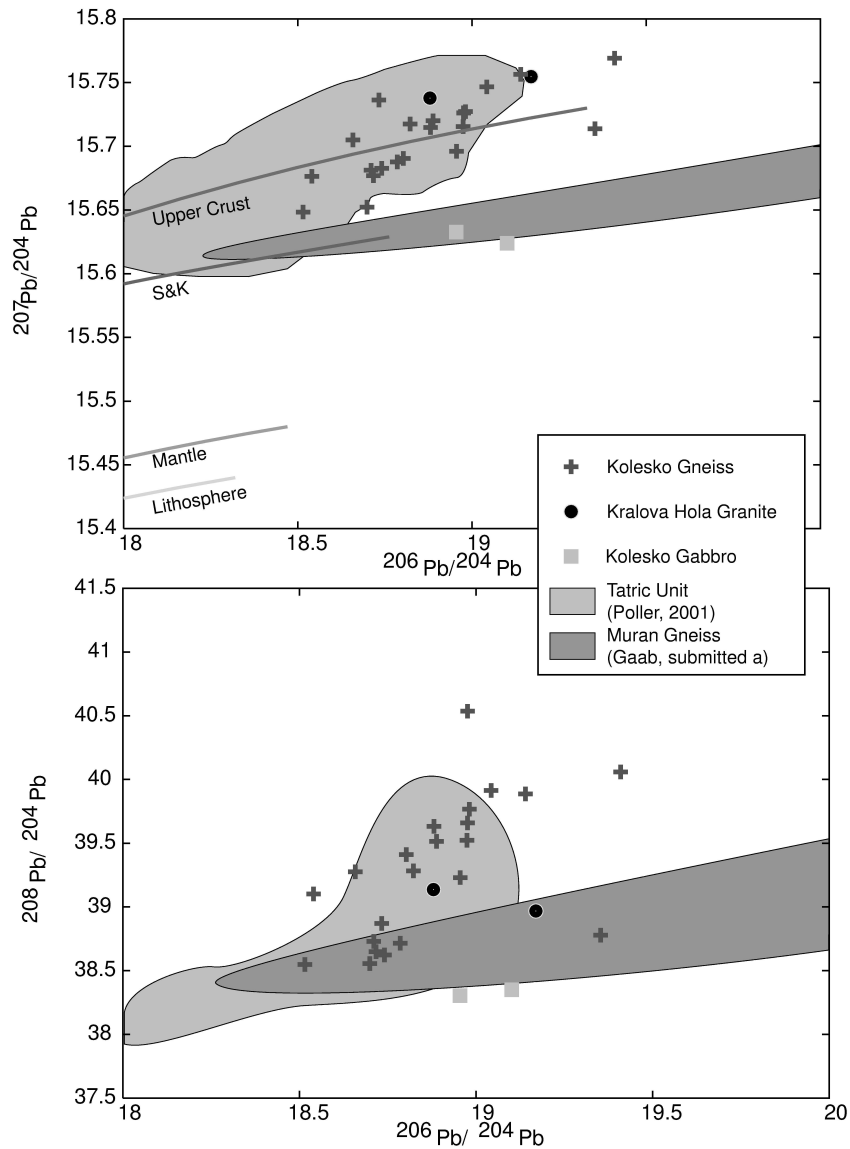


Fig. 6.  $^{206}\text{Pb}/^{204}\text{Pb}$  vs.  $^{207}\text{Pb}/^{204}\text{Pb}$  and  $^{206}\text{Pb}/^{204}\text{Pb}$  vs.  $^{208}\text{Pb}/^{204}\text{Pb}$  diagrams for the samples presented in table 6. Evolution lines in the upper diagram drawn for the reservoirs after Zindler and Hart (1986) and the model after Stacey and Kramers (S&K; 1975).

$^{208}\text{Pb}/^{204}\text{Pb}$ . This indicates a more primitive source for this gabbro with a lower Th/U ratio compared to the other samples.

In comparison to the Muráň gneiss, the felsic gneisses plot at more radiogenic values in the  $^{207}\text{Pb}/^{204}\text{Pb}$  vs.  $^{206}\text{Pb}/^{204}\text{Pb}$  as well as in the  $^{208}\text{Pb}/^{204}\text{Pb}$  vs.  $^{206}\text{Pb}/^{204}\text{Pb}$  diagram. The slope of a reference line would be larger for the Kolesko samples than for the Muráň samples. Nevertheless point the two datasets to a similar unradiogenic component. The principal component analysis (Fig. 7) clarifies the relation of these two datasets and will be discussed later.

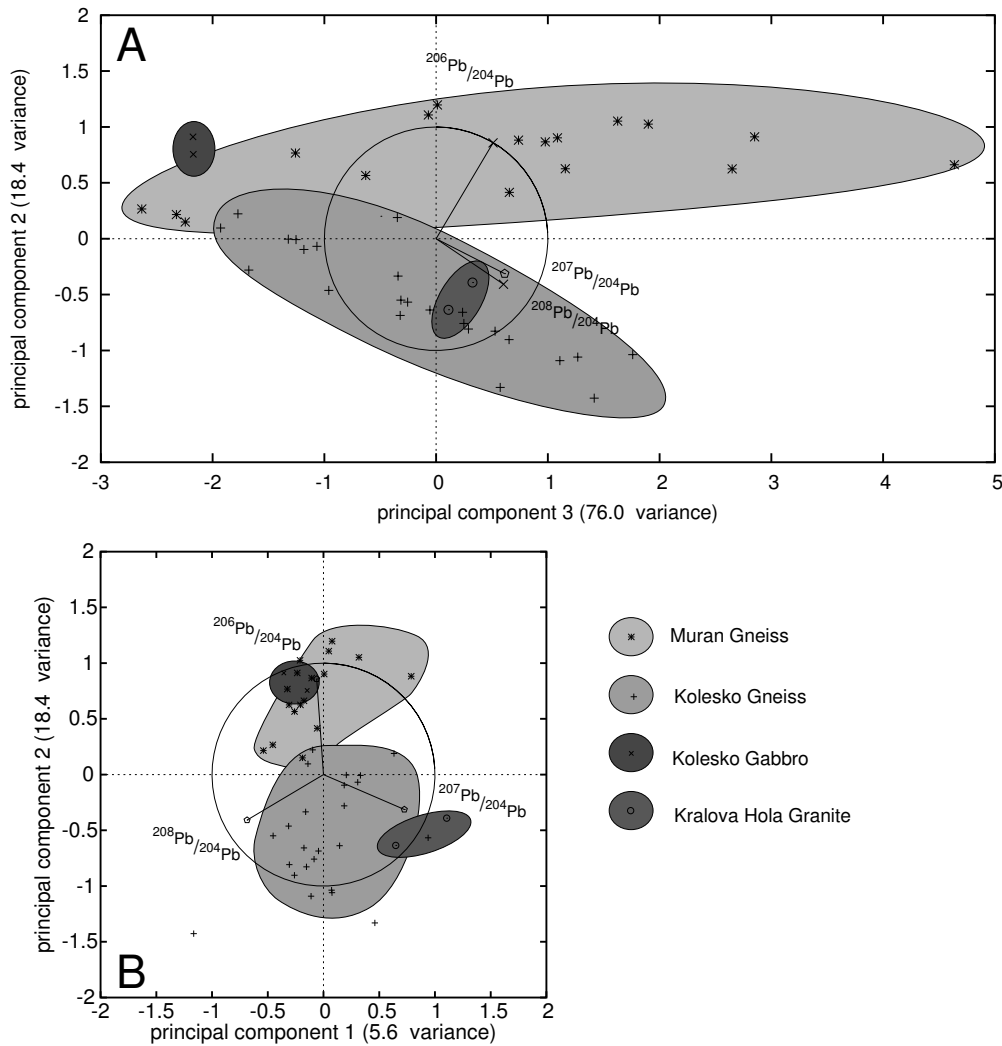


Fig. 7. Principal component analyses of the common lead data presented in this study (table 6) together with the common lead data published in Gaab et al. (in press).

Compared to the WR-Pb-Pb data published by Poller et al. (2001), the data for the Koleso gneisses fall mostly within the range of values observed for the Tatric Unit in the  $^{207}\text{Pb}/^{204}\text{Pb}$ - $^{206}\text{Pb}/^{204}\text{Pb}$  and the  $^{208}\text{Pb}/^{204}\text{Pb}$ - $^{206}\text{Pb}/^{204}\text{Pb}$  diagram (Fig. 6). They display relative radiogenic values and few samples plot at more radiogenic values outside the field for the Tatric unit. The samples from Kralova Hola fall in the same array at relatively high  $^{207}\text{Pb}/^{204}\text{Pb}$  ratios, whereas the gabbro plots outside this array at low  $^{207}\text{Pb}/^{204}\text{Pb}$  ratios.

With the principal component analysis the differences between the datasets for the Koleso gneisses and for the Muráň gneisses can be shown:

The principal component 3 observes the largest variance of 76% for the Koleso and the Muráň dataset (Fig. 7A). The  $^{206}\text{Pb}/^{204}\text{Pb}$ ,  $^{207}\text{Pb}/^{204}\text{Pb}$  and the  $^{208}\text{Pb}/^{204}\text{Pb}$  ratios have nearly the same influence on this main principal com-



ponent. The range of the Muráň samples overlap the range of the Koleso samples. This principal component is interpreted to display mostly the radiogenic growth of Pb from U and Th. The Muráň dataset plots nearly parallel to this principal component. This corresponds to the interpretation of Gaab et al. (in press) that the dataset displays the metamorphic Pb equilibration around 134 Ma reflecting the Alpine overprint.

The principal component 2 with 18.4% variance displays only a minor overlap of the two datasets. The  $^{206}\text{Pb}/^{204}\text{Pb}$  correlates positively with this principle component, whereas the  $^{207}\text{Pb}/^{204}\text{Pb}$  and  $^{208}\text{Pb}/^{204}\text{Pb}$  are negatively correlated. In the plot of the two principal components with the largest variance, two different trends can be observed for the Muráň and the Koleso samples (Fig. 7A). This reflects a distinct evolution for both units. Nevertheless both units have an overlap at unradiogenic values. This indicates a common source for both units. For the samples from Koleso this trend is interpreted to reflect a mixing with a radiogenic component.

The principal component 1 with 5.6% variance is plotted against the principal component 2 in Fig. 7B. The Kralova Hola granits plot distinct from the Koleso samples showing that the Kralova Hola samples do not represent the radiogenic component responsible for the variations of the Koleso samples.

The gabbro in the Koleso valley plot completely distinct from the other samples in Fig. 7, thus reflecting a distinct source.

The Pb isotopic variation of the Koleso samples can be interpreted as a mixing between a less evolved mantle reservoir and more evolved crustal reservoir. The timing of this mixing can not be inferred from this dataset. The less evolved lead reservoir is comparable with the unradiogenic samples observed in the Muráň area, therefore a similar geodynamic setting for both units is inferred. The evolved crustal reservoir is characterized by high  $^{207}\text{Pb}/^{204}\text{Pb}$  and  $^{208}\text{Pb}/^{204}\text{Pb}$  ratios as identified by the principal component 2. This radiogenic component is not observed in the Muráň area. The Kralova Hola samples also are influenced by a crustal component. But this crustal component is distinct from the crustal component observed in the Koleso samples (Fig. 7), revealing a distinct history for these units.

### 6.3 Sr and Nd Isotopes

The available  $^{87}\text{Sr}/^{86}\text{Sr}$  and  $\epsilon\text{Nd}$  data for rocks from the Central Western Carpathians are presented in Fig. 8 to reveal different sources in these samples. The data are compared to published data on the Muráň gneiss (Gaab et al., in press) and to the Tatric unit (Poller et al., 2001, in press). In this diagram, the isotopic compositions are calculated back in time according to Ordovician or

sample	$^{87}\text{Sr}/^{86}\text{Sr}$ <sup>1</sup> <sub>tod</sub>	$\pm 2\sigma$	$^{87}\text{Rb}/^{86}\text{Sr}$	$^{87}\text{Sr}/^{86}\text{Sr}$ <sub>ini</sub>	$^{143}\text{Nd}/^{144}\text{Nd}$ <sup>1</sup> <sub>tod</sub>	$\pm 2\sigma$	$^{147}\text{Sm}/^{144}\text{Nd}$ <sup>2</sup>	$\epsilon_{\text{Nd,tod}}$	$\epsilon_{\text{Nd,ini}}$	$T_{DM}^{\text{Nd}}[\text{Ga}]$ <sup>4</sup>
02GA01 <sup>6</sup>	0.720803	16	1.27 <sup>2</sup>	0.712401	0.511881	13	0.097	-15	-8.8	1.8 <sup>5</sup>
02GA06 <sup>6</sup>	0.721154	16	1.21 <sup>2</sup>	0.713151	0.511912	25	0.13	-14	-10	1.9 <sup>5</sup>
02GA10 <sup>6</sup>	0.738932	92	3.73 <sup>2</sup>	0.714286	0.511921	12	0.14	-14	-10	2.0 <sup>5</sup>
02GA04 <sup>6</sup>	0.708375	23	0.02 <sup>2</sup>	0.708230	0.512782	09	0.17	2.8	4.5	1.1
02GA11 <sup>6</sup>	0.715292	25	1.03 <sup>2</sup>	0.708458	0.512519	99	0.063	-2.3	5.6	0.62
02GA12 <sup>6</sup>	0.711133	44	0.18 <sup>2</sup>	0.709944	0.512856	10	0.19	4.3	4.7	1.5
02GA08 <sup>6</sup>	0.704393	10	0.34 <sup>2</sup>	0.702813	0.512920	16	0.19	5.5	5.9	1.2
02GA14 <sup>7</sup>	0.707460	17	0.93 <sup>3</sup>	0.701336	0.512400	12	0.098	-4.6	1.2	0.94
02GA17 <sup>7</sup>	0.711901	15	1.55 <sup>3</sup>	0.701669	0.512398	06	0.12	-4.7	-0.4	1.2

<sup>1</sup> measured on TIMS *MAT261* multicollection. Errors are given as  $2\sigma$  deviation of the weighted mean (6-25 blocks)

<sup>2</sup> calculated from the RFA measurement (Tab. 5)

<sup>3</sup> measured on single collector ICP-MS *Element2*

<sup>4</sup> calculated using the depleted mantle model after Liew and Hofmann (1988)

<sup>5</sup> two step model at 460 Ma ( $^{147}\text{Sm}/^{144}\text{Nd} = 0.12$ ) according Liew and Hofmann (1988)

<sup>6</sup> initial values calculated for 460 Ma

<sup>7</sup> initial values calculated for 330 Ma

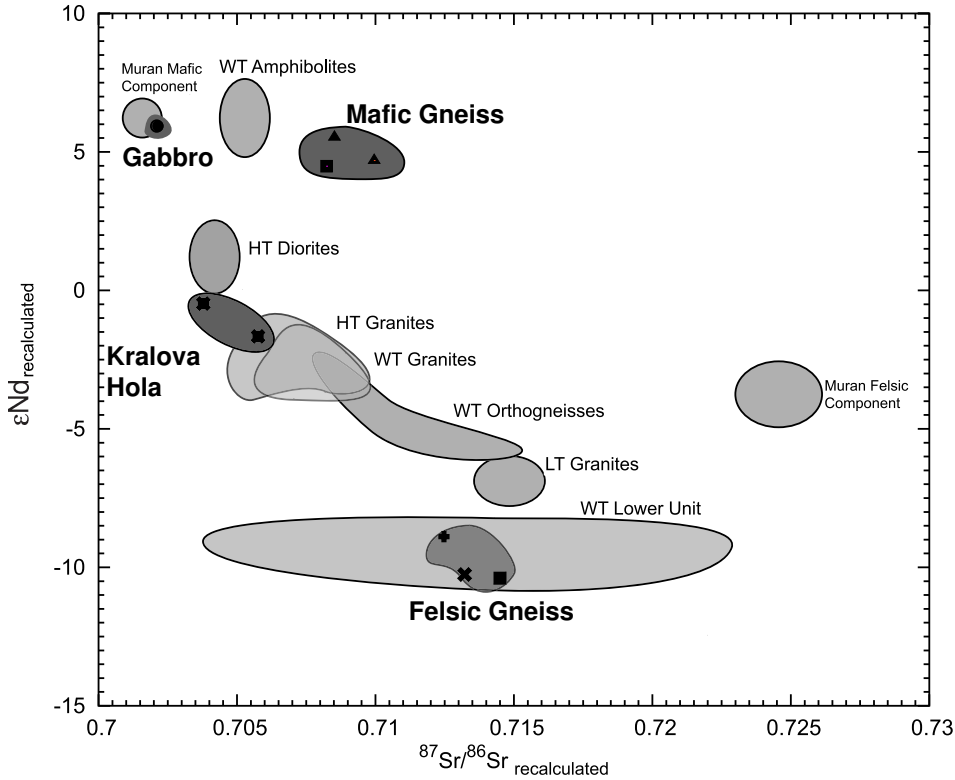


Fig. 8.  $\epsilon Nd$  vs.  $^{87}Sr/^{86}Sr$  diagram. Isotopic compositions are calculated back to initial values. Data for the High Tatra (HT), Western Tatra (WT), Low Tatra (LT) (Poller et al., 2001, in press) and the Kralova Hola samples are calculated to 330 Ma, data from the Koleso valley and the Muráň area (Gaab et al., in press) are calculated to 460 Ma.

Carboniferous formation age. In order not to over interpret the datasets and to include additional uncertainties of the exact formation age, the samples are either recalculated to initial values at 460 Ma or to at 330 Ma, respectively. The data for the Tatra mountains from Poller et al. (2001, in press) are recalculated to 330 Ma, except the data for the metasediments from the Lower Unit in the Western Tatra Mountains, which are recalculated to 460 Ma. The samples presented in this study are recalculated to 460 Ma, except the Kralova Hola samples, which formed during the Variscan orogeny (see Fig. 5). The data of the Muráň area are plotted according to the interpretation presented in (Gaab et al., in press).

The basement samples from the Koleso area are calculated to initial values at 460 Ma. Two distinct groups can be recognized in Fig 8. The mafic samples form a small array at un-radiogenic  $^{87}Sr/^{86}Sr_{ini,460}$  values of .705 to .715 with radiogenic  $\epsilon Nd_{ini,460}$  values between 4 and 6. This array does not coincide with the primitive mantle composition of Zindler and Hart (1986), thus indicating either a crustal contamination or a non-primitive source composition. All felsic samples plot in a narrow array between .712 to .715 and -11 to 8 for  $^{87}Sr/^{86}Sr_{ini,460}$  and  $\epsilon Nd_{ini,460}$ , respectively. These values reflect a major

influence of an evolved crustal component in these samples.

The gabbro sample from the Koleso area plots at low  $^{87}\text{Sr}/^{86}\text{Sr}_{ini,460}$  values of .703 and  $\epsilon Nd_{ini,460}$  values of 6, reflecting a more primitive source as the mafic gneisses. Initial values for this sample are also calculated using 460 Ma.

The Kralova Hola samples vary between .703 to .705 for  $^{87}\text{Sr}/^{86}\text{Sr}_{ini,330}$  and -1.5 to -0.5 for  $\epsilon Nd_{ini,330}$ , which are values close to the bulk earth composition after Zindler and Hart (1986). The mylonitized sample plots at slightly higher  $\epsilon Nd_{ini}$  and lower  $^{87}\text{Sr}/^{86}\text{Sr}_{ini}$ , which probably is caused by deformation and metamorphism.

The mean crustal resident ages,  $T_{DM}^{Nd}$  for the samples are presented in table 7. Two age groups become evident. The felsic samples result in old  $T_{DM}^{Nd}$  between 1.8 and 2.0 Ga using a two step approach with 460 Ma as age for the second step. These results fit well with  $T_{DM}^{Nd}$  for the Lower Unit in the Western Tatra between 1.8 and 2.0 Ga (Poller et al., 2001). All mafic sample reveal younger  $T_{DM}^{Nd}$  between 0.6 and 1.5 Ga and thus have crustal resident ages comparable to the diorites in the High Tatra mountains (1 Ga) and the Granites from the Tatra mountains (1.25-1.45 Ga, Poller et al., 2001). The Kralova Hola granite has  $T_{DM}^{Nd}$  between 1 and 1.2 Ga, the gabbro in the Koleso Valley has a  $T_{DM}^{Nd}$  of 1.2 Ga.

In comparison with published data for the West- and High Tatra Mountains (Poller et al., 2001), the basement rocks from the Koleso area can be clearly distinguished. The felsic gneisses have lower  $\epsilon Nd$  and are only comparable with the meta sediments of the Lower Unit in the Western Tatra Mountains. The mafic gneisses and the gabbro plot distinct from amphibolites from the Western Tatra (Poller et al., in press) and from the other reference fields from the Tatra Mountains (Poller et al., 2001). This indicates, that the Veporic basement has different sources as the Tatric unit which formed during the Variscan orogeny.

The samples from Kralova Hola on the other hand reveal an overlap in  $^{87}\text{Sr}/^{86}\text{Sr}$   $\epsilon Nd$  with diorites and granites from the High Tatra mountains (Poller et al., 2001). Thus the Kralova Hola is not only similar in age with the Tatric unit, but also in the isotopic composition.

The Muráň gneiss felsic component presented in Gaab et al. (in press) in the Southern Veporic Unit plot distinct from the Koleso samples. The felsic member has too high  $^{87}\text{Sr}/^{86}\text{Sr}$  ratios and too high  $\epsilon Nd$  values compared to the felsic gneisses. The Muráň mafic component coincides with the gabbro from the Koleso valley, but not with the amphibolites (Fig. 8).

## 7 Conclusion

A common evolution for the whole Veporic Unit in Paleozoic times can be inferred from the U-Pb zircon data presented in this study. The apparent dichotomy, which arises with comparison of literature data (Putiš et al., 2001), can be circumvented, if the literature data are reinterpreted.

At least three major events can be recognized in the U-Pb data from the Northern Veporic Unit:

- (1) Major Ordovician magmatic event (460-470 Ma), followed by minor magmatic activity ( $\approx 440$  Ma).
- (2) Variscan magmatic and metamorphic event (330-350 Ma) with formation of granitoids and re-crystallization of Ordovician basement.
- (3) Alpine metamorphic event during the Cretaceous time, which caused locally lead loss in the zircons. This event is mainly recorded in the Southern Veporic Unit (Gaab et al., in press), according to the increasing metamorphic grade observed by Janák et al. (2001a).

The common lead data together with the isotopic data from the Koleso valley reveal a marked difference between the Northern Veporic Unit and the Southern Veporic Unit (i.e. the Muráň gneiss). It reveals an important role of an additional source of radiogenic lead, which is absent in the Muráň Gneiss. This source could not be identified within the Veporic unit, but is characterized by high  $^{207}\text{Pb}/^{204}\text{Pb}$  and  $^{208}\text{Pb}/^{204}\text{Pb}$  ratios and therefore represents a typical crustal source. The Kralova Hora granites point in a similar direction as the Koleso gneisses, but do not coincide exactly with the observed variations as demonstrated by the principal component analysis.

The  $\epsilon\text{Nd}$  and the  $^{87}\text{Sr}/^{86}\text{Sr}$  isotopic compositions of the felsic gneisses in the Northern Veporic Unit are similar to the metasedimentary Lower Unit in the Western Tatra and distinct from the other units observed in the Tatra mountains and in the Veporic unit. The Lower Unit has a minimum sedimentation age of  $\approx 500$  Ma according to U-Pb zircon studies (Gurk, 1999; Gurk and Poller, 1999) and therefore can not be attributed as sediments derived from these rocks. But a common source of both units can be assumed.

The amphibolites in the Koleso valley, which were metamorphosed under HP metamorphic conditions (Janák et al., 2003), are distinct in their  $\epsilon\text{Nd}$  and  $^{87}\text{Sr}/^{86}\text{Sr}$  isotopic composition from the amphibolites from the Western Tatra mountains Poller et al. (in press). They are characterized by relatively high  $^{87}\text{Sr}/^{86}\text{Sr}_{ini}$  and low  $\epsilon\text{Nd}$  thus reflecting a crustal component. They are also distinct in their  $\epsilon\text{Nd}$  and  $^{87}\text{Sr}/^{86}\text{Sr}$  composition from Muráň mafic member observed in the Southern Veporic Unit (Gaab et al., in press). Only the gabbro from the Koleso valley depicts marked similarities with the Muráň mafic component, suggesting common sources.

## Acknowledgements

JH is thanked for help at the electron microscope for cathodo-luminescence imaging. DN for her help and presence at the clean-lab. AH is gratefully acknowledged for providing the opportunity to perform this study at MPI, Mainz. The field work has been partly supported (to MJ) from grants APVT-20-020002 and VEGA 3167.

## References

- Bezák, V., 1991. Metamorphic conditions of the Veporic unit in the Western Carpathians. *Geologický Zborník - Geologica Carpathica* 42, 219–222.
- Cambel, B., Král, J., Burchart, J., 1990. Izotopová geochronológia kryštálinka západných karpát. VEDA.
- Compston, W., Williams, I., Meyer, C., 1984. U-Pb geochronology of zircons from lunar breccia 73217 using a sensitive high mass-resolution ion microprobe. *Journal of Geophysical Research* 89, B525–B534. Supplement.
- Dallmeyer, R. D., Neubauer, F., Handler, R., Fritz, H., Müller, W., Pana, D., Putiš, M., 1996. Tectonothermal evolution of the internal Alps and Carpathians: Evidence from  $^{40}\text{Ar}/^{39}\text{Ar}$  mineral and whole-rock data. *Ecolgae geol. Helv.* 89, 203–227.
- Finger, F., Broska, I., Haunschmid, B., Hraško, L., Kohút, M., Krenn, E., Petřík, I., Riegler, G., Uher, P., 2003. Electron-microprobe dating of monazites from Western Carpathian basement granitoids: plutonic evidence for an important Permian rifting event subsequent to Variscan crustal anatexis. *Int. J. Earth Sci.* , 86–98.
- Gaab, A., Janák, M., Poller, U., Todt, W., in press. Alpine reworking of Ordovician protoliths in the Western Carpathians: Geochronological and geochemical data on the Muráň Gneiss Complex. *Lithos* .
- Gaab, A., Todt, W., Poller, U., submitted. CLEO: Common lead evaluation using Octave. *Computers & Geosciences* .
- Gurk, C., 1999. Petrographie, Geochemie und Geochronologie der unteren Einheit, Tatricum, Westliche Tatra (Slovakei). Unpublished Diploma Thesis, University of Mainz.
- Gurk, C., Poller, U., 1999. Petrography, geochemistry and geochronology of the Lower Unit, Western Tatra Mts (Slovakia). *Journal of Conference Abstracts* 4, 809.
- Janák, M., Cosca, M., Finger, F., Plašienka, D., Koroknai, B., Lupták, B., Horváth, P., 2001a. Alpine (Cretaceous) metamorphism in the Western Carpathians: P-T-t paths and exhumation of the Veporic core complex. *Geologisch-Paläontologische Mitteilungen Innsbruck* 25, 115–118.
- Janák, M., Finger, F., Plašienka, D., Petřík, I., Humer, B., Méres, Š., Lupták,

- B., 2002. Variscan high P-T recrystallization of Ordovician granitoids in the Veporic unit (Nízke Tatry Mountains, Western Carpathians): new petrological and geochronological data. *Geolines* 14, 38–39.
- Janák, M., Méres, Š., Ivan, P., 2003. First evidence for omphacite and eclogite facies metamorphism in the veporic unit of the Western Carpathians. *Journal of the Czech Geological Society* 48, 69.
- Janák, M., Plašienka, D., Frey, M., Cosca, M., Schmidt, S., Lupták, B., Méres, Š., 2001b. Cretaceous evolution of a metamorphic core complex, the Veporic unit, Western Carpathians (Slovakia): P-T conditions and *in situ*  $^{40}\text{Ar}/^{39}\text{Ar}$  UV laser probe dating of metapelites. *J. Metamorphic Geol.* 19, 197–216.
- Koroknai, B., Horvath, P., Balogh, I., K. Dunkl, 2001. Alpine metamorphic evolution and cooling history of the Veporic basement in northern Hungary: new petrological and geochronological constraints. *Int. J. Earth Sci.* 90, 740–751.
- Kováčik, M., Král', J., Maluski, H., 1996. Metamorphic rocks in the Southern Veporicum basement: their Alpine metamorphism and thermochronologic evolution. *Mineralia Slovaca* 28, 185–202.
- Král', J., Frank, W., Bezák, V., 1996.  $^{40}\text{Ar}$ - $^{39}\text{Ar}$  spectra from amphibole of veporic amphibolitic rocks. *Mineralia Slovaca* 28, 501–513.
- Liew, T., Hofmann, A., 1988. Precambrian crustal components, plutonic associations, plate environment of Hercynian Fold Belt of central Europe: Indications from a Nd and Sr isotopic study. *Contrib. Mineral. Petrol.* 98, 129–138.
- Ludwig, K. R., 2001a. Isoplot/ex rev. 3.49 A geochronological Toolkit for Microsoft Excel. Berkeley Geochronological Center; Special Publications No. 1a .
- Ludwig, K. R., 2001b. SQUID 1.02 - A user's Manual. Berkeley Geochronological Center; Special Publications No. 2 .
- Lupták, B., Janák, M., Plašienka, D., Schmidt, S. T., Frey, M., 2000. Chloritoid-kyanite schists from the Veporic unit, Western Carpathians, Slovakia: implications for Alpine (Cretaceous) metamorphism. *Schweiz. Mineral. Petrogr. Mitt.* 80, 211–222.
- Lupták, B., Janák, M., Plašienka, D., Schmidt, S. T., 2003. Alpine low-grade metamorphism of the Permian-Triassic sedimentary rocks from the Veporic Superunit, Western Carpathians: Phyllosilicate composition and "crystallinity" data. *Geologický Zborník - Geologica Carpathica* 54, 367–375.
- Lupták, B., Thöni, M., Janák, M., Petrík, I., 2004. Sm-Nd isotopic chronometry of garnets from the veporic unit, Western Carpathians: some preliminary age results and P-T constraints. *Geolines* 17.
- Maluski, H., Rajlich, P., Matte, P., 1993.  $^{40}\text{Ar}/^{39}\text{Ar}$  dating of the Inner Carpathians Variscan basement and Alpine mylonitic overprinting. *Tectonophysics* 223, 313–337.
- Plašienka, D., Grecula, P., Putiš, M., Hovorka, D., Kováčik, M., 1997. Evolution and structure of the Western Carpathians: an overview. In: *Grec*

- ula, P., Hovorka, D., Putiš, M. (Eds.), Geological Evolution of the Western Carpathians. Mineralia Slovaca - Monograph, 1–24.
- Poller, U., Janák, M., Kohút, M., Todt, W., 2000. Early Variscan Magmatism in the Western Carpathians: U-Pb zircon data from granitoids and orthogneisses of the Tatra Mts (Slovakia). *Int. J. Earth Sci.* 89, 336–349.
- Poller, U., Kohút, M., Gaab, A., Todt, W., in press. Pb, Sr and Nd isotope study of two co-existing magmas in the Nízke Tatry Mountains, Western Carpathians (Slovakia). *Mineralogy and Petrology*.
- Poller, U., Kohút, M., Todt, W., Janák, M., 2001. Nd, Sr, Pb isotope study of the Western Carpathians: implications for Palaeozoic evolution. *Schweiz. Mineral. Petrogr. Mitt.* 81, 159–174.
- Poller, U., Todt, W., 2000. U-Pb single zircon data of granites from the High Tatra Mountains (Slovakia): implications for the geodynamic evolution. *Trans. R. Soc.* 91, 235–243.
- Poller, U., Uher, P., Broska, I., Plasienska, D., Janák, M., 2002. First Permian-Early Triassic zircon ages for tin-bearing granites from the Gemeric unit (Western Carpathians, Slovakia): connection to the post-collisional extension of the Variscan orogen and S-type magmatism. *Terra Nova* 14, 41–48.
- Putiš, M., Filová, I., Korikovsky, S. P., Kotov, A. B., Madarás, J., 1997. Layered metaigneous complex of the veporic basement with features of the Variscan and Alpine thrust tectonics (Western Carpathians). In: Grecula, P., Hovorka, D., Putiš, M. (Eds.), Geological Evolution of the Western Carpathians. Mineralia Slovaca - Monograph, Geocomplex, 175–196.
- Putiš, M., Kotov, A., Korikovsky, S., Salnikova, E., Yakoleva, S., Berezhnaya, N., Kovach, V., Plotkina, J., 2001. U-Pb zircon ages of dioritic and trondhjemitic rocks from a layered amphibolitic complex crosscut by granite vein (Veporic basement, Western Carpathians). *Geologický Zborník - Geologica Carpathica* 52, 49–60.
- Stacey, J. S., Kramers, J. D., 1975. Approximation of terrestrial lead isotope evolution by a two-stage model. *Earth Planet. Sci. Lett.* 26, 207–221.
- Thöni, M., Petřík, I., Janák, M., Lupták, B., 2003. Preservation of Variscan garnet in Alpine metamorphosed pegmatite from the Veporic unit, Western Carpathians: evidence from Sm-Nd isotope data. *Journal of the Czech Geological Society* 48, 123–123.
- Vozárová, A., Sotáček, J., Ivanička, J., 1998. A new microfauna from the Early Paleozoic formations of the Gemericum (foraminifera): constraints for another fossils or subfossils. In: Rakús, M. (Ed.), Geodynamic development of the Western Carpathians. Dionýz Štúr Publication, 47–61.
- Wendt, J., Todt, W., 1991. A vapor digestion method for dating single zircons by direct measurement of U and Pb without chemical separation. *Terra Abstracts* 3, 507–508.
- White, W., Patchett, J., 1984. Hf-Nd-Sr isotopic and incompatible element abundances in island arcs: implications for magma origins and crust-mantle evolution. *Earth Planet. Sci. Lett.* 67, 167–185.
- Williams, I., 1998. U-Th-Pb Geochronology by Ion-Microprobe. In: McK-



- ibben, M., Shanks III, W., Ridley, W. (Eds.), Application of microanalytical techniques to understanding mineralization processes, vol. 7 of Reviews in Economic Geology. The Society of Economic Geologists, 1–35.
- Zartman, R., Haines, S., 1988. The plumbotectonic model for Pb isotopic systematics among major terrestrial reservoirs - A case for bi-directional transport. *Geochim. Cosmochim. Acta* 52, 1327–1339.
- Zindler, A., Hart, S., 1986. Chemical Geodynamics. *Annual Review of Earth and Planetary Sciences* 14, 493.

# Chapter 4

The magmatic and post-magmatic evolution recorded by REE, Pb and Sr isotopes of the Dlhá Dolina intrusive complex will be discussed in this chapter. This intrusive complex belongs to the sS-type granites occurring in several areas in the Gemeric Unit. They typically contain tourmaline and evolve in some places to W-Nb-Ta-Sn rich granites.

The manuscript and the analyses are prepared by A.S. Gaab. IB and MK motivated this study by introducing the author to the field geology. ID provided access to the drill core samples. IB also provided an additional dataset for main and trace elements and the reference dataset for Gemeric Granites. WT and UP introduced the author to the analytical methods and provided access to the clean lab and to the mass spectrometer.

The manuscript presented in the following will be submitted to *Geologica Carpathica*. First results from the Sr isotopes were presented by Gaab et al. (2003a) at the meeting of the Deutsche Mineralogische Gesellschaft.

# Redistribution of REE and of U, Th, Pb, Sr, and Rb during intrusion and auto-metasomatism of the Dlhá Dolina granite (Gemic Unit, Eastern Slovakia)

A.S. Gaab<sup>a,\*</sup> IB<sup>b</sup> ID<sup>b</sup> MK<sup>b</sup> UP<sup>a</sup> WT<sup>a</sup>

<sup>a</sup>*Max-Planck-Institut für Chemie; Abt. Geochemie; PF 3060; 55020 Mainz;  
Germany*

<sup>b</sup>*Geological Institute; Slovak Academy of Sciences; P.O. Box 106;  
84005 Bratislava 45; Slovak Republic*

---

## Abstract

The variations of REE within the magmatic complex in the Dlhá Dolina show a large range from 50 times chondritic to values below 0.1 times chondritic. Both, enrichment and depletion of the REE concentration, can be shown in this complex. Enrichment is due to magmatic fractionation, whereas the depletion is caused by intense auto-metasomatic processes, which also produce Tetrad effects of  $TE_{1,3} > 1.6$ .

These magmatic and metasomatic processes also led to a redistribution of U, Th, and Rb, which produced with time different signatures in the Pb and the Sr isotopic composition. The Pb isotopic composition constrains the minimum intrusion age of this complex to 241 Ma and records the intensive fractionation of U from Th during metasomatism. The Sr isotopic composition of the magmatic dominated samples agree with these age constraints and the initial  $^{87}\text{Sr}/^{86}\text{Sr}$  composition is estimated at 0.704. The strongly metasomatized samples show too radiogenic  $^{87}\text{Sr}/^{86}\text{Sr}_{ini}$  values, which are interpreted to be produced during metasomatism by intense depletion of Rb.

*Key words:* REE Tetrad effect, sS-type granite, metasomatism, Gemic Unit

---

---

\* Andreas S. Gaab

*Email address:* gaab at mpch-mainz.mpg.de (A.S. Gaab).

## 1 Introduction

Granites in Gemeric Unit show strong magmatic fractionation and metasomatic overprint. They form a large variety of granitoid rocks ranging from tourmaline bearing granites to Sn-bearing greisen. These Spiš-Gemer granites can be classified as so called specialized S-type granites (Broska et al., 2002). Often feldspatization, albitization, special mineralization and formation of greisenised cupolas can be observed (Malachovský et al., 1983; Dianiška et al., 2002).

The aim of this paper is to use the redistribution of trace elements, mainly REE, and radiogenic isotopes (Pb and Sr) within the granite complex of the Dlhá Dolina to gain information on the processes during formation as well as on the age of final fluid activity.

The Dlhá Dolina sS-type granitoid intrusion is build up by two main units, a barren Lower Complex and an ore-bearing Upper Complex with rare metal W-Nb-Ta-Sn mineralizations. Due to the available drill cores a vertical profile is sampled and the evolution from the barren granite to the rare-metal-rich granite can be studied in detail.

## 2 Geological Setting

The sub-surface granite complex is located in the Dlhá Dolina valley near Gemerská Poloma in Eastern Slovakia (Fig. 1). It belongs to the specialized S-type granite suite of the Gemeric superunit (Broska and Uher, 2001). This represents the uppermost of three thick skinned Alpine nappes (Plašienka, 1997). The Gemeric superunit forms a mega-anticline and is build up by meta-volcanosedimentary rocks belonging to the Gelnica and the Rakovec Group.

To the NE the Veporic superunit underlies the Gemeric superunit. The Veporic superunit consist mainly of Pre-Variscan basement units (Gaab et al., in press), magmatites (e.g. Poller et al., 2000) and paragneisses (Lupták et al., 2000). The Northernmost and tectonic highest unit is the Tatric superunit, which consists mainly of I- and S-type granites, orthogneisses, amphibolites and to a minor extend paragneisses (Poller et al., 2000).

The intensively folded Lower Palaeozoic volcano-sedimentary complexes of the Gemeric superunit (see Fig. 1) consist mainly of phyllites and pyroclastites with rhyolitic to dacitic composition as well as lenses of coarse-grained carbonates (dolomites, ankerites, siderites and magnesites). The magnesites are intensively steatitized and they represent a potential source for talk (Kilík,

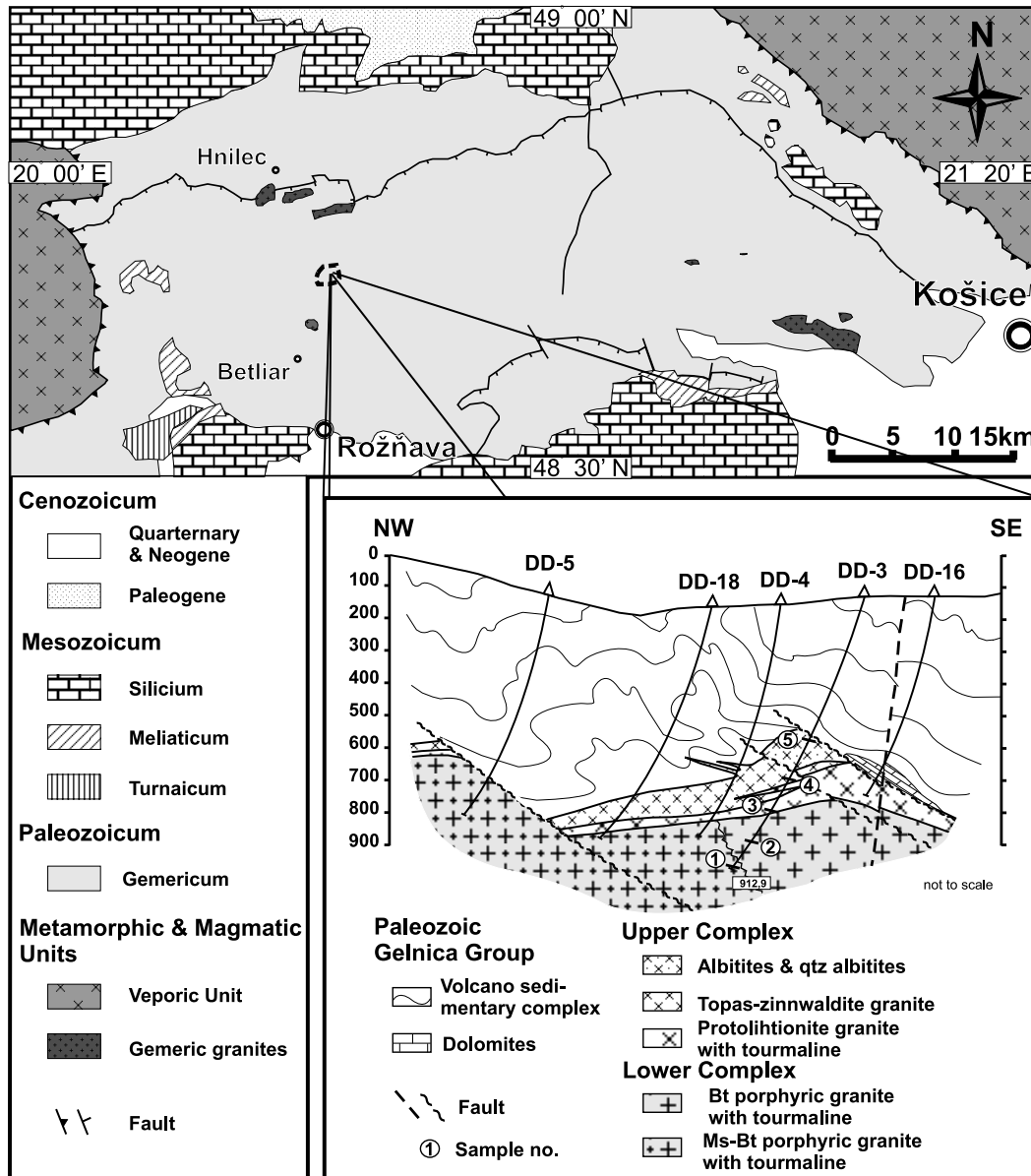


Fig. 1. Simplified geological map of the Gemeric Unit modified after Broska et al. (2002) and cross section through the Dlhá Dolina subsurface granite modified after Dianiška et al. (2002). Vertical position of the samples indicated by numbers (compare with table 1).

1997). Sedimentary ages are early Ordovician to early Silurian for the lowermost and most prominent Gelnica Group (e.g. Vozárová, 1998) The Gemeric Unit underwent green-schist facies metamorphism with 300-350°C and 0.5-0.7 GPa during Alpine orogeny (Krist et al., 1992; Faryad and Dianska, 1999).

Numerous granites were emplaced into these Palaeozoic metasediments (Fig. 1). All granites occurring in the Gemeric Unit show typical features of the S-type peraluminous leucogranite suite. The chemical composition is generally characterized by high  $SiO_2$  contents (usually up to 77 wt%), relatively high alkali

elements, especially  $K_2O$  (around 5 wt%) and relatively low MgO and CaO (0.3 wt% and 0.6 wt%, respectively). High volatile contents ( $H_2O$ ,  $B^-$ ,  $F^-$ ) are typical for these rocks (e.g. Kubiš and Broska, 2005).

The REE show relatively flat normalized pattern with significant negative Eu anomalies ( $Eu/Eu^* \leq 0.2$ ). The S-type character is also demonstrated by high  $^{87}Sr/^{86}Sr_{ini}$  ratio (Cambel et al., 1990). The special compositional character of the Spiš-Gemer granites is also reflected in the rare-metal mineralization of these granites (Malachovský et al., 1983; Dianiška et al., 2002).

The Permian age of these specialized S-type granites was previously detected by whole rock Rb-Sr analyses (Cambel et al., 1990, see Fig. 6), by chemical Th-U-Pb monazite dating ( $276 \pm 13$  Ma; Finger and Broska, 1999) and also by U-Pb CLC single zircon dating ( $243 \pm 18$  Ma; Poller et al., 2002). Chemical Th-U-Pb age determinations on monazite from the lower part of the Dlhá Dolina granite complex show an age of  $282 \pm 16$  Ma (Kubiš, 2004). A Permian intrusion age is also indirectly indicated by Re-Os dating of associated ore mineralization on molybdenite of the Hnilec granite ( $262.2 \pm 0.9$  Ma; Kohút et al., 2004).  $^{40}Ar - ^{39}Ar$  dating of amphibolites from the contact aureole of Súlová granite (Hnilec area) result in an age of 140 Ma indicating an Paleo-Alpine metamorphic superimposed event (Vozárová et al., 2000).

The specialized S-type granites in Gemeric Unit may have resulted from melting triggered by increased heat flow from the mantle below the continental crust during the post-collisional extension after the main Variscan orogeny. In this sense the specialized S-type granites are Variscan postorogenic granites (Broska and Uher, 2001).

### 3 Sample Description

The Dlhá Dolina granite is a subsurface granitoid body which was investigated by a intense drilling program in the 1980s. This area is located in Eastern Slovakia at  $48^\circ 46'N$ ;  $20^\circ 32'E$ , 12 km north of Rožňáva. The samples of the drill core DD-3 are used for this study. Thus samples are available in a vertical section through the body (see cross section in Fig. 1). This core is 912 m long and samples are from 910 m, 786 m, 691 m, 577 m and 504 m depth (table 1). The first two sections are representatives of the Lower Complex barren granites which occur from 718,5 m depth to the base of drill core at 912,9 m depth. The next two sections (691 m and 577 m) represent highly evolved Li-micas and topas bearing granites from the Upper Complex occurring from 558,5-718,5 m. The uppermost specimen typifies albitites found within 454,5-558,5 m depth.

No.	sample name	rock name	depth (m)	main minerals	main accessory minerals
①	DD-908	porphyric	910-908	kfs, qtz, ab, bt,	tur, ap, mnz, zrn, grt, phe
①	GA-908	biotite granite		porphyric kfs, qtz	fl, thor, xt
②	DD-783	two mica	788-783	qtz, kfs, ab, bt, ms,	tur, ap, zrn, ilm, rt
②	GA-783	porphyric granite		porphyric kfs	mnz, thor, bast
③	GA-691	proto-lithionite granite	691-681	qtz, kfs, ab, Li-ms, lith, tur	zrn, mnz, xt, ap, fl, thor, ura, cst, wf, col, goy
④	DD-577	topas-zinnwaldite	582-577	qtz, ab, kfs,	zrn, ap, mnz, xt, fl, wf, cst
④	GA-577	albite granite		Li-ms, tp	NB-Ta minerals, W-ixiolite, ilm
⑤	DD-504	albitite	507-504	ab, qtz	cst, ap, zrn, Nb-Ta minerals
⑤	GA-504				ura

Table 1. Short description of the samples used for this study, more detailed description in Dianiška et al. (2002). Numbers refer to location in cross section (Fig. 1). Mineral abbreviations are given on page 77.

### 3.1 Petrographical Description

As shown in the cross section (see Fig. 1), the granite complex in Dlhá Dolina is comprised of several primary granitoid and metasomatized granitoid rocks (Dianiška et al., 2002). In general, this intrusion consists of two distinct complexes. The barren Lower Complex is formed by a porphyric two-mica granite and a porphyric biotite granite, whereas the ore-bearing Upper Complex is formed by evolved rare-metal Li-mica and topas bearing granites. These show intense alterations in the roof zone.

The barren Lower Complex is mainly build up of the following two rock types: The porphyric biotite granite (910-908 m) shows 1-3 cm long alkali feldspar phenocryst of euhedral shape and is fine-grained. It consists of quartz, plagioclase and biotite. Typical accessory minerals are tourmaline, apatite, zircon, garnet, fluorite.

The barren porphyric two-mica granite (788-783 m) is medium-grained and quartz, K-feldspar, plagioclase, biotite, muscovite, and tourmaline are present in thin-sections. Also perthitic alkali feldspar of up to 4 cm in length is abundant. Main accessory minerals except tourmaline are zircon, apatite and monazite.

The lower part of ore-bearing Upper Complex from 691 to 681 m depth consists of a coarse-grained tourmaline-bearing, proto-lithionite leucogranite. Typical modal composition is quartz (40 vol.%), alkali feldspar (36 vol.%), albite (14 vol.%), Li-mica (3.5 vol.%), proto-lithionite (3 vol.%) and tourmaline (2.7 vol.%). Accessory minerals present are zircon, monazite, xenotime, apatite, fluorite, wolframite, cassiterite.

Upper parts of the Upper Complex (582 to 504 m) is formed by topas-zinnwaldite granite and resembles the most evolved samples of the Dlhá Dolina pluton, which crystallized in the cupolas. This is composed of quartz, alkali

feldspars, topas and Li-mica. Typical accessory minerals are apatite, fluorite, xenotime, wolframite, cassiterite, Nb-Ta minerals.

In high-level cupolas the topaz-zinnwaldite granites are overprinted to quartz-albitites and albitites (Fig. 1). The thickness of albitite cupola in the drill core DD-3 is more than 100 m. A representative sample for the albitite cupola has been taken at 507 m. It consists of quartz and albite or of mono-mineralic albite with a fine grained hypidiomorphic structure. Accessory minerals such as cassiterite, uranite, Mn-tantalocolumbite, tantalocolumbite, struverite, and others.

## 4 Geochemistry

Main and trace elements are analysed for 9 samples from the drill core DD-3 (table 2). Depth are given in table 1 and shown in Figure 1B. Samples named 'DD' were analysed at the ACME Laboratory (Vancouver, Canada), samples named 'GA' were analyzed at MPI for chemistry in Mainz.

### 4.1 Main and trace elements

The  $SiO_2$  is very similar for all samples between 73 and 77 wt%, whereas the  $Al_2O_3$  increases from the lower to the upper parts (table 2 and Fig. 2).  $Fe_2O_3$  is decreasing drastically from 1.3-1.5 to <0.2 wt%. The alkali elements  $Na_2O$  and  $K_2O$  are present in a comparable amount for the samples between 910 m and 577 m, only the uppermost sample reflects a drastic increase in  $Na_2O$  accompanied by a decrease of  $K_2O$ . This exchange of  $Na_2O$  vs.  $K_2O$  is already recognized in the intense albitisation of these samples. The increase of  $P_2O_5$  in the upper samples in comparison to the lower samples is significant and thus classifies the granites from the Upper Complex as P-rich granites, which typically develop in highly evolved granite systems (Fig. 2).

The trace elements  $Sn$ ,  $Ta$  and  $Nb$  increase from the Lower Complex to the Upper Complex (20 to 350 ppm, 3 to 40 ppm and 9 to 57 ppm, respectively), whereas  $Zr$  and  $Ba$  decrease (76 to 19 ppm and 66 to 12 ppm, table 2).  $Rb$  and  $Sr$  first increase for the samples between 910 m and 577 m from  $\approx 400$  and  $\approx 25$  ppm to  $\approx 1900$  and  $\approx 400$  ppm, respectively and then decrease significantly for the uppermost samples to  $\approx 80$  and  $\approx 40$  ppm, thus these elements behave similar to  $K_2O$ .



Sample	deph	SiO <sub>2</sub>	TiO <sub>2</sub>	Al <sub>2</sub> O <sub>3</sub>	Fe <sub>2</sub> O <sub>3</sub>	MnO	MgO	CaO	Na <sub>2</sub> O	K <sub>2</sub> O	P <sub>2</sub> O <sub>5</sub>	L.O.I.	TOTAL	Sr/Eu	K/Rb				
DD – 504	507-504	74.49	0.02	15.40	0.20	0.01	0.19	0.55	7.89	0.51	0.31	0.5	100.07	NA	48				
GA – 504	507-504	74.28	0.03	15.09	0.19	0.01	0.14	0.52	8.5	0.39	0.27	0.6	100.05	NA	60				
DD – 577	582-577	73.24	0.02	15.37	0.78	0.05	0.02	0.7	3.96	4.19	0.52	1.4	100.25	NA	18				
GA – 577	582-577	73.91	0.03	16.22	0.66	0.04	BD	0.48	4.44	4.81	0.4	1.1	102.07	NA	20				
GA – 681	691-681	76.70	0.07	13.07	1.08	0.01	0.56	0.37	3.44	2.76	0.27	1.0	99.37	287	35				
DD – 783	788-783	76.42	0.15	12.39	1.58	0.03	0.21	0.56	2.84	4.88	0.16	1.1	100.32	157	94				
GA – 783	788-783	74.77	0.19	12.80	1.90	0.03	0.18	0.63	3.16	4.53	0.15	0.9	99.32	100	88				
DD – 908	910-908	76.72	0.09	12.73	1.21	0.03	0.16	0.52	3.07	4.88	0.12	1.0	100.53	140	92				
GA – 908	910-908	75.92	0.10	12.86	1.32	0.03	0.09	0.46	3.35	4.79	0.12	0.8	99.84	138	95				
	V	Sc	Sn	Ta	Nb	Ga	Cs	Mo	Cu	As	Zn	Zr	Ba	Rb	Sr	Pb	Th	U	
DD – 504	< 5	3	347	40.5	57	56	7	5.4	1.0	8	2.2	7	19	12	88	40	2	7.6	12.2
GA – 504	2	2	NA	NA	57	46	NA	NA	1	NA	NA	33	26	54	36	3	6.5	10.1	
DD – 577	< 5	6	79	19.7	66	43	72.4	5.0	1	17.6	28	25	53	1866	170	5	8.6	19.4	
GA – 577	2	2	NA	NA	48	42	NA	NA	4	NA	NA	29	112	1919	456	9	12.0	12.1	
GA – 681	4	4	NA	NA	15	23	NA	NA	8	NA	NA	59	53	650	23	7	8.3	14.3	
DD – 783	10	3	31	2.7	12	22	18.1	2.2	8	9.8	23	88	108	430	27	9	14.8	15.7	
GA – 783	9	4	NA	NA	13	20	NA	NA	5	NA	NA	115	70	425	26	17	16.6	11.3	
DD – 908	6	2	21	2.8	10	20	14.0	2.8	2	55.3	13	63	76	439	20	8	12.3	13.6	
GA – 908	6	3	NA	NA	9	19	NA	NA	2	NA	NA	76	66	418	18	10	12.0	16.9	
	Y	La	Ce	Pr	Nd	Sm	Eu	Gd	Tb	Dy	Ho	Er	Tm	Yb	Lu	TE <sub>1,3</sub>	Eu/Eu*		
DD – 504	0.7	BD	BD	BD	BD	BD	BD	BD	BD	BD	BD	BD	BD	BD	BD	NA	NA		
GA – 504	3	BD	BD	BD	BD	BD	BD	BD	BD	BD	BD	BD	BD	BD	BD	NA	NA		
DD – 577	5.6	0.7	3.1	0.31	1.2	0.8	< 0.006	0.62	0.2	1.11	0.15	0.37	0.06	0.52	0.08	1.62	< 0.03		
GA – 577	1	0.37	1.7	0.21	0.76	0.47	< 0.006	0.43	0.12	0.69	0.091	0.25	0.04	0.38	0.038	1.6	< 0.04		
GA – 681	12	3.6	9.9	1.3	5.1	1.7	0.08	1.79	0.37	2.27	0.395	1.1	0.17	1.2	0.14	1.2	0.14		
DD – 783	30.8	15.2	32.2	3.62	13.2	4.2	0.17	3.92	0.8	5.03	1.03	2.68	0.43	3.14	0.43	1.1	0.12		
GA – 783	30	20	47	5.4	19	4.7	0.26	4.4	0.86	5.6	1.1	3.2	0.48	3.2	0.41	1.14	0.17		
DD – 908	24.1	9.6	20.5	2.42	8.7	3.1	0.14	2.52	0.55	4.06	0.84	2.47	0.4	3	0.44	1.12	0.15		
GA – 908	20	10	25	2.9	10.3	2.9	0.13	3.1	0.62	4.6	0.9	2.9	0.47	3.5	0.46	1.16	0.13		

Table 2. Geochemical data for the Dlhá Dolina complex. Main and trace elements analysed with XRF, REE analysed with ICPMS. *NA* for not available, *BD* for below detection. 0.006 ppm Eu assumed for samples with Eu below detection limit. Tetrad effect ( $TE_{1,3}$ ) calculated according Irber (1999).  $Eu/Eu^* = \frac{Eu_N}{\sqrt{Gd_N * Sm_N}}$ .

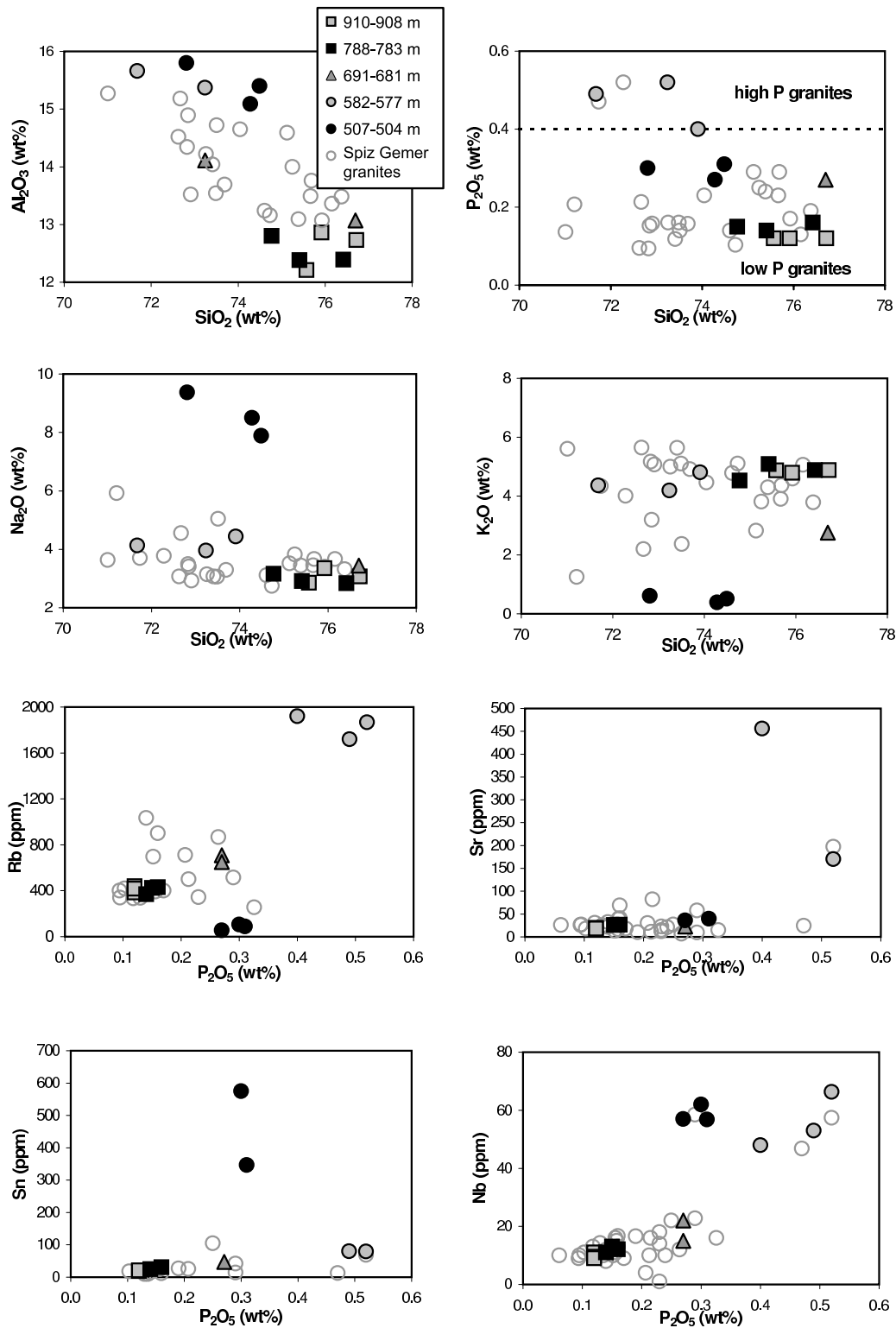


Fig. 2. Harker diagrams for the granites occurring in the Gemic Unit. Data for the Dlhá Dolina (black rimmed symbols) given in table 2. Reference data (grey circles) for the Gemic Granites from (Broska and Uher, 2001).

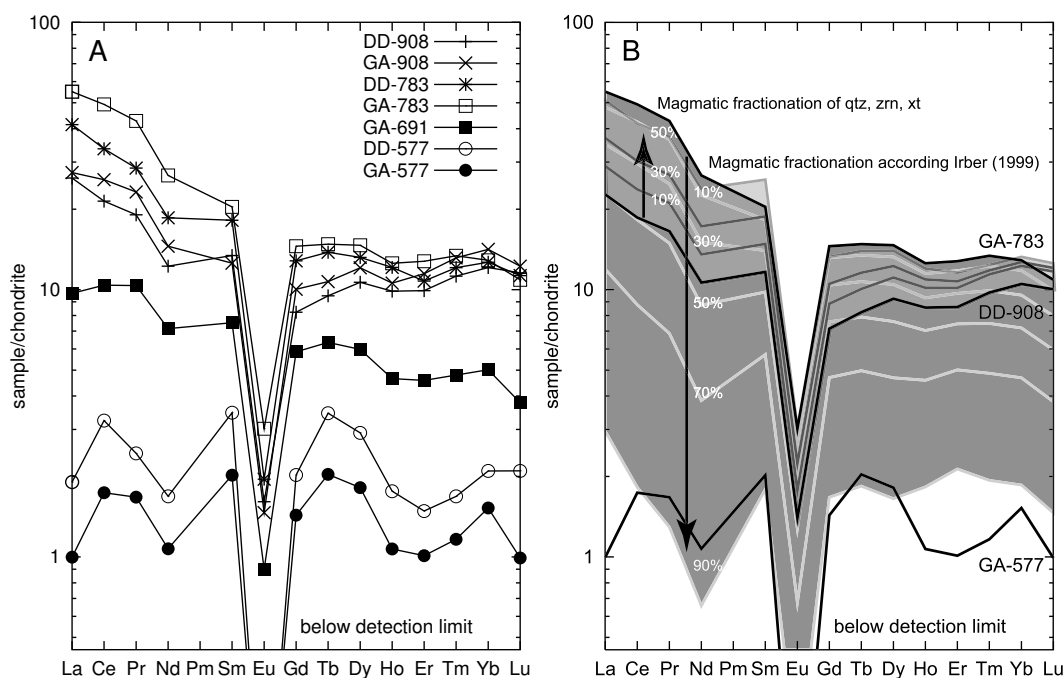


Fig. 3. REE diagram normalized to chondrite (Taylor and McLennan, 1985). A: The drill core samples. Data given in table 2. B: Modelling of crystal fractionation for this dataset. Sample DD-908 and DD-783 shown in solid used as initial composition, sample GA-577 shown as reference. Grey lines represent 10, 30, 50, 70, and 90 % of fractionation. Detailed discussion in the text.

#### 4.2 REE and Tetrad effect

The samples from the Lower Complex show moderate steep REE pattern. Chondrite (Taylor and McLennan, 1985) normalized  $La_N$  concentrations ( $La_N$ ) vary from 20 to 60 and  $Lu_N$  is nearly constant at 10 times chondritic (see Fig. 3A). The Eu anomaly ( $Eu_N/Eu_N^*$ ) increases slightly from 0.13 to 0.17 from the lower samples to the upper samples (table 2). These samples show a small Tetrad effect of 1.1 (calculated according to Irber, 1999).

The REE concentrations decrease significantly for the Upper Complex from 10 times chondrite normalized values for  $La$  to values below detection limit for the albitized samples. Together with the decrease of REE, the Tetrad effect increases from 1.2 to 1.6 (table 2).

Two different effects influencing the concentrations of the REE can be recognized in the Dlhá Dolina intrusive complex:

A fractional crystallisation trend can be observed for the samples from 908 m to the samples from 783 m. This leads to a three to four times enrichment of the light REE and up to a two times enrichment for the heavy REE. The Eu-anomaly does only increase to a minor extent with fractionation.

The second trend observable is the depletion of REE for the Upper Complex. This develops, with respect to the most fractionated sample GA-783, from a five times depletion for the 681 m sample to a 20 times depletion for the 577 m samples and further to a depletion below the detection limit for the samples at 504 m (table 2 and Fig. 3A). Simultaneously to this depletion of the REE, the Tetrad effect evolves from  $<1.2$  for the samples below 681 m to 1.6 for the samples above 577 m. The Tetrad effect is, according to Irber (1999), calculated as the geometric mean of the first (La, Ce, Pr, Nd) and the third (Gd, Tb, Dy, Ho) tetrad (see Fig. 3).

Modelling of fractional crystallization using the partition coefficients summarized by Irber (1999) with sample DD-908 as initial composition this enrichment can be modelled by fractionating mainly quartz (99.88%) and a small amount of accessory minerals (0.113% zircon and 0.007% of xenotime) with 50% of fractionation. The effect of fractionating such a mineral assemblage is shown in Fig. 3B by the dark grey lines. In this diagram the sample DD-908 and sample GA-783 are shown as reference. If feldspar is assumed to fractionate, it is expected that the Eu-anomaly increases with increasing fractionation. Because this is not observed to the extent expected if feldspar is fractionating, the modelling was calculated using quartz. The exact amount of the accessory minerals fractionating is difficult to estimate, but because of the only small enrichment of the heavy REE, the presence of such phases must be assumed. The assumed fractionation of 0.113% zircon and 0.007% of xenotime result in a good approximation of the composition of the sample GA-783.

For the more evolved samples from the Upper Complex such a good approximation can not be reached. The same mineral assemblage as used by Irber (1999) to model the Tetrad effect was used with sample GA-783 as initial composition. As can be seen in Fig. 3B (light grey lines) such an assemblage can diminish the REE concentration to a similar extent as observed for sample GA-577 by assuming 90% fractional crystallization. But neither can the Tetrad effect be reproduced by this modelling, nor can the very low REE concentrations in the uppermost samples be explained. This corresponds to the results by Irber (1999), where the Tetrad effect could also not be modelled by fractional crystallization.

According to Bau (1996) the Tetrad effect is caused by complexation of the REE with ligands as e.g.  $H_2O$ ,  $CO_2$ ,  $F^-$ , and  $Li$ . If such complexation occur, the behavior of the REE is no longer simply dependent on the ionic radii, which are comparable for all REE (Onuma et al., 1968), but is dependent on the filling stages of the 4f orbitals (Irber, 1999). Thus REEs with 0/4 (La), 1/4 (Nd, Pm), 2/4 (Gd), 3/4 (Ho, Er) and 4/4 (Lu) filled 4f orbitals can be fractionated from the other REEs.

Comparing the Tetrad effect and the Eu anomaly observed for the Dlhá Dolina intrusive complex with data compiled by Irber (1999), the effect for the Lower

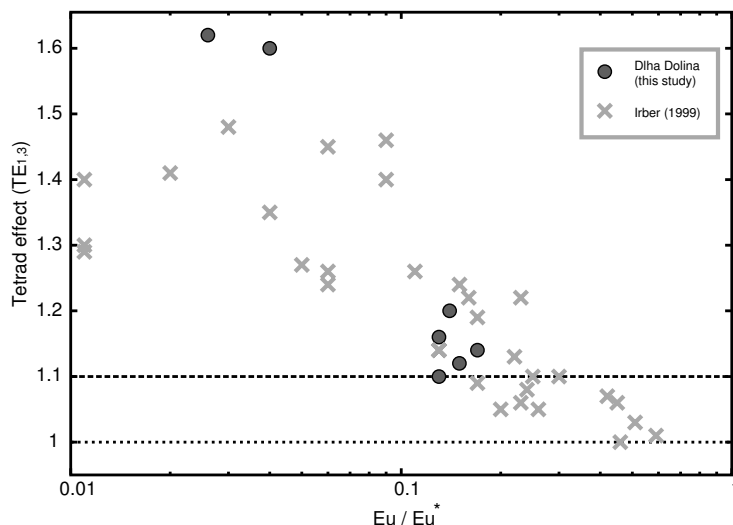


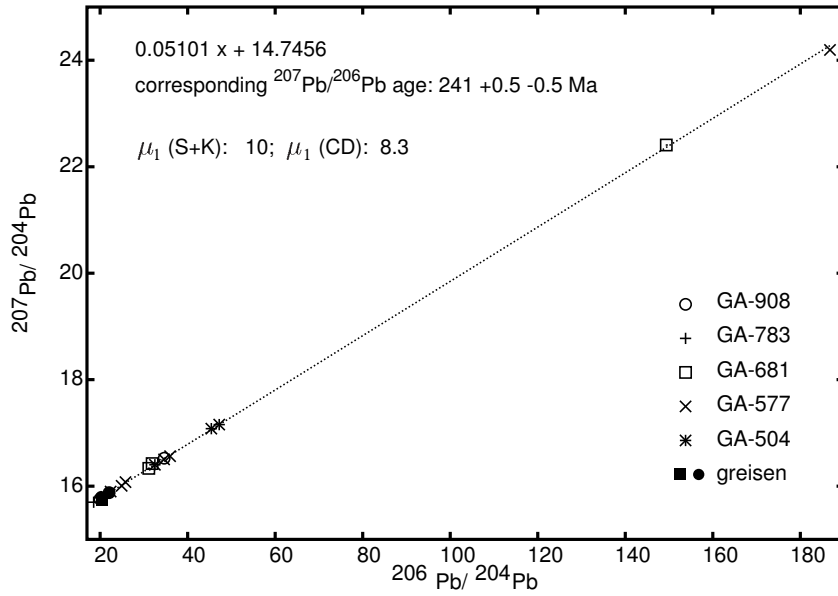
Fig. 4. Comparison of the Tetrad effect observed in the Dlhá Dolina samples with the data from Irber (1999). Data given in table 2.

Complex plots well within the range of the published data at typical values for granites (Fig. 4). The samples from the Upper Complex extend the range of presented values, nevertheless are in good agreement with the negative correlation observed for all data. This suggest that the Tetrad effect observed in the Dlhá Dolina granitic suite is in correspondence with similar evolved granitoid suites.

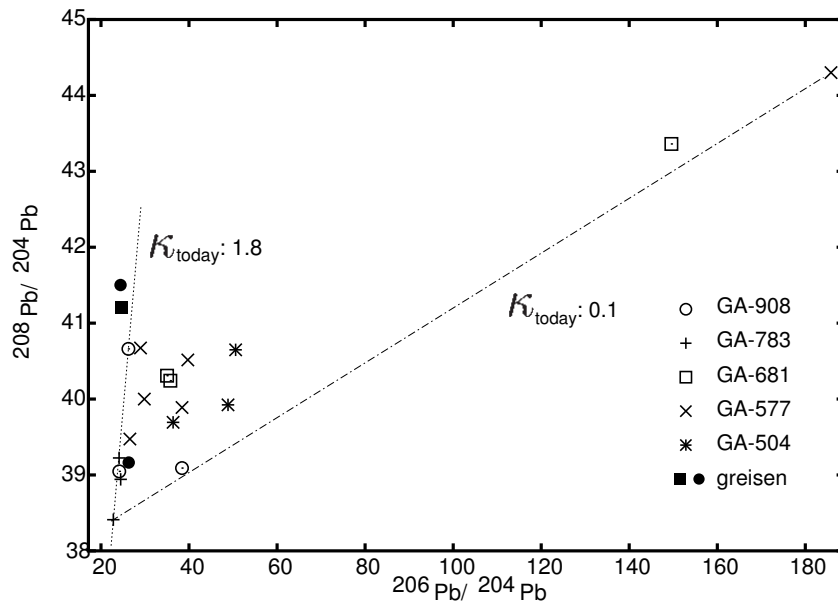
### 4.3 Lead Isotopes

WR-PbPb data for the drill cores and cassiterite bearing greisen from an outcrop in the Dlhá Dolina are presented by Gaab et al. (submitted) and shown in Fig. 5. According to this study the *Pb* isotopes yield a good constraint for the age of the last magmatic activity of this intrusive complex. The data for the drill core and for the cassiterite greisen show a good correlation in the  $^{207}\text{Pb}/^{204}\text{Pb}$  vs.  $^{206}\text{Pb}/^{204}\text{Pb}$  diagram with  $^{206}\text{Pb}/^{204}\text{Pb}$  ranging from 19.9 to 170 (Fig. 5(a)). This correlation is interpreted as the uranogenic *Pb* growth after the last *Pb* isotopic homogenization due to magmatic activity. Therefore a minimum age for this intrusion can be estimated at 241 Ma from the linear regression of this data (Gaab et al., submitted). The corresponding  $\mu_1$  values for this regression line of 10 using the Stacey and Kramers (1975) modell is typical for a crustal evolution.

This magmatic activity also led to a redistribution of *U* and *Th* and fractionated these elements from each other, which becomes visible in the  $^{208}\text{Pb}/^{204}\text{Pb}$  vs.  $^{206}\text{Pb}/^{204}\text{Pb}$  diagram (Fig. 5(b)). The samples from the Lower Complex (circles and pluses in Fig. 5(b)) reflect a more or less undisturbed system



(a)



(b)

Fig. 5.  $^{207}\text{Pb}/^{204}\text{Pb}$  vs.  $^{206}\text{Pb}/^{204}\text{Pb}$  diagram and  $^{208}\text{Pb}/^{204}\text{Pb}$  vs.  $^{206}\text{Pb}/^{204}\text{Pb}$  for the samples of the Dlhá Dolina subsurface granite.  $\kappa_{\text{today}}$  calculated for reference lines and the age of 241 Ma. Data published by Gaab et al. (submitted).

sample	$^{87}\text{Sr}/^{86}\text{Sr}$ <sup>1</sup>	$\pm 2\sigma$	$^{87}\text{Rb}/^{86}\text{Sr}$ <sup>2</sup>	$^{87}\text{Sr}/^{86}\text{Sr}$ 241 Ma
GA-908 I	0.9996	6	83.0	0.715
GA-908 II	1.0047	4	83.0	0.720
GA-783 I	0.8869	5	50.3	0.714
GA-783 II	0.8879	2	50.3	0.715
GA-577 I	0.7809	2	11.6	0.741
GA-577 II	0.7833	3	11.6	0.744
GA-504 I	0.7420	2	4.7	0.726
GA-504 II	0.7420	5	4.7	0.726

<sup>1</sup>measured on TIMS *MAT261* in static mode. Errors are given as  $2\sigma$  deviation of the weighted mean (6-25 blocks)

<sup>2</sup>measured on single collector ICP-MS *Element2*

Table 3. Sr isotopic composition of the Dlhá Dolina drill core samples. Isotopic analyses are reproduced twice.

with  $\kappa$  values between 1.5-1.8 calculated from the slopes of lines connecting the samples with the least radiogenic sample and the age obtained from the  $^{207}\text{Pb}/^{204}\text{Pb}$ - $^{206}\text{Pb}/^{204}\text{Pb}$  diagram (Gaab et al., submitted). With lower  $\kappa$  values plot the samples from the Upper Complex (squares, crosses, and stars). Thus these were depleted in *Th* vs. *U* during the last magmatic activity. In contrast to this the greisen (filled symbols) are enriched in *Th* vs. *U* and plot left of the samples from the Lower Complex (i.e. left of the line connecting these samples, except one outlier). Thus a *Th*-rich fluid, probably which depleted *Th* in the Upper Complex, generated the greisen in the country rock.

#### 4.4 Sr isotopes

The two mica granite of the Lower Complex (sample GA-908) reveal very high  $^{87}\text{Sr}/^{86}\text{Sr}$  ratios of  $\approx 1$  and an extremely high  $^{87}\text{Rb}/^{86}\text{Sr}$  ratio of 83. Also very radiogenic values of  $\approx 0.89$  are obtained for the biotite granite of the Lower Complex. In contrast, un-radiogenic  $^{87}\text{Sr}/^{86}\text{Sr}$  ratios between  $\approx 0.74$  and  $\approx 0.78$  have been measured for the Upper Complex (table 3).

The Sr isotopes of the drill core samples do not result in an isochron (Fig. 6). If a reference line with a slope corresponding to 241 Ma, according to the last magmatic activity revealed by the WR-PbPb data, is drawn for the radiogenic sample GA-908II, the data of the sample GA-783 plot nicely on this line (Fig. 6). This line corresponds results in a  $^{87}\text{Sr}/^{86}\text{Sr}_{ini}$  of .704, which is in the range of the expected values (Poller et al., 2001; Cambel et al., 1990).

The samples from the Upper Complex plot at too radiogenic  $^{87}\text{Sr}/^{86}\text{Sr}$  ratios for the measured  $^{87}\text{Rb}/^{86}\text{Sr}$  ratios, thus they plot above the previously mentioned reference line. This indicates either recent Rb loss or too radiogenic initial  $^{87}\text{Sr}/^{86}\text{Sr}$  values. The too radiogenic values could be generated by late

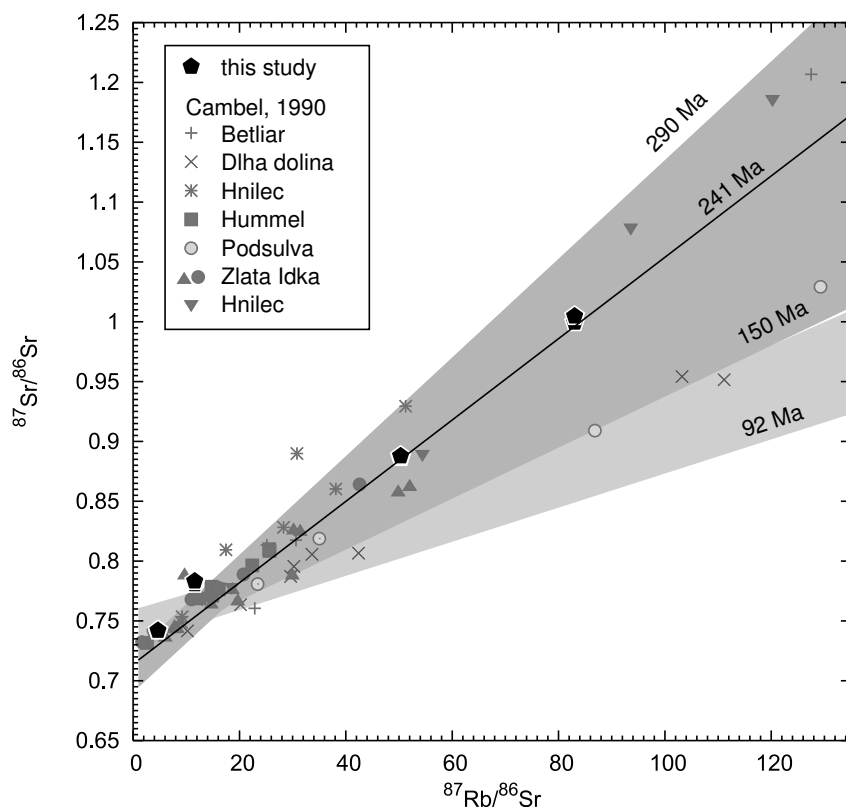


Fig. 6.  $^{87}\text{Rb}/^{86}\text{Sr}$  vs.  $^{87}\text{Sr}/^{86}\text{Sr}$  diagram for Gemicic Granites. Black symbols are the data presented in this study (table 3). WR data compiled by Cambel et al. (1990) shown in grey, localities given in the key. Reference line corresponding to 241 Ma shown (black line). Fields of the WR “isochrons” (dark grey field) and the WR-Biotite “isochrons” (light grey field) of the Cambel et al. (1990) dataset indicated. Biotite data points are not shown due to their high  $^{87}\text{Rb}/^{86}\text{Sr}$ .

magmatic albitization and thus an intense loss of Rb, which is observed for the uppermost sample (table 2).

In comparison with Sr WR analyses compiled by Cambel et al. (1990, dark shaded area in Fig. 6), the data for the drill cores have similar affinities. The  $^{87}\text{Sr}/^{86}\text{Sr}_{ini}$  of this compilation vary between 0.690 and 0.728, with a mean value of 0.720. This large spread and the existence of geological meaningless  $^{87}\text{Sr}/^{86}\text{Sr}_{ini}$  values below the BABI composition of 0.699 (Papanastassiou and Wasserburg, 1969) shows that the Rb-Sr systematics of the Gemicic granites was disturbed by co-magmatic processes, as shown by the data presented in this study, or by metamorphic processes.

Alpine metamorphism disturbed by Rb-Sr systematics of these samples as can be seen from the WR-Bt pairs from the compilation by Cambel et al. (1990). The WR-Bt pairs result in consistently higher  $^{87}\text{Sr}/^{86}\text{Sr}_{ini}$  between 0.722 and 0.759 with a mean value of 0.743 as the corresponding WR “isochrons” and correspondingly lower ages between 92 and 142 Ma (light grey shaded area



in Fig. 6). All data points for biotites plot below the WR regression lines at high  $^{87}\text{Rb}/^{86}\text{Sr}$  values, showing that during metamorphism the biotites re-equilibrated partially.

## 5 Conclusions

The intrusive complex of Dlhá Dolina shows magmatic fractionation and intense metasomatic activity. The Lower Complex is dominated by magmatic processes, but already shows metasomatic influences like the presence of tourmaline and a minor Tetradeffect. The Upper Complex is strongly influenced by a fluid phase and shows a strong Tetradeffect and strong fractionation of e.g. U from Th. Nevertheless the Pb isotopic data show a contemporaneous emplacement of both complexes. Thus the metasomatic overprint is interpreted to be co-magmatic and the observed variations are due to the different mechanisms of magmatic evolution.

The Tetradeffect observed for this suites evolves from a only minor effect for the magmatic dominated samples of the Lower Complex ( $TE_{1,3} < 1.1$ ) to a very high Tetradeffect for the evolved and metasomatized samples from the Upper Complex ( $TE_{1,3} = 1.2 - 1.6$ ). The REE data of this complex is consistent with published data on the Tetradeffect by Irber (1999) and extends the range of observed Tetradeffect slightly. This show that metasomatic overprint was very intense during intrusion of the Dlhá Dolina pluton.

This is also recorded by the Sr isotopes of the Upper Complex with too radiogenic  $^{87}\text{Sr}/^{86}\text{Sr}_{ini}$ , thus reflecting late-magmatic redistribution of Rb and Sr. The Sr data for the samples from the Lower Complex, which are dominated by magmatic processes are in good agreement with the timing of intrusion constrained by the WR-Pb-Pb isotopes published in Gaab et al. (in press).

Published ages for intrusion age of the granites in the Gemeric Unit do show a wide age range from 300 to 240 Ma.

Chemical U-Th-Pb ages record the oldest ages. They range from 282 Ma for the Dlhá Dolina (Kubiš, 2004) complex to 276 Ma for the Hnilec complex (Finger and Broska, 1999). Re-Os work in the Hnilec area (Kohút et al., 2004) points to a younger age of intrusion of the granites at 262 Ma. A wide variety of ages are documented by WR Sr isotopic analyses compiled by Cambel et al. (1990) from 290 to 150 Ma, with even younger ages obtained by WR-Bt pairs. This and the Sr data presented in this work suggest that the Sr isotopic systematics were strongly disturbed by metasomatism during intrusion of the granites and during later metamorphic overprint. Thus very much care must be taken, if these data are used for geochronologic purpose. Nevertheless is the Sr data presented in this study for the Lower Complex consistent with the

timing of Pb isotopic homogenization presented by Gaab et al. (in press). Both datasets imply a young intrusion age around 241 Ma. This young intrusion age is confirmed by U-Pb single zircon dating (Poller et al., 2002) for the Hnilec and the Betliar granites with ages of  $250\pm 18$  and  $246\pm 5$ , respectively.

If intrusion ages for the granites in the Spiš-Gemer can be restricted to a period between 260-240 Ma or if the granites intruded during a longer time span must be clarified by further studies. At least the minimum age of these granites is constrained by this study to 240 Ma.

### Acknowledgements

We would like to thank MK, MJ, IP and DP for their help during field work and for fruitful discussions. AH is gratefully acknowledged for providing the opportunity to perform this study at MPI, Mainz.

### References

- Bau, M., 1996. Controls on the fractionation of isovalent trace elements in magmatic and aqueous systems: evidence from Y/Ho, Zr/Hf, and lanthanide tetrad effect. *Contributions to Mineralogy and Petrology* 123, 323–333.
- Broska, I., Kubiš, M., Williams, C., Konečný, P., 2002. The compositions of rock-forming and accessory minerals from the Gemeric granites (Hnilec area, Gemeric Superunit, Western Carpathians). *Bulletin of the Czech Geological Survey* 77, 147–155.
- Broska, I., Uher, P., 2001. Whole-rock chemistry and genetic typology of the West-Carpathian Variscan granites. *Geologický Zborník - Geologica Carpathica* 52, 79–90.
- Cambel, B., Král, J., Burchart, J., 1990. *Izotopová geochronológia kryštálikov západných karpát*. VEDA.
- Dianiška, I., Breitner, K., Broska, I., Kubiš, M., Malachovský, 2002. First Phosphorus-rich Nb-Ta-Sn-specialised granite from the Carpathians - Dlhá Dolina vally granite pluton, Gemeric Superunit, Slovakia. *Geologický Zborník - Geologica Carpathica* 53.
- Faryad, S., Dianiška, I., 1999. Alpine overprint in the early Paleozoic of the Gemericum. *Mineralia Slovaca* 5.
- Finger, F., Broska, I., 1999. The Gemeric S-type granites in southern Slovakia: Late Paleozoic or Alpine intrusion? Evidence from electron-microprobe dating of monazite. *Swiss Bulletin of Mineralogy and Petrology* 79, 439–443.
- Gaab, A., Janák, M., Poller, U., Todt, W., in press. Alpine reworking of Ordovician protoliths in the Western Carpathians: Geochronological and geochemical data on the Muráň Gneiss Complex. *Lithos* .

- Gaab, A., Todt, W., Poller, U., submitted. CLEO: Common lead evaluation using Octave. *Computers & Geosciences* .
- Irber, W., 1999. The lanthanide tetrad effect and its correlation with K/Rb, Eu/Eu\*, Sr/Eu, Y/Ho, and Zr/Hf of evolving per-aluminous granite suites. *Geochimica et Cosmochimica Acta* 63, 489–508.
- Kilík, J., 1997. Geologická charakteristika mastencového ložiska Gemerská Poloma - Dlhá Dolina. *Acta Montanistica Slovaca* 2.
- Kohút, M., Stein, H., Radvanec, M., 2004. Re-Os dating of molybdenite from the Hnilec Permian granite-related mineralisation - its tectonic significance (Gemic unit, Slovakia). *Geolines* 17, 54–55.
- Krist, E., Korikovskij, S. P., Putiš, M., M., Janák, Faryad, S. W., 1992. *Geology and Petrology of Metamorphic rocks of the Western Carpathian Crystalline Complexes*. Comenius University Press, Bratislava.
- Kubiš, M., 2004. Origin and evolution of the Spi-Gemer granites. Ph.D. thesis, GIU SAV, Bratislava.
- Kubiš, M., Broska, I., 2005. Role of boron and fluorine in evolved granitic rock systems (on an example of the Hnilec area, Western Carpathians). *Geologický Zborník - Geologica Carpathica* .
- Lupták, B., Janák, M., Plašienka, D., Schmidt, S. T., Frey, M., 2000. Chloritoid-kyanite schists from the Veporic unit, Western Carpathians, Slovakia: implications for Alpine (Cretaceous) metamorphism. *Swiss Bulletin of Mineralogy and Petrology* 80, 211–222.
- Malachovský, P., et al., 1983. Final report SGR, high-temperature mineralization - Sn, W, Mo ores. Tech. rep., Geofond Bratislava.
- Onuma, N., Higuchi, H., Wakita, H., Nagasawa, H., 1968. Trace element partitioning between two pyroxenes and the host lava. *Earth Planetary Science Letters* 5, 47–51.
- Papanastassiou, D., Wasserburg, G., 1969. Initial Strontium isotopic abundances and the resolution of small time differences in the formation of planetary object. *Earth Planetary Science Letters* 5, 361–376.
- Plašienka, D., 1997. Cretaceous tectonochronology of the Central Western Carpathians, Slovakia. *Geologický Zborník - Geologica Carpathica* 48, 99–111.
- Poller, U., Janák, M., Kohút, M., Todt, W., 2000. Early Variscan Magmatism in the Western Carpathians: U-Pb zircon data from granitoids and orthogneisses of the Tatra Mts (Slovakia). *International Journal of Earth Science* 89, 336–349.
- Poller, U., Kohút, M., Todt, W., Janák, M., 2001. Nd, Sr, Pb isotope study of the Western Carpathians: implications for Palaeozoic evolution. *Swiss Bulletin of Mineralogy and Petrology* 81, 159–174.
- Poller, U., Uher, P., Broska, I., Plašienka, D., Janák, M., 2002. First Permian-Early Triassic zircon ages for tin-bearing granites from the Gemic unit (Western Carpathians, Slovakia): connection to the post-collisional extension of the Variscan orogen and S-type magmatism. *Terra Nova* 14, 41–48.
- Stacey, J. S., Kramers, J. D., 1975. Approximation of terrestrial lead isotope

- evolution by a two-stage model. *Earth Planetary Science Letters* 26, 207–221.
- Taylor, S., McLennan, S., 1985. *The continental crust: its composition and evolution*. Blackwell, Oxford.
- Vozárová, A., 1998. Hercynian development of the external-Gemeric zone. In: Rakús, M. (Ed.), *Geodynamic development of the Western Carpathians*. Dionýz Štúr Publication, 47–61.
- Vozárová, A., Frank, W., Král', J., 2000.  $^{40}\text{Ar}/^{39}\text{Ar}$  data from contact aureole of Súľ'ová granite (Gemicum, Western Carpathians). *Slovak Geological Magazine* 6, 363–366.

**A mineral abbreviations**

kfs alkali-feldspar  
qtz quartz  
ab albite  
bt biotite  
ms muscovite  
Li-ms Li-mica  
lith proto-lithionite  
tur tourmalin  
ap apatite  
mnz monazite  
zrn zirkon  
grt garnet  
fl fluorite  
thor thorite  
xt xenotime  
ilm ilmenite  
rt rutile  
bast bastnezite  
ura uranite  
cst cassiterite  
wf wolframite  
col columbite  
goy goyazite  
tp topas

# Chapter 5

All Pb isotopic analyses on whole rock samples were evaluated using the script *CLEO* for *Octave*. This script and its capabilities will be described in this chapter.

It can be used to correct the measurements for fractionation, to generate diagrams for evaluation of WR-Pb-Pb isotopic datasets or to calculate a principal component analysis. The capabilities of the script are demonstrated by evaluating the WR-Pb-Pb dataset for the Dlhá Dolina intrusion presented in Chapter 4.

The script and the manuscript is written by A.S. Gaab. WT provided access to the mass spectrometer for Pb isotopic measurements and supported this work by extensive discussions about evaluation. UP provided access to the clean lab and introduced the author to Pb column chemistry.

The manuscript and the computer script are submitted to Computers & Geosciences.

# CLEO: Common Lead Evaluation using Octave

A.S. Gaab<sup>a,\*</sup> WT<sup>a</sup> UP<sup>a</sup>

<sup>a</sup>*Max-Planck-Institut für Chemie; Abt. Geochemie; PF 3060; 55020 Mainz; Germany*

---

## Abstract

Common lead isotopic data can provide important informations on the history and the evolution of geological samples.

To evaluate common lead data specific calculations are needed, which are not always trivial, especially in a non-programming environment. Therefore a set of pre-defined functions are helpful.

This paper presents an implementation of some basic functions for *Octave*, a GNU Public License program, for the evaluation of common lead data. To show the capability of the script a common lead data set for the Dlhá Dolina intrusion is presented and evaluated using *CLEO*. The timing of this evolved magmatic body can be constrained by the WR-Pb-Pb method to a minimum age of  $241 \pm 0.5$  Ma.

*Key words:* Lead isotopes, Octave, geochemical modeling, magmatic fractionation, principal component analysis

---

## 1 Introduction

Common lead is useful for environmental (e.g. Chillrud et al., 2003; Charalampides and Manoliadis, 2002), climatological (e.g. Abouchami and Zabel, 2003; Planchon et al., 2003), archaeological (e.g. Schettler and Romer, 1998; Habicht-Mauche et al., 2002), volcanological (e.g. Abouchami et al., 2000) and geochronological studies (e.g. Poller et al., 2004). It is analyzed on whole rock splits (WR-Pb-Pb) or on feldspar separates, which contain significant

---

\* Andreas S. Gaab

*Email address:* gaab at mpch-mainz.mpg.de (A.S. Gaab).

amounts of the non-radiogenic  $^{204}\text{Pb}$ , together with  $U$ -genic  $^{206}\text{Pb}$  and  $^{207}\text{Pb}$ , and  $Th$ -genic  $^{208}\text{Pb}$ .

To evaluate lead isotopic data, complex calculations and iterations are frequently needed. These can be solved easily with a mathematical programming environment like *Octave*. This study presents a script with some tools to evaluate lead isotopic data together with a dataset measured with TIMS (Thermal-Ionisation-Mass-Spectrometry).

As the evaluation is not always trivial, e.g. Ludwig (2001) has developed Isoplot for geochronological applications as for calculation of isochrons, evaluation of  $U$ - $Pb$  zircon data and more. This program can only be used with MsExcel<sup>TM</sup>. Thus the usability of that program is limited to people with Windows<sup>TM</sup> or Macintosh<sup>TM</sup> operated computer systems with a commercial version of MsExcel<sup>TM</sup> installed. Additional it is not possible to read or modify the source code of Isoplot, e.g. to check the calculations performed or to extend the abilities of the program.

Because of the fast enhancing user-friendliness of Linux based computer systems, alternatives for commercial programs are provided. As shown by Janousek et al. (2003), who presents a tool for modeling and displaying geochemical data, GNU GPL (General Public License, <http://www.gnu.org/copyleft/gpl.html>) software can be very helpful for geochemical applications. Also the usage of a mathematical programming environment for evaluation of geochemical data proved useful and applicable for scientists as well as for students (Middleton, 2000; Grunsky, 2002). A further advantage of programs under the GNU GPL is that they can be obtained free of charge in the Internet for most operating systems.

This study presents a script written for *Octave*, which introduces many useful functions for evaluation of  $Pb$  isotopic data. The script can be executed without knowledge of the *Octave* language, because all functions are included in the script and no further installation is needed. By a more experienced user these functions can be used for further calculations by entering *Octave* from within the script. The main purpose of *CLEO* is the calculation of regressions using the algorithm after York (1969) and of the corresponding  $^{207}\text{Pb}/^{206}\text{Pb}$  age for WR-Pb-Pb dating. This method yields good results for differentiated magmatic bodies (this paper), for inhomogeneous metamorphic bodies (Gaab et al., in press), or on a regional scale (Poller et al., 2004). Additional, diagrams and tables can be easily generated with *CLEO*, e.g. all diagrams and tables in this paper are generated with this script. Some further tools are included, like plotting lead evolution curves, principal components analysis and radiogenic  $Pb$  diagrams.

To demonstrate an application of the WR-Pb-Pb method evaluated using



*CLEO*, a specialized S-type granitoid body with extensive fractionation in the apical parts drilled in the Gemeric Unit (Central Slovakia) was chosen. During evolution of such a magmatic system, the elements are redistributed by magmatic fractionation or by hydrothermal processes. This leads to enrichment or depletion of *U* vs. *Th* vs. *Pb* and therefore determines the subsequent evolution of the *Pb* isotopes with time. The aim of this study is to evaluate, whether the observed mineralogical variations of these rocks were generated by one or more events and to gain an age information on those events.

## 2 WR-Pb-Pb dating

The basis of dating with naturally occurring lead isotopes is the radioactive decay of *U* and *Th* to *Pb*: ( $^{238}\text{U} \rightarrow ^{206}\text{Pb}$ ,  $^{235}\text{U} \rightarrow ^{207}\text{Pb}$  and  $^{232}\text{Th} \rightarrow ^{208}\text{Pb}$ ). The  $^{238}\text{U}/^{204}\text{Pb}$  ( $\mu$ ) and the  $^{232}\text{Th}/^{238}\text{U}$  ( $\kappa$ ) ratios determine the *Pb* isotopic evolution of geological samples with time.

These decays are in fact complex decay series, but for geological time-spans (generally  $> 10^6$  a, which are at least 4 times larger than longest half life of an intermediate isotope) the decay chain can be simplified as a single decay reaction.  $^{204}\text{Pb}$  is a stable isotope, which is not produced by decay, and is used for normalization of the measurements.

Due to the fact, that two distinct *U* isotopes decay to two distinct *Pb* isotopes, measuring only the lead isotopic composition can yield age information by the following equation:

$$\frac{^{207}\text{Pb}^*}{^{206}\text{Pb}^*} = \frac{^{235}\text{U}(e^{\lambda_{235}t} - 1)}{^{238}\text{U}(e^{\lambda_{238}t} - 1)}$$

, with a uniform  $\frac{^{238}\text{U}}{^{235}\text{U}}$  ratio on earth (= 137.88) and known decay constants ( $\lambda_{238}$  and  $\lambda_{235}$ , Steiger and Jäger, 1977), the age can be solved iteratively. The  $\frac{^{207}\text{Pb}^*}{^{206}\text{Pb}^*}$  (the ratio of the radiogenic isotopes) is a function of the slope of a straight line in a  $^{207}\text{Pb}/^{204}\text{Pb}$  vs.  $^{206}\text{Pb}/^{204}\text{Pb}$  diagram and the age can be interpreted as the time of the final *Pb* isotopic homogenization of samples defining this line.

The errors of the measurement of the *Pb* isotopic composition are mainly dependent on the accuracy of the  $^{204}\text{Pb}$  measurement, which is the least abundant isotope of common lead. Thus the errors of the  $^{206}\text{Pb}/^{204}\text{Pb}$  and the  $^{207}\text{Pb}/^{204}\text{Pb}$  ratios are highly correlated. *CLEO* calculates the error correlation between the  $^{206}\text{Pb}/^{204}\text{Pb}$ ,  $^{207}\text{Pb}/^{204}\text{Pb}$  and  $^{207}\text{Pb}/^{206}\text{Pb}$  measurements, if all three isotope ratios are given with their analytical error. For calculation of the regression line, the algorithm according York (1969) can be used, which

[ 1] add new data	
[ 2] load/save/import/export dataset	[ 1] load CLEO data file [ 2] save CLEO data file [ 3] save as CLEO data file [ 4] import space separated file [ 5] export space separated file [ 6] export as .tex table [ 7] export as .cvs file
[ 3] modify data	[ 1] save dataset [ 2] save dataset as [ 3] delete data point [ 4] change data point [ 5] add dataset [ 6] sort data [ 7] display dataset [ 8] display regressions [ 9] delete regressions
[ 4] plot diagram	[ 1] 207/204-206/204 [ 2] 208/204-206/204 [ 3] 208/204-207/204 [ 4] 207/204+208/204-206/204 (w/o multiplot) [ 5] 207/206-206/204 [ 6] 207/206-204/206 [ 7] define symbols for this dataset [ 8] principal components
[ 5] modify diagram	[ 2] add title [ 3] remove legend [ 4] add legend [ 5] edit labels [ 6] re-show labels [ 7] rescale axes [ 8] calculate regression (selected samples only) [ 9] define regression line by coefficients or display previous [10] display evolution lines [11] intersection of regressions with evolution lines [12] export diagram
[ 6] exit	
[ 7] switch to octave	

Table 1. Main and sub menu of *CLEO*

respects the error on both variables and the correlation between these errors. The correct error calculation for this regression is adopted from Titterington and Halliday (1979).

In a  $^{207}\text{Pb}/^{204}\text{Pb}$  vs.  $^{206}\text{Pb}/^{204}\text{Pb}$  diagram a straight line can also be interpreted as mixing between two distinct isotopic reservoirs, thus care must be taken in interpreting such datasets.

### 3 CLEO

*CLEO* is a script written for *Octave*. It can be used and modified without commercial programs, requiring only an installation of *Octave*, which is available for most operating systems (<http://www.octave.org>). The script can be executed within *Octave* or depending on the operation system be executed interactively (see appendix A).

### 3.1 Capabilities

*CLEO* is used to input the *Pb* isotopic data and to correct them for mass fractionation (the mass-spectrometer dependent fractionation values must be modified in the script. Already defined values are 3.5‰ per  $\Delta amu$  for dynamic measurements using the SEM, 1.45‰ per  $\Delta amu$  for static measurements using the Faraday cups). Loaded data can be converted into a .txt file to use the data with other applications or into a .tex file to produce tables with L<sup>A</sup>T<sub>E</sub>X (as Table 2).

Additionally, text files can be imported, if the data are already in a computer readable format. Thus *Pb* data can be imported from MsExcel<sup>TM</sup> or from an electronic document by pasting the data to a text file.

Data can be saved and reloaded, data points can be removed, or new data can be appended. If a dataset is available, it can be resorted according to the sample names or to a selected variable. Additional previous datasets can be appended.

For geological samples it is often useful to compare the samples with lead evolution models. *CLEO* can display the most important evolution lines (i.e. Stacey and Kramers (1975), Cumming and Richards (1975), Canyon Diabolo Troilite (Doe and Zartman, 1979) and the reservoirs used in Zartman and Haines (1988)) and calculate the intersections of a regression line with these evolution lines. Additionally it calculates the  $\mu_1$  values for the Stacey and Kramers (1975) and the Canyon Diabolo Troilite (Doe and Zartman, 1979) initial lead compositions, if a regression line is calculated in a  $^{207}Pb/^{204}Pb$  vs.  $^{206}Pb/^{204}Pb$  diagram. The  $\mu_1$  value is the average  $\mu$  value, which is needed to produce the initial *Pb* isotopic composition of the samples from the initial *Pb* isotopic composition of the according model.

*CLEO* is capable of calculating a Principal Component Analysis (PCA) according to Albarède (1995) and of displaying a two dimensional diagram with two principal components as x- and y-axis. The original  $^{206}Pb/^{204}Pb$ ,  $^{207}Pb/^{204}Pb$  and  $^{208}Pb/^{204}Pb$  axes and the scaled data are also projected to this plane in the diagram. PCA of lead isotopic data reduces the three-dimensional isotopic space to a two dimensional space with the main variances as axes. The percentage of variance along the PCA axes measures the number of independent influences on the dataset and helps to identify different processes (this study) or helps to identify parallel trends (e.g. Abouchami et al., 2000).

All diagrams created with *CLEO* can be exported as postscript file (used for Figure 1-3) or as enhanced meta-file. Using Windows<sup>TM</sup> or Macintosh OsX<sup>TM</sup>, the diagrams can also be directly copied to the clipboard by clicking the main bar with the left mouse button.

sample	$\frac{^{206}\text{Pb}}{^{204}\text{Pb}}$	$\frac{2\sigma}{10^4}$	$\frac{^{207}\text{Pb}}{^{204}\text{Pb}}$	$\frac{2\sigma}{10^4}$	$\frac{^{208}\text{Pb}}{^{204}\text{Pb}}$	$\frac{2\sigma}{10^4}$	$\frac{^{207}\text{Pb}}{^{206}\text{Pb}}$	$\frac{2\sigma}{10^4}$	$R$
02GA70	19.9457	9	15.7566	8	39.2465	19	0.7900	0.01	0.99
02GA70-2	22.0632	106	15.8753	82	40.7129	194	0.7195	0.88	0.97
02GA70-3	34.6379	23	16.5222	13	39.2866	29	0.4770	0.03	0.99
02GA71	20.2585	109	15.8036	85	39.1506	210	0.7801	0.94	0.97
02GA71-2	18.5374	13	15.6984	7	38.6688	27	0.8468	0.01	0.99
02GA71-3	19.8953	12	15.7831	9	39.4074	20	0.7933	0.01	0.99
02GA74-1	31.1250	71	16.3334	40	40.3913	95	0.5248	0.29	0.97
02GA74-2	149.3610	437	22.4068	64	43.1648	96	0.1500	0.02	1.00
02GA74-3	31.8925	121	16.4252	39	40.3311	148	0.5150	0.48	0.95
02GA72	35.9993	20	16.5629	10	40.5800	22	0.4601	0.02	0.99
02GA72-2	34.6311	12	16.5021	5	40.0104	14	0.4765	0.01	0.99
02GA72-4	22.4035	23	15.8978	16	39.6341	41	0.7096	0.04	0.99
02GA72B	186.7779	3791	24.1928	483	44.0186	896	0.1293	0.01	1.00
02GA72B-2F	25.8040	9	16.0756	7	40.1118	15	0.6230	0.01	0.99
02GA72B-2T	24.9118	40	16.0073	7	40.7234	65	0.6426	0.03	0.99
02GA73	47.2085	123	17.1557	34	40.7020	103	0.3634	0.43	0.88
02GA73-2	32.5299	69	16.4013	29	39.8335	81	0.5042	0.20	0.97
02GA73-3	45.4237	31	17.0810	10	40.0430	26	0.3760	0.03	0.99
03GA75-1	20.4210	48	15.7468	35	41.2052	98	0.7711	0.18	0.99
03GA77-1	22.1189	20	15.8790	13	39.3518	35	0.7179	0.03	0.99
03GA77-2	20.2040	42	15.8041	34	41.4763	86	0.7822	0.15	0.99

Table 2.  $^{206}\text{Pb}/^{204}\text{Pb}$ ,  $^{207}\text{Pb}/^{204}\text{Pb}$ ,  $^{208}\text{Pb}/^{204}\text{Pb}$ ,  $^{207}\text{Pb}/^{206}\text{Pb}$  ratios for the samples of the Dlhá Dolina drill core. Measurements are corrected for fractionation. Errors are absolute.  $R$  gives the correlation of the error on the  $^{206}\text{Pb}/^{204}\text{Pb}$ ,  $^{207}\text{Pb}/^{204}\text{Pb}$  and  $^{207}\text{Pb}/^{206}\text{Pb}$  measurements.

### 3.2 Usage

The script is menu based, which is summarized in Tab. 1. The main menu, which appears directly at the start of *CLEO*, is for adding new data, entering the load-data, the modify-data, the plot-data and edit-plot sub menus and for exiting *CLEO*. After entering data, it should be saved and diagrams can be created with 'plot diagram'. Here the user can decide, what isotope ratios should be plotted ( $^{207}\text{Pb}/^{204}\text{Pb}$  vs.  $^{206}\text{Pb}/^{204}\text{Pb}$ ,  $^{208}\text{Pb}/^{204}\text{Pb}$  vs.  $^{206}\text{Pb}/^{204}\text{Pb}$ ,  $^{208}\text{Pb}/^{204}\text{Pb}$  vs.  $^{207}\text{Pb}/^{204}\text{Pb}$ , or a combined  $^{207}\text{Pb}/^{204}\text{Pb}$  and  $^{208}\text{Pb}/^{204}\text{Pb}$  vs.  $^{206}\text{Pb}/^{204}\text{Pb}$ . For radiogenic lead data a  $^{206}\text{Pb}/^{204}\text{Pb}$  vs.  $^{207}\text{Pb}/^{206}\text{Pb}$  and a  $^{204}\text{Pb}/^{206}\text{Pb}$  vs.  $^{207}\text{Pb}/^{206}\text{Pb}$  can also be useful) and specific symbols to group the samples can be defined. Diagrams can be edited using the 'modify diagram' sub-menu. This is the most important menu for calculating ages and modeling the dataset.

## 4 The Dlhá Dolina granite

The intrusive complex of Dlhá Dolina, located in Central Slovakia at 48°46'N; 20°32'E, resembles a tourmaline bearing granite, which is typical for the Gemeric unit. These specialized S-type granites are rich in Li, B and rare metals (Broska and Uher, 2001). *U-Pb* zircon vapor digestion dating and EMPA chemical *U-Th-Pb* monazite dating result in a Permian age for these granites (Monazite: 260-290 Ma, Finger and Broska (1999); Zircon: 241-303 Ma, Poller et al. (2002)). Outcrops of the Dlhá Dolina intrusion are not found, only cassiterite bearing greisens, which were formed due to this intrusion, crop out. Several authors suggest two separated intrusions for this complex, because of the sharp evolution from a barren granite to a rare-metal rich granite (for detailed description of the granites see Dianiška et al., 2002; Dianiška, 1983; Broska and Uher, 2001).

The Dlhá Dolina granite was drilled in 1980s. The core DD-3 is 912 m long and samples used for this study are from 908 m (03GA70), 783 m (03GA71), 691 m (03GA74), 577 m (03GA72) and 504 m (03GA73) depth. These samples evolve from a barren lower granite to a highly evolved granite on the top. Additional to the drill core samples, cassiterite bearing greisen from the outcrop (03GA75 and 03GA77) were analyzed for their lead isotopic composition following the method after Arndt and Todt (1994). The data is given in Table 2.

### 4.1 The *WR-Pb-Pb* data

The samples show a very large spread in the *Pb* isotope space and all drill core samples reflect a good correlation in the  $^{207}\text{Pb}/^{204}\text{Pb}$ - $^{206}\text{Pb}/^{204}\text{Pb}$  space (Figure 1). The un-fractionated granite samples (02GA70 and 02GA71) have normal (“common”)  $^{206}\text{Pb}/^{204}\text{Pb}$  ratios between 18.5 and 22.1. The more evolved samples (02GA72 to 02GA74) have  $^{206}\text{Pb}/^{204}\text{Pb}$  ratios between 22.4 to 35.9, which is a large spread for whole-rock samples. Few splits yielded higher  $^{206}\text{Pb}/^{204}\text{Pb}$  ratios, which is due to grain effects when a *U*-rich mineral is present in the rock split. One fraction even had  $^{206}\text{Pb}/^{204}\text{Pb}$  ratio of 186 (see Table 2). Nevertheless, all data points fall on a common regression line. The sample from the cassiterite greisen on the surface have  $^{206}\text{Pb}/^{204}\text{Pb}$  ratios between 20.2 and 22.1, which is comparable to the barren granite and plot on the same regression line.

The slope of the regression line of the samples corresponds to an  $^{207}\text{Pb}/^{206}\text{Pb}$  age of  $241\pm 0.5$  Ma, which reflects a Permian to Early-Triassic age.

In the  $^{208}\text{Pb}/^{204}\text{Pb}$ - $^{206}\text{Pb}/^{204}\text{Pb}$  space (Figure 1), the situation is completely different. Here no correlation of all data can be observed, only most of the

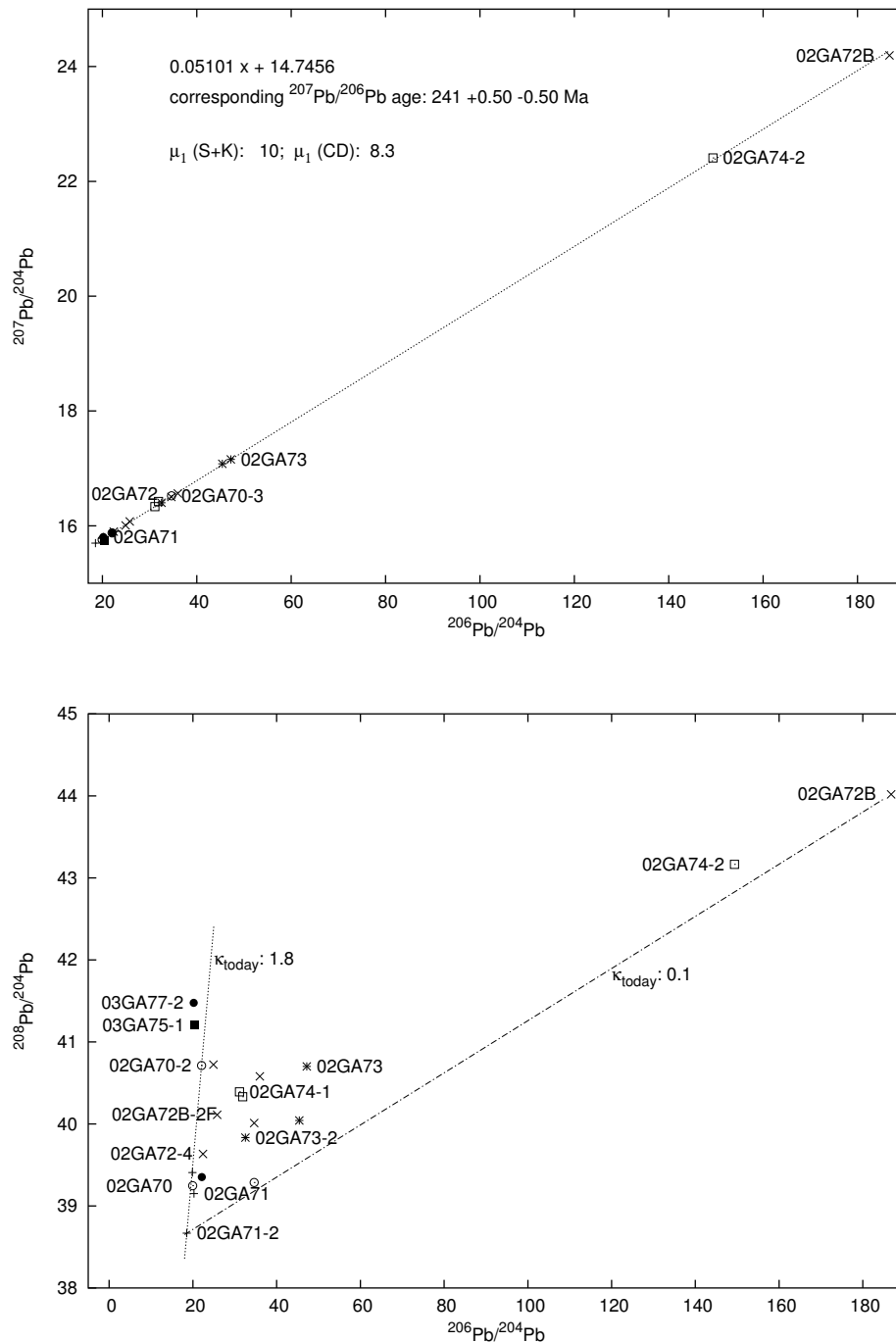


Fig. 1.  $^{207}\text{Pb}/^{204}\text{Pb}$  vs.  $^{206}\text{Pb}/^{204}\text{Pb}$  diagram and  $^{208}\text{Pb}/^{204}\text{Pb}$  vs.  $^{206}\text{Pb}/^{204}\text{Pb}$  for the samples of the Dlhá Dolina subsurface granite. Note the good linear correlation in the  $^{207}\text{Pb}/^{204}\text{Pb}$  vs.  $^{206}\text{Pb}/^{204}\text{Pb}$  diagram, which corresponds to an  $^{207}\text{Pb}/^{206}\text{Pb}$  age of  $241 \pm 0.5$  Ma. Same symbols for samples used in all diagrams.  $\kappa_{\text{today}}$  calculated for reference lines and the age of 241 Ma.

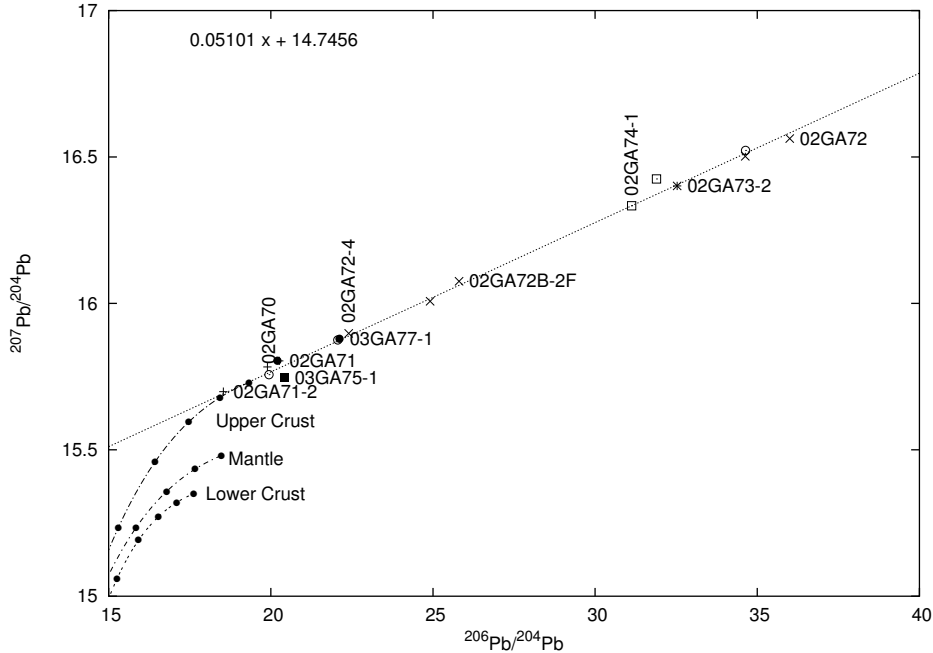


Fig. 2. Detail from the  $^{207}\text{Pb}/^{204}\text{Pb}$  vs.  $^{206}\text{Pb}/^{204}\text{Pb}$  diagram with lead evolution curves drawn for the reservoirs after Zartman and Haines (1988). Ticks on the evolution curves for 0 (right), 500, 1000, 1500 and 2000 Ma (left).

barren granite samples are aligned along a straight line. With the previously calculated  $^{207}\text{Pb}/^{206}\text{Pb}$  age, a  $\kappa$ -value (i.e.  $^{232}\text{Th}/^{238}\text{U}$  ratio) of 1.8 can be calculated from the slope in the  $^{208}\text{Pb}/^{204}\text{Pb}$  vs.  $^{206}\text{Pb}/^{204}\text{Pb}$  diagram. The data points for the more evolved samples plot right of this reference line at lower  $^{208}\text{Pb}/^{204}\text{Pb}$  ratios with high  $^{206}\text{Pb}/^{204}\text{Pb}$  ratios. In Fig. 1 a reference line is also drawn for these samples. This reference line corresponds to a  $\kappa$  value of 0.1, thus  $\text{Th}$  is depleted with respect to  $\text{U}$ . All greisen samples from the outcrop plot left to the reference line at high  $^{208}\text{Pb}/^{204}\text{Pb}$  values. Thus these samples are enriched in  $\text{Th}$  vs.  $\text{U}$  relative to the barren granite. Therefore a effective fractionation of  $\text{U}$  from  $\text{Th}$ , which behave different in oxidizing environments, can be observed in this dataset. The  $\text{U}$  is connected to the magmatic phase and immobile in the fluid phase, whereas the  $\text{Th}$  is transported in a fluid phase, which caused the greisenization.

$\text{Pb}$  evolution lines for the reservoirs after Zartman and Haines (1988) are drawn in Figure 2. The evolution line for Upper Crustal lead plots close to the regression line and the most unradiogenic samples, whereas the evolution lines for Mantle lead and Lower Crustal lead plot distinct from the regression line. This indicates that only lead from an Upper Crustal reservoir, extracted at ages similar to the intrusion age, contributed to the initial lead composition of the granite complex. This can be also seen with the  $\mu_1$  value of 10 for Stacey and Kramers (1975) model composition, which reflects a crustal precursor for the magmatic intrusion.

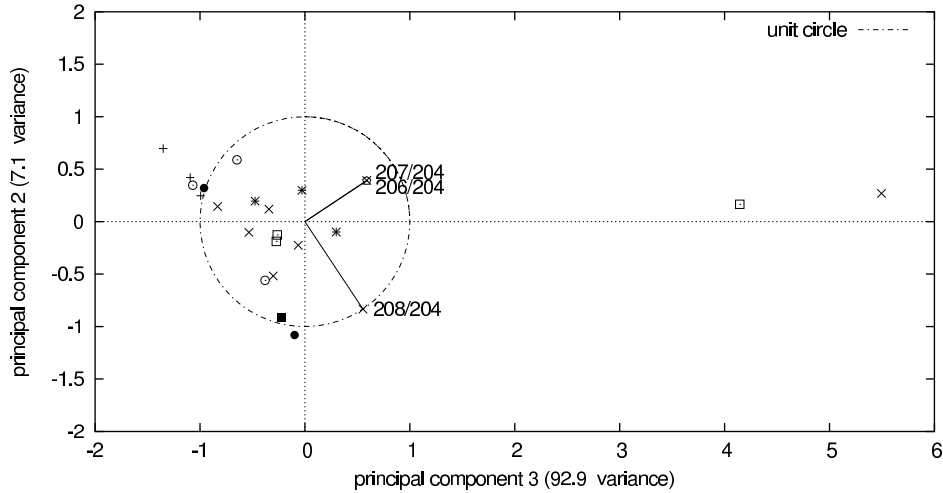


Fig. 3. Two dimensional diagram for the two principal components with the largest variance.

#### 4.1.1 Principal Component Analysis of the Dlhá Dolina data

With PCA the evolution of the granite body can be depicted. The PCA shows that two components result in a total variance of 100% and even one component is accountable for 92.9% of the total variance observed in this dataset. Thus this system is influenced by two effects, radioactive decay and fractionation of  $U$  from  $Th$ , which leads with time to a distinct evolution in the lead isotopes, whereas the radioactive decay results by far in the largest variance.

Fig. 3 shows that the  $^{206}Pb/^{204}Pb$ ,  $^{207}Pb/^{204}Pb$  and  $^{208}Pb/^{204}Pb$  vectors have a positive influence on the main principal component, whereas the second principal component, is negatively correlated to the  $^{208}Pb/^{204}Pb$  and positively correlated to the  $^{206}Pb/^{204}Pb$  and  $^{207}Pb/^{204}Pb$  vectors. The main principal component thus displays the radioactive decay and the second principal component measures the fractionation of  $Th$  from  $U$ .

#### 4.2 Discussion

The  $^{207}Pb/^{206}Pb$  age of  $241 \pm 0.5$  Ma is in good accordance to  $U-Pb$  dating of similar granite bodies in the Špis Gemer ( $(U-Pb)$  zircon age: 241-303 Ma Poller et al., 2002); (chemical monazite age: 260-290 Ma Finger and Broska, 1999)). The younger age reflects the lower closing temperature for the whole rock  $Pb$  system, which corresponds to the last magmatic/hydrothermal activity of this granitoid system. The good correlation of  $^{206}Pb/^{204}Pb$  with  $^{207}Pb/^{204}Pb$  proves a common evolution of the lower barren parts and the upper evolved parts of the Dlhá Dolina granite body and no different timing of these intrusions can be inferred. Because of the different pattern in  $^{208}Pb/^{204}Pb$  for the lower



and the upper parts different mechanism of fractionation must be employed. Fluids probably played a major role in the development of the upper, more evolved parts, which led to a extensive depletion in *Th*. The greisenisation was produced by these fluids, which are enriched in *Th*. The lower parts reflect a normal magmatic fractionation and only a small amount of fractionation of *U* vs. *Th* is observed.

## 5 Summary

Lead isotopic studies are useful in environmental and geological studies and evaluation of these datasets is mathematical not trivial (i.e. York (1969) regressions and iterative  $^{207}\text{Pb}/^{206}\text{Pb}$  age calculations). With *CLEO* a tool for the most important calculations needed for the evaluation of WR-Pb-Pb data is available for non-commercial program users, which can be distributed and modified freely.

## Acknowledgements

IB, ID and MK are thanked for their help during field work and providing the samples. MT is acknowledged for his courses using Matlab. VJ is acknowledged for GCDkit providing a GNU GPL based tool for geochemist and motivating AG for this work.

This program will continuously be enhanced and any critic or contribution is welcome and greatly acknowledged.

## A Octave

*Octave* is a free GNU public license program for mathematical calculations. Installation instructions can be found on the Website <http://octave.org> and downloaded for most recent operating systems. The *CLEO* code is tested on a SUSE Linux 8.0 (*Octave* 2.1.57), Windows<sup>TM</sup> 2k (*Octave* 2.1.36) and Macintosh OsX<sup>TM</sup> (*Octave* 2.1.46).

In a Linux/Unix platform the script can be executed directly from the shell (*chmod +x ./CLEO.oct* and execute with *./CLEO.oct*), whereas on a Windows<sup>TM</sup> platform the the extension *.oct* can be linked with the *Octave* program file (*select "open with .." and select the octave program*). Double-clicking will then invoke the script. With Macintosh OsX<sup>TM</sup> the script can be executed directly

from a Terminal (*./CLEO.oct*), if the first line in the script is changed to */sw/bin/octave -qf*. Alternatively on all platforms it can be started directly from the *Octave* prompt using *source("PATH\_TO\_CLEO/CLEO.oct")*.

Prior to the use of *CLEO*, some values have to be modified in the script. Therefore open the script in a simple text editor and go to line no. 47. Here the correct values for the machine dependend mass fractionation has to be modified, and according to the operating system the according line should be uncommented two lines below.

## B Analytical Technique

Fresh rock splits are used for the analysis of the WR-Pb-Pb isotopic data. On the one hand this eliminates contamination with *Pb* during crushing and milling of the sample and on the other hand it enhances the spread of the WR-Pb-Pb data due to inhomogeneities in the rock splits. The splits are leached with *HF – HNO<sub>3</sub>* mixture overnight on a hotplate. After drying, the sample is taken up in 7n *HBr*, heated for several hours and dried down again. 1 ml of 0.6n *HBr* is used to extract the leachate. Teflon columns with 0.1 ml resin are used to separate the *Pb* to provide a clean fraction for TIMS measurement. *Pb* is eluated with 6n *HCl*. This fraction is loaded with silica gel onto a Re single filament and measured on Finnigan MAT 261 in static mode with multi-collection.

The results of the measurement must be corrected for machine dependent mass fractionation. The correction factors are determined for the international standard NBS 981 (Todt et al., 1996) and a exponential correction with a fractionation coefficient of 1.45 ‰ per  $\Delta amu$  for static mode on the Faraday Cups is applied using *CLEO*.

## References

- Abouchami, W., Galer, S. J. G., Hofmann, A. W., 2000. High precision lead isotope systematics of lavas from the Hawaiian Scientific Drilling Project. *Chemical Geology* 169, 187–209.
- Abouchami, W., Zabel, M., 2003. Climate forcing of the Pb isotope record of terrigenous input into the Equatorial Atlantic. *Earth Planetary Science Letters* 213, 221–234.
- Albarède, F., 1995. *Introduction to geochemical modeling*. Cambridge University Press.
- Arndt, N., Todt, W., 1994. Formation of 1.9 Ga Old Trans-Hudson Continental Crust: Pb Isotopic Data. *Chemical Geology* 118, 9–26.

- Broska, I., Uher, P., 2001. Whole-rock chemistry and genetic typology of the West-Carpathian Variscan granites. *Geologický Zborník - Geologica Carpathica* 52, 79–90.
- Charalampides, G., Manoliadis, O., 2002. Sr and Pb isotopes as environmental indicators in environmental studies. *Environment International* 28, 147–151.
- Chillrud, S. N., Hemming, S., Shuster, E. L., Simpson, H. J., Bopp, R. F., Ross, J. M., Pederson, D. C., Chaky, D. A., Tolley, L.-R., Estabrooks, F., 2003. Stable lead isotopes, contaminant metals and radionuclides in upper Hudson River sediment cores: implications for improved time stratigraphy and transport processes. *Chemical Geology* 199, 53–70.
- Cumming, G., Richards, J., 1975. Ore lead isotope ratios in a continuously changing earth. *Earth Planetary Science Letters* , 155–171.
- Dianiška, I., 1983. Endo- and Exo contact post-magmatic alteration of granites from the eastern part of Špis Gemer Ore Mountains (in Slovak). Ph.D. thesis, Comenius University, Bratislava.
- Dianiška, I., Breitner, K., Broska, I., Kubiš, M., Malachovský, 2002. First Phosphorus-rich Nb-Ta-Sn-specialised granite from the Carpathians - Dlhá Dolina valey granite pluton, Gemeric Superunit, Slovakia. *Geologický Zborník - Geologica Carpathica* 53.
- Doe, B., Zartman, R., 1979. *Geochemistry of Hydrothermal Ore Deposits*, chap. 2: Plumbotectonics, The Phanerozoic. Wiley Interscience Publication, New York, 22–70.
- Finger, F., Broska, I., 1999. The Gemeric S-type granites in southern Slovakia: Late Paleozoic or Alpine intrusion? Evidence from electron-microprobe dating of monazite. *Swiss Bulletin of Mineralogy and Petrology* 79, 439–443.
- Gaab, A., Janák, M., Poller, U., Todt, W., in press. Alpine reworking of Ordovician protoliths in the Western Carpathians: Geochronological and geochemical data on the Muráň Gneiss Complex. *Lithos* .
- Grunsky, E., 2002. R: a data analysis and statistical programming environment - an emerging tool for the geosciences. *Computers & Geosciences* 28, 1219–1222.
- Habicht-Mauche, J. A., Glenn, S. T., Schmidt, M. P., Franks, R., Milford, H., Flegal, A. R., 2002. Stable Lead Isotope Analysis of Rio Grande Glaze Paints and Ores Using ICP-MS: A Comparison of Acid Dissolution and Laser Ablation Techniques. *Journal of Archaeological Science* 29, 1043–1053.
- Janousek, V., Farrow, C., Erban, V., 2003. GCDkit: New PC software for interpretation of whole-rock geochemical data for igneous rocks. *Goldschmidt Conference Abstracts 2003* .
- Ludwig, K. R., 2001. Isoplot/ex rev. 3.49 A geochronological Toolkit for Microsoft Excel. Berkeley Geochronological Center; Special Publications No. 1a .
- Middleton, G., 2000. *Data analysis in Earth sciences using Matlab*. Prentice-Hall, Upper Saddle River, NJ.
- Planchon, F. A. M., van de Velde, K., Rosman, K. J. R., Wolff, E. W., Ferrari,

- C. P., Boutron, C. F., 2003. One hundred fifty year record of lead isotopes in Antarctic snow from Coats Land. *Geochimica et Cosmochimica Acta* 67, 693–708.
- Poller, U., Gladkochub, D., Donskaya, T., Mazukabzov, A., Sklyarov, E., Todt, W., 2004. Timing of Early Proterozoic magmatism along the Southern margin of the Siberian Craton (Kitoy area). *Transactions of the Royal Society* 95. In press.
- Poller, U., Uher, P., Broska, I., Plasienska, D., Janaák, M., 2002. First Permian-Early Triassic zircon ages for tin-bearing granites from the Gemeric unit (Western Carpathians, Slovakia): connection to the post-collisional extension of the Variscan orogen and S-type magmatism. *Terra Nova* 14, 41–48.
- Schettler, G., Romer, R. L., 1998. Anthropogenic influences on Pb/Al and lead isotope signature in annually layered Holocene Maar lake sediments. *Applied Geochemistry* 13, 787–797.
- Stacey, J. S., Kramers, J. D., 1975. Approximation of terrestrial lead isotope evolution by a two-stage model. *Earth Planetary Science Letters* 26, 207–221.
- Steiger, R. H., Jäger, E., 1977. Subcommittee on geochronology: Convention on the use of decay constants in geo- and cosmochronology. *Earth Planetary Science Letters* 36, 359–362.
- Titterton, D. M., Halliday, A. N., 1979. On the fitting of parallel isochrons and the method of maximum likelihood. *Chemical Geology* 26, 183–195.
- Todt, W., Cliff, R., Hanser, A., Hofmann, A., 1996. Earth Processes: Reading the Isotopic Code, vol. 95, chap. 202Pb + 205Pb double spike for lead isotopic analyses. *Geophysikal Monograph*, 429–437.
- York, D., 1969. Least squares fitting of a straight line with correlated errors. *Earth Planetary Science Letters* 5, 320–324.
- Zartman, R., Haines, S., 1988. The plumbotectonic model for Pb isotopic systematics among major terrestrial reservoirs - A case for bi-directional transport. *Geochimica et Cosmochimica Acta* 52, 1327–1339.

# Chapter 6

## Analytical techniques

For the Sr and Nd isotopic analyses and the determination of the Rb/Sr and Sm/Nd elemental ratios, a combined approach was established during the course of this PhD study. The goal was to circumvent the need of isotopic tracer for determining the elemental ratios and to enhance the digestion procedure by using a microwave oven. The isotopic Sr and Nd composition, the Rb/Sr and Sm/Nd ratios, and the complete REE pattern can be obtained using the same digestion solution. This method yields an accuracy of  $\approx 10\%$  for the REE concentrations and  $\approx 5\%$  for the elemental ratios as is demonstrated by first results on international reference material (IRM) (table 2 to 4).

This approach uses a TIMS (Finnigan MAT 261) in multi-collection mode for isotopic and an ICPMS (Finnigan Element2) with a single collector for elemental analyses. For the microwave assisted digestion a *CEM Mars5* with temperature control equipped with 12 pressure safe XP-1500 vessels was used (Fig. 2).

In order to enhance cleanliness and to facilitate the weighing procedures, only small PTFE beakers (7 ml) are used for the sample digestion. These beakers are introduced to pressure-safe microwave digestion vessel and *HCl* is added to ensure pressure equilibrium outside and inside the PTFE beaker



Figure 1: Detail for the assembly of the vessels for the microwave assisted digestion. PTFE beakers containing the sample and acid are introduced to the pressure safe microwave vessel.  $HCl$  is added outside the beaker to the vessel to ensure pressure equilibrium.

analogously to Parr bombs classically used.

For quantification and drift correction of the ICPMS measurements two stock solution were added to the samples. A 2 ppm  $In$  solution is added directly at the weighing step for quantification and a 2 ppm  $Re - Ru$  mixed solution is added prior to ICPMS measurement for drift correction.

In the following section details about this approach will be given.

## 1 Microwave assisted digestion of granitoid material

To facilitate the sample preparation and digestion, a microwave assisted technique was used. Similar approaches are described by Das et al. (2001),

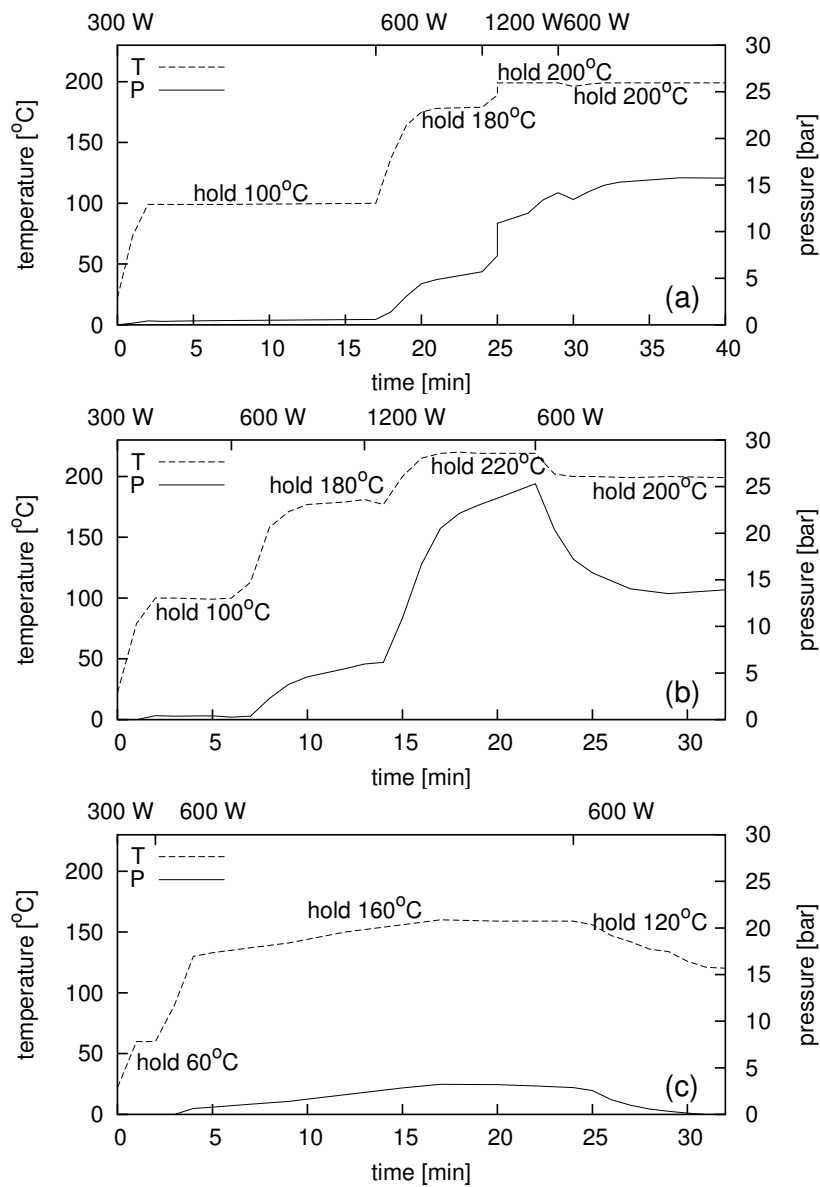


Figure 2: P-T diagram for the three digestion steps used for microwave assisted digestion. Acids used for the first and second step are  $HF - HNO_3$ , for the last step  $HCl$ . Temperature limits shown in the diagram, energy of the microwave oven indicated at the top of each diagram.

Sen Gupta and Bertrand (1995), Totland et al. (1992) and Totland et al. (1995). For digesting granitoid material, having a high  $SiO_2$  content, these approaches were slightly modified for this procedure:

The powdered sample is weighted into 7 ml PTFE beakers. 50  $\mu$ l of the *In* stock solution is added to each sample and weighings are recorded. To the beakers  $\approx 3$  ml *HF* and  $\approx 1$  ml  $HNO_3$  is added so that the beakers are filled to two-third and introduced to the pressure-safe microwave digestion vessels (Fig. 2). Into these vessels 5 ml of *HCl* is added to provide high pressure environment outside the beakers. These vessels are closed tightly and introduced to the microwave *CEM Mars5* and radiated for 18 min with 300 W, 7 min with 600 W, 5 min with 1200 W and finally 10 min with 600 W. These steps are temperature controlled, thus that 100°C, 180°C and 200°C, respectively, are not exceeded (Fig. 2a). Maximum pressure attained during this step is  $\approx 16$  bar at the end. After cooling, the vessels are opened and the *HCl* is discarded. The beakers, which lost approximately 50% of acid, are refilled with *HF* and  $HNO_3$  so that the beakers are again filled to two-third. Between the microwave digestion steps the samples are not evaporated to complete dryness to prevent formation of insoluble residue. The loss of acid can not be prevented, because *HF* dissolves silicate minerals and forms  $SiF_4$ , which is gaseous. Thus a over pressures forms inside the beaker and the  $SiF_4$  is expected to be lost from the beaker. To prevent loss of sample during digestion, the temperature is hold at 100°C for 18 min to ensure pressure equilibrium and minimize excessive boiling. The beakers are re-assembled together *HCl* into the vessels. The second *HF-HNO<sub>3</sub>* step is irradiated for 6 min at 300 W, for 7 min at 600 W, for 9 min at 1200 W, and for 10 min at 600 W. Maximum temperature and pressure during the 1200 W step is 220°C and 25 bar (Fig. 2b). After cooling, the beakers are refilled with *HCl* and introduced once more to the microwave. This last step heats the samples for 25 min at 160°C using 600 W. After the last *HCl* microwave



step the samples are evaporated to incipient dryness on a hotplate, refilled with  $HCl$  and left overnight on a warm hotplate for equilibration. These solutions are checked for clearness and evaporated to complete dryness.

Loss of sample from the beaker to the vessel during microwave digestion was monitored once and the loss from the beaker was generally less than 1%. The blank level in the closed PTFE beakers is below 15  $\mu g$  for  $Sr$ , whereas the blank level outside the closed beaker can be up to 10 ng due to the handling of the beakers. This shows that contamination from the vessel to the beaker is very low (Poller and Neuhäuser, pers. comm).

For splitting, the dried sample is dissolved in 5n  $HNO_3$ . After overnight equilibration on hotplate a clear solution is obtained. This is split in two halves, one split for isotopic analysis, one split for elemental analysis. There is no need of weighing the splits exactly, because the quantification will be obtained by the sample-to- $In$  ratio and the isotopic composition is independent of the amount of split used. The split for isotopic analysis is again dried down and preserved for column chemistry (section 2).

The ICPMS split is transferred to 50 ml PE tube, 50  $\mu l$  of  $Re - Ru$  solution is added, and the exact weight of this is recorded. This is important for the drift correction. The 50 ml PE tube is then filled to 50 ml with 5n  $HNO_3$  to provide the solution for ICPMS analysis (section 3).

## 2 Column chemistry for Sr and Nd separation and loading for TIMS measurements

Column chemistry for separation of  $Sr$  and  $Nd$  is applied to the samples according White and Patchett (1984).

This method applies standard ion exchange procedures. The sample is dissolved in 2.5n  $HCl$  and transferred to the prepared 5ml columns filled with AG50W-X12 resin.  $Sr$  is eluted from the column after 42 ml 2.5n  $HCl$  with

8 ml 2.5n *HCl* and the REE consecutively eluted with 13 ml 6n *HCl* after an additional wash step with 5 ml 6n *HCl*. The *Sr* fraction is cleaned on 1 ml resin columns with an according smaller amount of 2.5n *HCl*. *Nd* is separated from the REE fraction using columns filled with 2 ml Teflon powder coated with di-2-ethylhexyl orthophosphoric acid. It is eluted with 6 ml 0.18n *HCl* after 10 ml 0.18n *HCl* wash.

Measurements were made on a Finnigan MAT261 in static mode. A fraction of the cleaned *Sr* ( $\approx 50$  ng), depending on the concentration of the sample, is loaded using 2n *HCl* on *W* single filaments. The *W* filaments were prepared with 1 $\mu$ l *TaF* prior to loading the sample. The filament is dried at 2.5A and heated for 30 sec with 4.2A.

Also a fraction of the cleaned *Nd* ( $\approx 50$  ng) is loaded on *Re* double filaments with 2n *HCl*. The sample is dried at 1.2A and glowed shortly at 2A.

### 3 Relative-Sensitivity-Factor quantification for ICPMS analysis

The ICPMS solutions were measured on the ICPMS *Element2* using medium and high resolution mode to analyze Sr, Rb, and the REE. The high resolution mode is necessary for the HREE to resolve isobaric interferences. Table 1 lists details for the measurement. Measuring time for each sample was  $\approx 5$  min with 30 individual scans summarized to 3 runs for each resolution. Together with the wash and the takeup time one sample was measured within 10 min.

The quantification was obtained using a dissolution of the IRM GSP-2 with known concentrations (Raczek et al., 2001). This standard is prepared analogously as the samples and used as standard for calculation of the relative sensitivity factors (RSF) relative to the added *In*. These RSF are then applied to the samples after a linear mass dependent drift correction using *Re* – *Ru* (Eggins et al., 1997; Cheatham et al., 1993).

measured isotope	resolution	mass window <sup>2</sup> [%]	integration window <sup>3</sup> [%]	settling time [s]	samples per peak <sup>4</sup>
<sup>85</sup> Rb	MR	120	80	0.300	20
<sup>88</sup> Sr	MR	120	80	0.001	20
<b><sup>101</sup>Ru</b>	MR	120	80	0.037	20
<b><sup>115</sup>In</b>	MR	120	80	0.001	20
<sup>139</sup> La <sup>1</sup>	MR	180	80	0.050	25
<sup>140</sup> Ce	MR	120	80	0.001	20
<sup>141</sup> Pr	MR	120	80	0.001	20
<sup>143</sup> Nd	MR	120	80	0.001	20
<sup>147</sup> Sm	MR	120	80	0.001	20
<b><sup>187</sup>Re</b>	MR	120	80	0.051	20
<b><sup>101</sup>Ru</b>	HR	200	80	0.300	20
<b><sup>115</sup>In</b>	HR	200	80	0.001	20
<sup>151</sup> Eu	HR	200	80	0.057	20
<sup>158</sup> Gd	HR	200	80	0.001	20
<sup>159</sup> Tb	HR	200	80	0.001	20
<sup>163</sup> Dy <sup>1</sup>	HR	230	80	0.001	25
<sup>165</sup> Ho	HR	200	80	0.001	20
<sup>167</sup> Er	HR	200	80	0.001	20
<sup>169</sup> Tm	HR	200	80	0.001	20
<sup>172</sup> Yb	HR	200	80	0.001	20
<sup>175</sup> Lu	HR	200	80	0.038	20
<b><sup>187</sup>Re</b>	HR	200	80	0.001	20

<sup>1</sup>used as locked mass

<sup>2</sup>width actually measured

<sup>3</sup>width used for quantification by integration

<sup>4</sup>samples measured during one scan over 100% of the peak width.

Table 1: Details for the method used for measurements on *Element2*.

In the following the calculation for evaluation will be described:

**Blank correction:**

A blank correction was applied by the software of the *Element2*. Therefore the 5n  $HNO_3$  was analyzed at the start of a sequence. Blank level was in general below 0.1% of the analyte intensity.

**Drift correction:** The drift was corrected with a linear correction using the *Re – Ru* mixed solution added prior to measurement. A correction factor  $x$  is calculated for *Re* and *Ru* and the intermediate masses corrected according to:

$$x = \frac{I_{smp}/m_{ReRu,smp}}{I_{std}/m_{ReRu,std}}$$

$$x = \frac{I_{smp}/(w_{ReRu,smp} * c_{ReRu})}{I_{std}/(w_{ReRu,std} * c_{ReRu})}$$

because  $c_{ReRu}$  is equal for sample and initial sample:

$$x = \frac{I_{smp}/w_{ReRu,smp}}{I_{std}/w_{ReRu,std}}$$

Correction for each analyte isotope is accordingly obtained by:

$$x_{isotop} = \frac{(x_{Re} - x_{Ru})}{M_{Re} - M_{Ru}} * (M_{Re} - M_{isotop}) + x_{Re}$$

$$I_{corr} = I_{meas} * x_{isotop}M$$

, with

<i>smp</i>	-	sample
<i>std</i>	-	standard
<i>ReRu</i>	-	stock solution used for drift correction
$c_{ReRu}$	-	concentration of the stock solution [ppm]
$x$	-	correction factor [1]
$I$	-	Intensity [cps]
$m$	-	amount of internal standard in sample [ $\mu$ g]
$w$	-	weight of internal standard stock solution [mg]
<i>meas</i>	-	measured
<i>corr</i>	-	corrected

**Relative Standard Factor Quantification:**

The general formula for **SF** (Sensitivity Factors) according to Doherty (1989):

$$SF = \frac{c}{I * H} = \frac{\frac{m}{D}}{I * H}$$

formula to calculate the **RSF** (Relative Sensitivity Factors) for an isotope of a standard sample:

$$RSF_A = \frac{SF_A}{SF_N} = \frac{\frac{\frac{m_A}{D_A}}{I_A * H_A}}{\frac{\frac{m_N}{D_N}}{I_N * H_N}} = \frac{\frac{m_A}{D_A}}{I_A * H_A} * \frac{I_N * H_N}{\frac{m_N}{D_N}} =$$

, because the dilution factor  $D = D_A = D_N$

$$= \frac{m_A}{m_N} * \frac{I_N * H_N}{I_A * H_A} = \frac{(c_A * w_{std})}{(c_N * w_{Instock, std})} * \frac{I_N}{I_A} * \frac{H_N}{H_A}$$

to calculate the concentration in the samples using the previously calculated RSF:

$$c_{smp,A} = RSF_A * \frac{I_{smp,A}}{I_{smp,N}} * \frac{H_A}{H_N} * \frac{(c_N * w_{Instock,smp})}{w_{smp}}$$

, with

- $H$  - isotopic abundance
- $A$  - analyte isotope
- $N$  - normalizing isotope
- $smp$  - sample
- $std$  - standard
- $SF$  - sensitivity factor [ng/ml/cps]
- $RSF$  - relative sensitivity factor [1]
- $m$  - amount of element [ng]
- $D$  - final Dilution [ml]
- $I$  - intensity [cps]
- $c$  - concentration [ppm]
- $c_N$  - concentration of In stock solution
- $w$  - weight [mg]

	GSP-2 <sub>ref</sub>	GSP-2c	GSP-2a	GSP-2b <sup>1</sup>	GSP-2b <sup>1</sup>	GSP-2b <sup>1</sup>	GSP-2c <sup>1</sup>	GSP-2d	GSP-2eI <sup>1</sup>	GSP-2eII <sup>2</sup>	mean	RSD [%]
used as standard measured on				GSP-2b 31.7.03				GSP-2eI 2.2.04				
Rb	242	245	202	239	237	235	239	247	243	243	237	5.5
Sr	238	242	228	237	237	237	234	240	236	239	237	1.6
La	186.0	177.3	138.2	184.4	188.0	191.4	192.2	198.4	183.7	185.0	182.5	9.1
Ce	445.0	440.0	349.0	452.8	448.6	464.0	453.1	460.6	422.6	426.6	436.2	7.7
Pr	50.7	50.2	38.5	51.0	49.9	49.9	55.0	57.0	50.5	50.2	50.3	9.5
Nd	207.0	177.3	165.4	207.6	196.8	204.4	222.8	224.6	206.7	210.5	202.3	9.1
Sm	26.2	24.7	21.3	26.3	26.1	25.4	27.2	27.3	25.9	26.0	25.6	6.7
Eu	2.3	2.2	1.9	2.2	2.2	2.2	2.4	2.3	2.2	2.3	2.2	5.6
Gd	12.2	12.2	10.5	12.9	13.0	13.2	12.5	12.3	11.8	12.3	12.3	6.1
Tb	1.3	1.4	1.2	1.5	1.4	1.4	1.4	1.3	1.3	1.4	1.4	5.3
Dy	5.7	5.4	4.9	5.7	5.6	5.6	5.9	5.5	5.3	5.7	5.5	5.0
Ho	1.0	1.0	1.0	1.1	1.1	1.1	1.0	1.0	1.0	1.0	1.0	3.8
Er	2.3	2.3	2.2	2.4	2.4	2.4	2.3	2.2	2.2	2.3	2.3	3.2
Tm	0.3	0.3	0.3	0.3	0.3	0.3	0.3	0.3	0.3	0.3	0.3	4.7
Yb	1.6	1.6	1.6	1.7	1.7	1.7	1.7	1.6	1.6	1.7	1.7	2.1
Rb/Sr	1.017	1.014	0.886	1.005	1.002	0.993	1.022	1.031	1.028	1.018	1.002	4.2
Sm/Nd	0.127	0.140	0.129	0.127	0.132	0.124	0.122	0.122	0.125	0.124	0.127	4.3

<sup>1</sup>double measurement on same dilution <sup>2</sup>analysis on second split

Table 2: Analyses of IRM GSP-2 of two independent microwave dissolution procedures and two independent analysis sequences. GSP-2b and GSP-2eI used as standard. Reference value after Raczek et al. (2001).

	JG-1 <sub>ref</sub>	JG-1a	JG-1b	JG-1c	JG-1d	mean	RSD [%]
used as standard measured on		GSP-2b 31.7.03		GSP-2eI 2.2.04			
Rb	178	138	131	179	180	179	0.1
Sr	186	174	178	187	188	187	0.4
La	20	18.8	15.6	24.0	24.0	24.0	0.1
Ce	43	40.7	35.4	50.2	49.7	50.0	0.7
Pr	4.9	4.3	3.9	5.8	5.7	5.7	0.5
Nd	17.8	18.8	17.4	23.5	23.6	23.5	0.3
Sm	4.14	4.2	4.2	5.1	5.1	5.1	0.5
Eu	0.67	0.7	0.7	0.8	0.8	0.8	1.0
Gd	4.4	4.1	4.5	4.5	4.6	4.5	1.4
Tb	0.75	0.7	0.8	0.8	0.8	0.8	1.7
Dy	4.75	3.8	4.5	4.2	4.1	4.1	2.3
Ho	0.99	0.8	1.0	0.8	0.8	0.8	0.8
Er	2.99	2.4	2.9	2.3	2.3	2.3	1.0
Tm	0.46	0.4	0.5	0.4	0.4	0.4	3.0
Yb	3	2.4	3.1	2.6	2.5	2.6	2.7
Rb/Sr	0.957	0.792	0.735	0.962	0.956	0.959	0.4
Sm/Nd	0.233	0.221	0.238	0.216	0.217	0.217	0.2

Table 3: Analyses of IRM JG-1 of two independent microwave dissolution procedures and two independent analysis sequences. GSP-2b and GSP-2eI used as standard. Reference value after Dulski (2001). For JG-1a and JG-1b too low concentrations were measured and these analyses are classified as outliers.

### 3.1 Results on IRM

Two digestion runs and measurement sequences of IRM were performed to check the precision of the RSF evaluation (tables 2 to 3).

Within each digestion run, GSP-2 was dissolved thrice (a-c and d-f), JG-1 and JG-2 twice (a-b and c-d). Every dissolution was spit in two fractions and one split diluted for ICPMS analysis. The two digestion runs were prepared and analyzed separately.

For the first run, GSP-2b was used as standard to calculate the RSF and re-measured thrice during the measuring sequence to check for drift effects. Also GSP-2c was re-measured once to check for drift effects (table 2). JG-1a, JG-1b, JG-2a and JG-2b were quantified using the RSF determined for the GSP-2b in the beginning of this sequence (table 3 and 4).

CHAPTER 6: ANALYTICAL TECHNIQUES

JG-2 <sub>ref</sub> used as standard measured on	JG-2a	JG-2b	JG-2cI <sup>2</sup>	JG-2d	JG-2d <sup>1</sup>	JG-2cII <sup>2</sup>	mean	RSD [%]	
	GSP-2b 31.7.03		GSP-2eI 2.2.04						
Rb	293	298	301	302	302	303	306	302	0.9
Sr	16.2	17	17	17	17	17	17	17	1.1
La	19	21.5	21.0	23.9	23.9	24.1	24.1	23.1	6.2
Ce	45	54.7	52.4	57.3	57.8	57.4	58.3	56.3	4.0
Pr	6.0	6.4	6.1	7.4	7.3	7.3	7.4	7.0	8.3
Nd	24	29.7	27.5	32.3	31.4	31.9	32.2	30.8	6.1
Sm	7.5	9.0	8.1	9.4	9.1	9.2	9.3	9.0	5.2
Eu	0.09	0.1	0.1	0.1	0.1	0.1	0.1	0.1	6.7
Gd	9.3	11.3	9.6	10.4	10.0	9.9	9.7	10.1	6.0
Tb	1.74	2.2	1.9	2.0	2.0	1.9	1.9	2.0	6.5
Dy	11.7	12.9	10.9	12.0	11.8	11.3	11.6	11.8	5.9
Ho	2.5	3.1	2.7	2.7	2.7	2.6	2.5	2.7	6.6
Er	7.8	8.7	7.6	8.0	7.8	7.8	7.5	7.9	5.6
Tm	1.2	1.5	1.3	1.3	1.3	1.3	1.3	1.3	5.2
Yb	8.1	9.5	8.3	9.1	9.0	8.7	8.9	8.9	4.4
Rb/Sr	18.086	17.716	18.011	17.765	18.130	17.864	17.876	17.894	0.9
Sm/Nd	0.313	0.304	0.295	0.292	0.288	0.290	0.288	0.293	2.1

<sup>1</sup>double measurement on same dilution <sup>2</sup>analysis on second split

Table 4: Analyses of IRM JG-2 of two independent microwave dissolution procedures and two independent analysis sequences. GSP-2b and GSP-2eI used as standard. Reference value after Dulski (2001).

For the second run, dissolution GSP-2e was used as standard and re-measured once. Additional for sample GSP-2e and JG-2c both splits (I and II, table 2 and 4) were diluted and measured to check for effects caused by the splitting.

The drift correction results in good results as can be seen for the re-measurements of the same solution. Also if the two splits were diluted individually, the results correspond within error (table 2 and 4).

As shown in table 2 to 4 result this method in a precision of  $\approx 10\%$  for elemental concentrations and  $\approx 5\%$  for elemental ratios. The results agree with the reference values for the samples, only two dissolutions, JG-1a and JG-1b, resulted in a too low concentrations probably due to problems during weighing of the samples and are classified as outliers (table 3). These results are comparable to the precision reported for external calibration as presented in Eggins et al. (1997). Eggins et al. (1997) even reports precision below 5%



for a *In* normalized external calibration procedure for the REE, indicating that the precision can be enhanced by prolonging measuring time.

The REE pattern and concentration obtained with this method are in good agreement with analyses from ACME Laboratories, Vancouver (Canada). This can be seen in Chapter 4 where two datasets, measured in Mainz and in Vancouver for samples from the same units, are joined and interpreted together. Also the Rb/Sr and Sm/Nd ratios obtained by this method result in reasonable values for the geodynamic calculations and interpretations.

# Danksagung

An dieser Stelle möchte ich mich ganz herzlich bei allen bedanken, die zur Entstehung dieser Arbeit beigetragen und mich während dieser Zeit unterstützt haben.

Dazu zählen vor allem meine Betreuer am MPI für Chemie, UP und WT, die mich in Analytik und die Auswertung von Isotopiedaten einführten und mir jederzeit mit Rat und Tat zur Seite standen. Ein riesiges Dankeschön geht an Beide für die excellenten Geländeaufenthalte und die Tage in der 'Chata Jochy', für deren Benutzung ich mich herzlich bei JW und seiner Familie bedanken möchte.

Meinen slovakischen Kollegen MJ, MK, IB, ID, DP, IP und MK danke ich für die ausführliche und freundliche Einführung in die Geologie der Slowakei und die Abende im 'Pilsener Pub', Bratislava. Für die Einführung in 'Fernet Stock' in Martin danke ich M, L, M und I.

Ein grosser Dank geht an die Laborantinnen des Reinraumlabor, Frau DN und Frau EM, für Ihre Unterstützung bei der Laborarbeit. Frau BS sei herzlich für die Unterstützung bei den Messungen am *Element2* gedankt.

Besonders möchte ich mich aber bei meiner Frau Simone und meiner Tochter Johanna für die positive Ablenkung in den letzten Wochen und die tatkräftige Unterstützung während der gesamten Zeit danken.

Meinen Eltern und meinen Grosseltern möchte ich ganz besonders für Ihr Vertrauen und Ihre Unterstützung während der letzten 29 Jahre danken.

# Complete Reference List

- Abouchami, W., Galer, S. J. G., Hofmann, A. W., 2000. High precision lead isotope systematics of lavas from the Hawaiian Scientific Drilling Project. *Chemical Geology* 169, 187–209.
- Abouchami, W., Zabel, M., 2003. Climate forcing of the Pb isotope record of terrigenous input into the Equatorial Atlantic. *Earth Planetary Science Letters* 213, 221–234.
- Albarède, F., 1995. *Introduction to geochemical modeling*. Cambridge University Press.
- Arndt, N., Todt, W., 1994. Formation of 1.9 Ga Old Trans-Hudson Continental Crust: Pb Isotopic Data. *Chemical Geology* 118, 9–26.
- Bajaník, Š., Hovorka, D., 1981. The amphibolite facies metabasites of the Rakovec Group of Gemericum (the Western Carpathians). *Geologický Zborník - Geologica Carpathica* 32, 679–705.
- Bau, M., 1996. Controls on the fractionation of isovalent trace elements in magmatic and aqueous systems: evidence from Y/Ho, Zr/Hf, and lanthanide tetrad effect. *Contributions to Mineralogy and Petrology* 123, 323–333.
- Bezák, V., 1991. Metamorphic conditions of the Veporic unit in the Western Carpathians. *Geologický Zborník - Geologica Carpathica* 42, 219–222.
- Broska, I., Kubiš, M., Williams, C., Konečný, P., 2002. The compositions of rock-forming and accessory minerals from the Gemeric granites (Hnilec

- area, Gemeric Superunit, Western Carpathians). *Bulletin of the Czech Geological Survey* 77, 147–155.
- Broska, I., Uher, P., 2001. Whole-rock chemistry and genetic typology of the West-Carpathian Variscan granites. *Geologický Zborník - Geologica Carpathica* 52, 79–90.
- Cambel, B., Král, J., Burchart, J., 1990. Izotopová geochronológia kryštálinka západných karpát. VEDA.
- Charalampides, G., Manoliadis, O., 2002. Sr and Pb isotopes as environmental indicators in environmental studies. *Environment International* 28, 147–151.
- Cheatham, M., Sangrey, W., White, W., 1993. Sources of error in external calibration ICP-MS analysis of geological samples and an improved non-linear drift correction procedure. *Spectrochimica Acta Part B* 48B, E487–E506.
- Chen, F., Hegner, E., Todt, W., 2000. Zircon ages and Nd isotopic and chemical compositions of orthogneisses from the Black Forest, Germany: evidence for a Cambrian magmatic arc. *International Journal of Earth Science* 88, 791–802.
- Chillrud, S. N., Hemming, S., Shuster, E. L., Simpson, H. J., Bopp, R. F., Ross, J. M., Pederson, D. C., Chaky, D. A., Tolley, L.-R., Estabrooks, F., 2003. Stable lead isotopes, contaminant metals and radionuclides in upper Hudson River sediment cores: implications for improved time stratigraphy and transport processes. *Chemical Geology* 199, 53–70.
- Compston, W., Williams, I., Meyer, C., 1984. U-Pb geochronology of zircons from lunar breccia 73217 using a sensitive high mass-resolution ion microprobe. *Journal of Geophysical Research* 89, B525–B534. Supplement.
- Cumming, G., Richards, J., 1975. Ore lead isotope ratios in a continuously changing earth. *Earth Planetary Science Letters* , 155–171.

- Dallmeyer, R. D., Neubauer, F., Handler, R., Fritz, H., Müller, W., Pana, D., Putiš, M., 1996. Tectonothermal evolution of the internal Alps and Carpathians: Evidence from  $^{40}\text{Ar}/^{39}\text{Ar}$  mineral and whole-rock data. *Ecolgae Helveticae* 89, 203–227.
- Das, A. K., Chakraborty, R., de la Guardia, M., Cervera, M. L., Goswami, D., 2001. ICP-MS multielement determination in fly ash after microwave-assisted digestion of samples. *Talanta* 54, 975–981.
- Dianiška, I., 1983. Endo- and Exo contact post-magmatic alteration of granites from the eastern part of Špis Gemer Ore Mountains (in Slovak). Ph.D. thesis, Comenius University, Bratislava.
- Dianiška, I., Breitner, K., Broska, I., Kubiš, M., Malachovský, 2002. First Phosphorus-rich Nb-Ta-Sn-specialised granite from the Carpathians - Dlhá Dolina valey granite pluton, Gemeric Superunit, Slovakia. *Geologický Zborník - Geologica Carpathica* 53.
- Doe, B., Zartman, R., 1979. *Geochemistry of Hydrothermal Ore Deposits*, chap. 2: Plumbotectonics, The Phanerozoic. Wiley Interscience Publication, New York, 22–70.
- Doherty, W., 1989. An internal standardization procedure for the determination of yttrium and the rare earth elements in geological materials by inductive coupled plasma-mass spectrometry. *Spectrochimica Acta Part A* 44B, 263–280.
- Dulski, P., 2001. Reference Materials for Geochemical Studies: New Analytical Data by ICP-MS and Critical Discussion of Reference Values. *Geostandard Newsletter* 25, 87–125.
- Eggins, S., Woodhead, J., Kinsley, L., Mortimer, G., Sylvester, P., McCulloch, M., Hergt, J., Handler, M., 1997. A simple method for the precise determination of > 40 trace elements in geological samples by ICPMS using enriched isotope internal standardisation. *Chemical Geology* 134, 311–326.

- Faryad, S., Dianška, I., 1999. Alpine overprint in the early Paleozoic of the Gemericum. *Mineralia Slovaca* 5.
- Faryad, S. W., 1995. Phase petrology and P-T conditions of mafic blueschists from the Meliata unit, West Carpathians, Slovakia. *Journal of Metamorphic Geology* 13, 701–714.
- Faryad, S. W., 1997. Metamorphic petrology of the Early Paleozoic low-grade rocks in the Gemericum. In: Grecula, P., Hovorka, D., Putiš, M. (Eds.), *Geological Evolution of the Western Carpathians. Mineralia Slovaca - Monograph, Geocomplex*, 309–314.
- Finger, F., Broska, I., 1999. The Gemeric S-type granites in southern Slovakia: Late Paleozoic or Alpine intrusion? Evidence from electron-microprobe dating of monazite. *Swiss Bulletin of Mineralogy and Petrology* 79, 439–443.
- Finger, F., Broska, I., Haunschmid, B., Hraško, L., Kohút, M., Krenn, E., Petřík, I., Riegler, G., Uher, P., 2003. Electron-microprobe dating of monazites from Western Carpathian basement granitoids: plutonic evidence for an important Permian rifting event subsequent to Variscan crustal anatexis. *International Journal of Earth Science* , 86–98.
- Gaab, A., Janák, M., Poller, U., Todt, W., in press. Alpine reworking of Ordovician protoliths in the Western Carpathians: Geochronological and geochemical data on the Muráň Gneiss Complex. *Lithos* .
- Gaab, A., Poller, U., Todt, W., Broska, I., Kubiš, M., 2003a. Constraints on Metasomatism of the Dhlá Dolina granite (Western Carpathians, Slovakia). *Beihefte zum European Journal of Mineralogy* 15, 59.
- Gaab, A., Poller, U., Todt, W., Janák, M., 2003b. Geochemical and Isotopic Characteristics of the Muráň Gneiss Complex, Veporic Unit (Slovakia). *Journal of the Czech Geological Society* 48, 52.
- Gaab, A., Poller, U., Todt, W., Janák, M., 2003c. Isotopic Pb-Pb and U-Pb Data in the Muran Gneiss Complex, Veporic Unit (Western Carpathians, Slovakia). *EGS-AGU-EUG Joint assembly* , 282.

- Gaab, A., Todt, W., Poller, U., submitted. CLEO: Common lead evaluation using Octave. *Computers & Geosciences* .
- Grecula, P., 1982. Gemericum: segment of the Paleotethyan riftogeneous basin within Alpine Variscides. *Mineralia Slovaca - Monograph 2*, 108pp.
- Grunsky, E., 2002. R: a data analysis and statistical programming environment - an emerging tool for the geosciences. *Computers & Geosciences* 28, 1219–1222.
- Gurk, C., 1999. Petrographie, Geochemie und Geochronologie der unteren Einheit, Tatricum, Westliche Tatra (Slovakie). Unpublished Diploma Thesis, University of Mainz.
- Gurk, C., Poller, U., 1999. Petrography, geochemistry and geochronology of the Lower Unit, Western Tatra Mts (Slovakia). *Journal of Conference Abstracts* 4, 809.
- Habicht-Mauche, J. A., Glenn, S. T., Schmidt, M. P., Franks, R., Milford, H., Flegal, A. R., 2002. Stable Lead Isotope Analysis of Rio Grande Glaze Paints and Ores Using ICP-MS: A Comparison of Acid Dissolution and Laser Ablation Techniques. *Journal of Archaeological Science* 29, 1043–1053.
- Hegner, E., Kröner, A., 2000. Review of Nd isotopic data and xenocrystic and detrital zircon ages from the pre-Variscan basement in the eastern Bohemian Massif: speculations on palinspastic reconstructions. In: Franke, W., Haak, V., Onken, O., Tanner, D. (Eds.), *Orogenic Processes: Quantification and Modelling in the Variscan Belt*, vol. 179. Geological Society, London, 113–129.
- Hovorka, D., Dávidová, M.-Ľ., Fejdi, P., Gregorová, Z., Határ, J., Kátlovský, V., Pramuka, S., Spišiak, J., 1987. The Muráň gneisses of the Kohút Crystalline Complex. *Acta Geologica et Geographica Universitatis Comenianae* 42, 5–101.

- Irber, W., 1999. The lanthanide tetrad effect and its correlation with K/Rb, Eu/Eu\*, Sr/Eu, Y/Ho, and Zr/Hf of evolving per-aluminous granite suites. *Geochimica et Cosmochimica Acta* 63, 489–508.
- Janák, M., Cosca, M., Finger, F., Plašienka, D., Koroknai, B., Lupták, B., Horváth, P., 2001a. Alpine (Cretaceous) metamorphism in the Western Carpathians: P-T-t paths and exhumation of the Veporic core complex. *Geologisch-Paläontologische Mitteilungen Innsbruck* 25, 115–118.
- Janák, M., Finger, F., Plašienka, D., Petrík, I., Humer, B., Méres, Š., Lupták, B., 2002. Variscan high P-T recrystallization of Ordovician granitoids in the Veporic unit (Nízke Tatry Mountains, Western Carpathians): new petrological and geochronological data. *Geolines* 14, 38–39.
- Janák, M., Méres, Š., Ivan, P., 2003. First evidence for omphacite and eclogite facies metamorphism in the veporic unit of the Western Carpathians. *Journal of the Czech Geological Society* 48, 69.
- Janák, M., O'Brien, P. J., Hurai, V., Reutel, C., 1996. Metamorphic evolution and fluid composition of garnet-clinopyroxene amphibolites from the Tatra Mountains, Western Carpathians. *Lithos* 39, 57–59.
- Janák, M., Plašienka, D., Frey, M., Cosca, M., Schmidt, S., Lupták, B., Méres, Š., 2001b. Cretaceous evolution of a metamorphic core complex, the Veporic unit, Western Carpathians (Slovakia): P-T conditions and *in situ*  $^{40}\text{Ar}/^{39}\text{Ar}$  UV laser probe dating of metapelites. *Journal of Metamorphic Geology* 19, 197–216.
- Janousek, V., Farrow, C., Erban, V., 2003. GCDkit: New PC software for interpretation of whole-rock geochemical data for igneous rocks. *Goldschmidt Conference Abstracts 2003*.
- Kilík, J., 1997. Geologická charakteristika mastencového ložiska Gemerská Poloma - Dlhá Dolina. *Acta Montanistica Slovaca* 2.
- Klinec, A., 1976. Geologická mapa Slovenského Rudohoria a Nízkyh Tatier. *Geologický Ústav Dionýza Štura, Bratislava*.



- Kohút, M., Stein, H., Radvanec, M., 2004. Re-Os dating of molybdenite from the Hnilec Permian granite-related mineralisation - its tectonic significance (Gemeric unit, Slovakia). *Geolines* 17, 54–55.
- Korikovskiy, S. P., Krist, E., Boronikhin, V. A., 1989. Staurolite-chloritoid schists from the Klenovec region: prograde metamorphism of high alumina rocks of the Kohút zone-Veporides. *Geologický Zborník - Geologica Carpathica* 39, 187–200.
- Koroknai, B., Horvath, P., Balogh, I., K. Dunkl, 2001. Alpine metamorphic evolution and cooling history of the Veporic basement in northern Hungary: new petrological and geochronological constraints. *International Journal of Earth Science* 90, 740–751.
- Kováčik, M., Král', J., Bachlinski, R., 2001. The "Muráň" orthogneisses: contribution to tectonics, origin, metamorphism and Sr-isotopes constraint (Southern Veporicum, Western Carpathians). *Slovak Geological Magazine* 7, 202–211.
- Kováčik, M., Král', J., Maluski, H., 1996. Metamorphic rocks in the Southern Veporicum basement: their Alpine metamorphism and thermochronologic evolution. *Mineralia Slovaca* 28, 185–202.
- Král', J., Frank, W., Bezák, V., 1996.  $^{40}\text{Ar}$ - $^{39}\text{Ar}$  spectra from amphibole of veporic amphibolic rocks. *Mineralia Slovaca* 28, 501–513.
- Krist, E., Korikovskij, S. P., Putiš, M., M., Janák, Faryad, S. W., 1992. *Geology and Petrology of Metamorphic rocks of the Western Carpathian Crystalline Complexes*. Comenius University Press, Bratislava.
- Kröner, A., Štípská, P., Schlumann, K., Jaeckel, P., 2000. Chronological constraints on the pre-Variscan evolution of the Bohemian Massif, Czech Republic. In: Franke, W., Haak, V., Onken, O., Tanner, D. (Eds.), *Orogenic Processes: Quantification and Modelling in the Variscan Belt*, vol. 179. Geological Society, London, 175–197.
- Kubiš, M., 2004. Origin and evolution of the Spi-Gemer granites. Ph.D. thesis, GIU SAV, Bratislava.

- Kubiš, M., Broska, I., 2005. Role of boron and fluorine in evolved granitic rock systems (on an example of the Hnilec area, Western Carpathians). *Geologický Zborník - Geologica Carpathica* .
- Langmuir, C. H., Vocke, R. D., Hanson, G. N., 1978. A general mixing equation with applications to Icelandic basalts. *Earth Planetary Science Letters* 37, 380–392.
- Liew, T., Hofmann, A., 1988. Precambrian crustal components, plutonic associations, plate environment of Hercynian Fold Belt of central Europe: Indications from a Nd and Sr isotopic study. *Contributions to Mineralogy and Petrology* 98, 129–138.
- Ludwig, K. R., 2001a. Isoplot/ex rev. 3.49 A geochronological Toolkit for Microsoft Excel. Berkeley Geochronological Center; Special Publications No. 1a .
- Ludwig, K. R., 2001b. SQUID 1.02 - A user's Manual. Berkeley Geochronological Center; Special Publications No. 2 .
- Lupták, B., Janák, M., Plašienka, D., Schmidt, S. T., Frey, M., 2000. Chloritoid-kyanite schists from the Veporic unit, Western Carpathians, Slovakia: implications for Alpine (Cretaceous) metamorphism. *Swiss Bulletin of Mineralogy and Petrology* 80, 211–222.
- Lupták, B., Janák, M., Plašienka, D., Schmidt, S. T., 2003. Alpine low-grade metamorphism of the Permian-Triassic sedimentary rocks from the Veporic Superunit, Western Carpathians: Phyllosilicate composition and "crystallinity" data. *Geologický Zborník - Geologica Carpathica* 54, 367–375.
- Lupták, B., Thöni, M., Janák, M., Petřík, I., 2004. Sm-Nd isotopic chronometry of garnets from the veporic unit, Western Carpathians: some preliminary age results and P-T constraints. *Geolines* 17.
- Malachovský, P., et al., 1983. Final report SGR, high-temperature mineralization - Sn, W, Mo ores. Tech. rep., Geofond Bratislava.

- Maluski, H., Rajlich, P., Matte, P., 1993.  $^{40}\text{Ar}/^{39}\text{Ar}$  dating of the Inner Carpathians Variscan basement and Alpine mylonitic overprinting. *Tectonophysics* 223, 313–337.
- McDonalds, G. A., 1986. Chemical composition of Hawaiian lavas. In: Coats, R. R., Hay, R. L., Anderson, C. A. (Eds.), *Studies in vulcanology: a memoir in honor of Howel Williams*, 116. Geological Society of America, 477–522.
- Méres, Š., Hovorka, D., 1991. Geochemistry and metamorphic evolution of the Kohút crystalline complex mica schists (Western Carpathians). *Acta Geologica et Geographica Universitatis Comenianae* 47, 15–66.
- Middleton, G., 2000. *Data analysis in Earth sciences using Matlab*. Prentice-Hall, Upper Saddle River, NJ.
- Miller, C., Thöni, M., 1995. Origin of eclogites from the Austroalpine Ötztal basement (Tirol, Austria) - Geochemistry and Sm-Nd vs. Rb-Sr isotope systematics. *Chem. Geol.* 122, 199–225.
- Murphy, J. B., Nance, R. D., 2002. Sm-Nd isotopic systematics as tectonic tracers: an example from West Avalonia in the Canadian Appalachians. *Earth-Science Reviews* 59, 77–100.
- Oliver, G., Corfu, F., Krogh, T., 1993. U-Pb ages from SW Poland: evidence for a Caledonian suture zone between Baltica and Gondwana. *Journal of the Geological Society, London* 150, 355–369.
- Onuma, N., Higuchi, H., Wakita, H., Nagasawa, H., 1968. Trace element partitioning between two pyroxenes and the host lava. *Earth Planetary Science Letters* 5, 47–51.
- Papanastassiou, D., Wasserburg, G., 1969. Initial Strontium isotopic abundances and the resolution of small time differences in the formation of planetary object. *Earth Planetary Science Letters* 5, 361–376.
- Pearce, J., Norry, M., 1979. Petrogenetic implications of Ti, Zr, Y and Nb variations in volcanic rocks. *Contrib. Mineral. Petrol.* 69, 33–47.

- Planchon, F. A. M., van de Velde, K., Rosman, K. J. R., Wolff, E. W., Ferrari, C. P., Boutron, C. F., 2003. One hundred fifty year record of lead isotopes in Antarctic snow from Coats Land. *Geochimica et Cosmochimica Acta* 67, 693–708.
- Plašienka, D., 1997. Cretaceous tectonochronology of the Central Western Carpathians, Slovakia. *Geologický Zborník - Geologica Carpathica* 48, 99–111.
- Plašienka, D., Grecula, P., Putiš, M., Hovorka, D., Kováčik, M., 1997. Evolution and structure of the Western Carpathians: an overview. In: Grecula, P., Hovorka, D., Putiš, M. (Eds.), *Geological Evolution of the Western Carpathians. Mineralia Slovaca - Monograph*, 1–24.
- Plašienka, D., Janák, M., Lupták, B., Milovský, R., Frey, M., 1999. Kinematics and metamorphism of a Cretaceous core complex: the Veporic unit of the Western Carpathians. *Physics and Chemistry of the Earth (A)* 24, 651–658.
- Poller, U., Gladkochub, D., Donskaya, T., Mazukabzov, A., Sklyarov, E., Todt, W., 2004. Timing of Early Proterozoic magmatism along the Southern margin of the Siberian Craton (Kitoy area). *Transactions of the Royal Society* 95. In press.
- Poller, U., Janák, M., Kohút, M., Todt, W., 2000. Early Variscan Magmatism in the Western Carpathians: U-Pb zircon data from granitoids and orthogneisses of the Tatra Mts (Slovakia). *International Journal of Earth Science* 89, 336–349.
- Poller, U., Kohút, M., Gaab, A., Todt, W., in press. Pb, Sr and Nd isotope study of two co-existing magmas in the Nízke Tatry Mountains, Western Carpathians (Slovakia). *Mineralogy and Petrology* .
- Poller, U., Kohút, M., Todt, W., Janák, M., 2001a. Nd, Sr, Pb isotope study of the Western Carpathians: implications for Palaeozoic evolution. *Swiss Bulletin of Mineralogy and Petrology* 81, 159–174.

- Poller, U., Nagler, T., Liebetrau, V., Galetti, G., 1997. The Monchalpgneiss - Geochemical characteristics and Sm-Nd data of a polymetamorphic S-type granitoid (Silvretta nappe / Switzerland). *European Journal of Mineralogy* 9, 411–422.
- Poller, U., Todt, W., 2000. U-Pb single zircon data of granites from the High Tatra Mountains (Slovakia): implications for the geodynamic evolution. *Transactions of the Royal Society* 91, 235–243.
- Poller, U., Uher, P., Broska, I., Plasienska, D., Janaak, M., 2002. First Permian-Early Triassic zircon ages for tin-bearing granites from the Gemeric unit (Western Carpathians, Slovakia): connection to the post-collisional extension of the Variscan orogen and S-type magmatism. *Terra Nova* 14, 41–48.
- Poller, U., Uher, P., Janak, M., Plasienska, D., Kohut, M., 2001b. Late Cretaceous age of the Rochovce granite, Western Carpathians, constrained by U/Pb single-zircon dating in combination with cathodoluminescence imaging. *Geologicky Zbornık - Geologica Carpathica* 52, 41–47.
- Putis, M., Filova, I., Korikovskyy, S. P., Kotov, A. B., Madaras, J., 1997. Layered metaigneous complex of the veporic basement with features of the Variscan and Alpine thrust tectonics (Western Carpathians). In: Grecula, P., Hovorka, D., Putis, M. (Eds.), *Geological Evolution of the Western Carpathians. Mineralia Slovaca - Monograph, Geocomplex*, 175–196.
- Putis, M., Kotov, A., Korikovskyy, S., Salnikova, E., Yakoleva, S., Berezhnaya, N., Kovach, V., Plotkina, J., 2001. U-Pb zircon ages of dioritic and trondhjemitic rocks from a layered amphibolitic complex crosscut by granite vein (Veporic basement, Western Carpathians). *Geologicky Zbornık - Geologica Carpathica* 52, 49–60.
- Raczek, I., Stoll, B., Hofmann, A. W., Jochum, K., 2001. High-Precision Trace Element Data for the USGS Reference Materials BCR-1, BCR-2, BHVO-1, BHVO-2, AGV-1, AGV-2, DTS-1, DTS-2, GSP-1 and GSP-2 by ID-TIMS and MIC-SSMS. *Geostandard Newsletter* 25, 77–86.

- Schaltegger, U., Nagler, T., Corfu, E., Maggetti, M., Galetti, M. G., Stosch, H., 1997. A Cambrian island arc in the Silvretta nappe, a comparison. *Swiss Bulletin of Mineralogy and Petrology* 77, 337–350.
- Schettler, G., Romer, R. L., 1998. Anthropogenic influences on Pb/Al and lead isotope signature in annually layered Holocene Maar lake sediments. *Applied Geochemistry* 13, 787–797.
- Sen Gupta, J., Bertrand, N., 1995. Direct ICP-MS determination of trace and ultratrace elements in geological materials after decomposition in a microwave oven I. Quantitation of Y, Th, U and the lanthanides. *Talanta* 42, 1595–1607.
- Stacey, J. S., Kramers, J. D., 1975. Approximation of terrestrial lead isotope evolution by a two-stage model. *Earth Planetary Science Letters* 26, 207–221.
- Stampfli, G., 1996. The intra-Alpine terrain: a palaeotethyan remnant in the Alpine Variscides. *Eclogae Helvetiae* 89, 12–42.
- Stampfli, G. M., Borel, G. D., 2002. A plate tectonic model for the Paleozoic and Mesozoic constrained by dynamic plate boundaries and restored synthetic oceanic isochrons. *Earth Planetary Science Letters* 196, 17–33.
- Steiger, R. H., Jager, E., 1977. Subcommission on geochronology: Convention on the use of decay constants in geo- and cosmochemistry. *Earth Planetary Science Letters* 36, 359–362.
- Sun, S.-S., 1980. Lead isotopic study of young volcanic rocks from mid-ocean ridges, ocean islands and island arcs. *Philosophical Transactions of The Royal Society* 297, 409–445.
- Taylor, S., McLennan, S., 1985. *The continental crust: its composition and evolution*. Blackwell, Oxford.
- Thoni, M., Petrık, I., Janak, M., Luptak, B., 2003. Preservation of Variscan garnet in Alpine metamorphosed pegmatite from the Veporic unit, Western Carpathians: evidence from Sm-Nd isotope data. *Journal of the Czech Geological Society* 48, 123–123.

- Titterton, D. M., Halliday, A. N., 1979. On the fitting of parallel isochrons and the method of maximum likelihood. *Chemical Geology* 26, 183–195.
- Todt, W., Cliff, R., Hanser, A., Hofmann, A., 1996. Earth Processes: Reading the Isotopic Code, vol. 95, chap. 202Pb + 205Pb double spike for lead isotopic analyses. *Geophysikal Monograph*, 429–437.
- Totland, M., Jarvis, I., Jarvis, K., 1992. An assessment of dissolution techniques for analysis of geological samples by plasma spectrometry. *Chemical Geology* 95, 35–62.
- Totland, M., Jarvis, I., Jarvis, K., 1995. Microwave digestion and alkali fusion procedures for the determination of platinum-group elements and gold in geological materials by ICP-MS. *Chemical Geology* 124, 21–36.
- von Raumer, J., Neubauer, F., 1993. Late Precambrian and Palaeozoic evolution of the Alpine basement - an overview. In: von Raumer, J., Neubauer, F. (Eds.), *Pre-Mesozoic geology in the Alps*. Springer-Verlag, Berlin, 625–639.
- von Raumer, J., Stampfli, G., Borel, G., Bussy, F., 2002. Organization of pre-Variscan basement areas at the north-Gondwanan margin. *International Journal of Earth Science* 91, 35–52.
- von Raumer, J. F., Stampfli, G. M., Bussy, F., 2003. Gondwana-derived microcontinents – the constituents of the Variscan and Alpine collisional orogens. *Tectonophysics* 365, 7–22.
- Vozárová, A., 1998. Hercynian development of the external-Gemeric zone. In: Rakús, M. (Ed.), *Geodynamic development of the Western Carpathians*. Dionýz Štúr Publication, 47–61.
- Vozárová, A., Frank, W., Král', J., 2000.  $^{40}\text{Ar}/^{39}\text{Ar}$  data from contact aureole of Súľ'ová granite (Gemericum, Western Carpathians). *Slovak Geological Magazine* 6, 363–366.
- Vozárová, A., Sotáček, J., Ivanička, J., 1998. A new microfauna from the Early Paleozoic formations of the Gemericum (foraminifera): constraints for an-

- other fossils or subfossils. In: Rakús, M. (Ed.), Geodynamic development of the Western Carpathians. Dionýz Štúr Publication, 47–61.
- Wendt, J., Todt, W., 1991. A vapor digestion method for dating single zircons by direct measurement of U and Pb without chemical separation. *Terra Abstracts* 3, 507–508.
- White, W., Patchett, J., 1984. Hf-Nd-Sr isotopic and incompatible element abundances in island arcs: implications for magma origins and crust-mantle evolution. *Earth Planetary Science Letters* 67, 167–185.
- Williams, I., 1998. U-Th-Pb Geochronology by Ion-Microprobe. In: McKibben, M., Shanks III, W., Ridley, W. (Eds.), Application of microanalytical techniques to understanding mineralization processes, vol. 7 of *Reviews in Economic Geology*. The Society of Economic Geologists, 1–35.
- York, D., 1969. Least squares fitting of a straight line with correlated errors. *Earth Planetary Science Letters* 5, 320–324.
- Zartman, R., Haines, S., 1988. The plumbotectonic model for Pb isotopic systematics among major terrestrial reservoirs - A case for bi-directional transport. *Geochimica et Cosmochimica Acta* 52, 1327–1339.
- Zindler, A., Hart, S., 1986. Chemical Geodynamics. *Annual Review of Earth and Planetary Sciences* 14, 493.

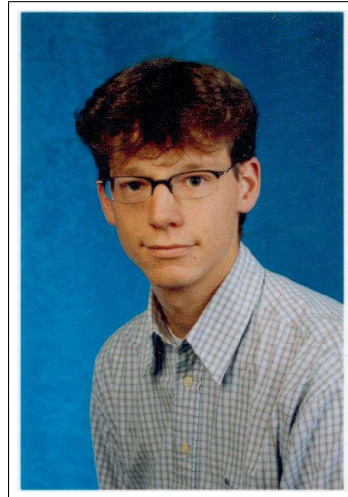


COMPLETE REFERENCE LIST

---

# CURRICULUM VITAE

ANDREAS S. GAAB



---

## ADRESSE

Karmeliterplatz 4  
55116 Mainz  
Telefon: +49-6131-6933482  
Email: a.s.gaab@gmx.de

---

## PERSÖNLICHE DATEN

Geburtstag: 2. April 1976  
Geburtsort: Gräfelfing, Deutschland  
  
Familienstand: verheiratet  
Kinder: Johanna M. Gaab, geb. 10 Oktober 2004

---

## BERUFSERFAHRUNG

seit 04.2002 Doktorand am Max-Planck-Institut für Chemie, Mainz

---

## AUSBILDUNG

10.1996–10.2001 Student der Geowissenschaften an der Universität Potsdam  
Abschluss: Diplom Mineraloge, Note 1.7  
  
08.1995–09.1996 Zivildienst im Altenpflegeheim der Inneren Mission, Planegg  
  
09.1986–06.1995 Kurt-Huber-Gymnasium  
Abschluss: Abitur, Note: 2.3  
  
09.1982–06.1986 Grundschule Gräfelfing

Mainz,